Stellingen

1. De vaak praktische aanpak van problemen door de verfindustrie, wordt zeker gekenmerkt door haar termen nagelhard, duimvast en stofdroog. Om deze problemen beter te kunnen karakteriseren cq. oplossen is een wetenschappelijker aanpak noodzakelijk
   OSV, Verfkroniek **64**, *250 (1991)*
   W.J. Nijveld, A.F. Ross, *De Praktische Controle van Droging, Verfkroniek* **57**, 424 (1984)

2. De benaming "Minimale Filmvormings Temperatuur" is misleidend, omdat deze parameter niet het filmvormingsproces van een drogende latexfilm karakteriseert, maar alleen die temperatuur waarbij de gedroogde latexfilm, onder standaard condities, homogeen en transparant wordt.
   Dit proefschrift

3. De invloed van deeltjesgrootte op de MFT kan grotendeels verklaard worden door de verschillen in het lichtverstrooiingsgedrag van latices met respectievelijk grote en kleine deeltjes.
   Eckersley, S.T., Rudin, A., J. Coat. Techn. **62**, *89 (1990).*
   Jenson, D.P., Morgan, L.W., J. Appl. Polym. Sci. **42**, *2845 (1991).*
   Dit proefschrift

4 De interne grenslagen die na de coalescentie van de latexdeeltjes nog zichtbaar zijn zullen pas verdwijnen wanneer de emulgatormolekulen migreren of oxideren.
   Dit proefschrift
   Chevalier, Y., Pichot, C., Graillat, C., Colloid Polym. Sci. **270**, *806 (1992).*
   Bradford, E.B., Vanderhoff, J.W., J. Macromol. Chem. **1**, *335 (1966).*

5 In het algemeen wordt vaak het isotrope deformatiemechanisme toegepast voor de beschrijving van latexcoalescentie. Dit is niet juist, want de latexdeeltjes coalesceren volgens een bi-axiaal mechanisme.
   Dit proefschrift
   Bierwagen, G.P., J. Coat. Techn. **51**, *117 (1979).*
   Kendall, K., Padget, J.C., Int. J. Adhesion and Adhesives **7**, *149 (1982).*

6. "Chemische" stoffen die op zichzelf niet milieuvriendelijk zijn, kunnen toch als milieuvriendelijk aangeduid worden indien zij de levensduur van schaarse, natuurlijke produkten verlengen.

7 De internationale gemeenschap is pas echt geïnteresseerd in mensenleed wanneer ook grote economische belangen een rol spelen. Doet zo een situatie zich voor, dan worden kosten nog middelen gespaard om de crisis het hoofd te bieden.

8 Om de bezettingsgraad van computers te verminderen, zouden computers niet meer van een kleurenmonitor voorzien dienen te worden.

9 Muziek is een kunstvorm die berust op het ordenen en harmoniseren van klankfenomenen. Daarom kan, in sommige gevallen, de hedendaagse electronische "popmuziek" niet meer tot deze kunstvorm worden gerekend, omdat in deze gevallen alleen nog maar sprake is van ordenen van klanken.
Webster's Third New International Dictionary of the English Language (1986)
Grote Winkler Prins, Encyclopedie, achtste druk, Elsevier (1980)
Rotterdam termination source, Midtown : Poing, Poing, Poing ....

10 Het kennisniveau van een afgestudeerd HTS- (*nu TH*) en TU-ingenieur verschilt op dit moment niet zo veel meer. Echter, andere minstens zo belangrijke aspecten van de opleiding als zelfstandigheid, inzicht, overzicht en kennisaccumulatie liggen bij een TU-ingenieur op een veel hoger niveau dan bij een HTS-ingenieur. Daarom is het egaliseren van HTS- en TU-opleidingen niet juist, omdat dit altijd ten koste zal gaan van de kwaliteit van de TU-ingenieur.

TURBIDITY STUDY OF THE PROCESS OF FILM FORMATION OF POLYMER PARTICLES IN DRYING THIN FILMS OF ACRYLIC LATICES

PROEFSCHRIFT

ter verkrijging van de graad van doctor
aan de Technische Universiteit Delft,
op gezag van de Rector Magnificus,
prof. drs. P.A. Schenck,
in het openbaar te verdedigen
ten overstaan van een commissie aangewezen
door het College van Dekanen
op maandag 12 oktober 1992 te 19.00 uur door

Abraham van Tent

Ingenieur in de Chemische Technologie
geboren te Ermelo

Dit proefschrift is goedgekeurd door promotor
Prof.dr.ir. A. Posthuma de Boer

en toegevoegd promotor
Dr.ir. K. te Nijenhuis

Voor mijn ouders

Publications

"Turbidity study of the process of film formation of thin films of aqueous acrylic dispersions"
by A. van Tent and K. te Nijenhuis
in *Journal of Polymer Science, Progress in Organic Coatings* **20**, 459 (1992).

Chapter 2
"Turbidity study of the process of film formation of polymer particles in drying thin films of acrylic latices I. Intrastructure of acrylic latices studied with transmission spectrophotometry"
by A. van Tent and K. te Nijenhuis
in *Journal of Colloid and Interface Science* **150**, 97 (1992).

Chapter 3 / 4 and 5
"Turbidity study of the process of film formation of polymer particles in drying thin films of acrylic latices II. The coalescence and autohesion process"
by A. van Tent and K. te Nijenhuis *in preparation, (1992).*

Chapter 6
"Turbidity study of the process of film formation of polymer particles in drying thin films of acrylic latices III. Influence of Core-shell morphology on latex coalescence"
by A. van Tent and K. te Nijenhuis *in preparation, (1992).*

CONTENTS

Chapter 1
Introduction
1.1. General Introduction 1
1.2. This Thesis 2
References 4

Chapter 2
Intrastructure of Thin Films of Acrylic Latices Determined with Transmission Spectrophotometry
2.1. Introduction 5
2.2. Theory 7
2.2.1. Multilayer Interference 7
2.2.2. Rayleigh Scattering 11
2.3. Model 13
2.3.1. The Particle Distance and the Layer Distance 14
2.3.2. The Average Refractive Index 15
2.3.3. The Rayleigh Scattering Models 17
2.4. Experimental 20
2.4.1. Materials 20
2.4.2. Influence of Weight Fraction on Transmission 21
2.4.3. Influence of Weight Fraction on λ_{min} 22
2.4.4. Influence of Angle of Incidence on λ_{min} 23
2.4.5. Influence of Film Thickness on the Interference Pattern 24
2.4.6. Influence of Particle Distribution on the Interference Pattern 24
2.5. Model Results and Discussions 25
2.5.1. The Particle Size 25
2.5.2. Interparticle Interference 27
2.5.3. Rayleigh Scattering Models 28
2.6. Conclusions 30
References 31

Chapter 3

The Film Formation Process of Drying Thin Films of Acrylic Latices

3.1. Introduction 33
3.2. Experimental 38
3.2.1. Materials. 38
3.2.1a. Procedure Semi-continue Emulsion Polymerization 38
3.2.2. Equipment and Measurements 39
3.3. Results and Discussions 42
3.3.1. Regularity of the Interparticle Structure 42
3.3.1a. Secondary Interference Minima 43
3.3.1b. Polymer Concentration Profiles 44
3.3.2. Critical Interparticle Distance 47
3.3.3. Size of Stabilizer Layer around the Latex Particles 48
3.4. Conclusions 49
References 50

Chapter 4

The Process of Coalescence of Latex Particles in Drying Thin Films of Acrylic Latices

4.1. Introduction 51
4.2. Latex Coalescence Theories 52
4.2.1. Dry Sintering 52
4.2.2. Wet Sintering 53
4.2.2a. Capillary Forces 54
4.2.2b. Deformation Forces of Viscoelastic Bodies 55
4.2.2c. Latex Coalescence 58
4.3. Experimental 60
4.3.1. Materials 60
4.3.2. Equipment 60
4.4. Results and Discussions 61
4.4.1. Determination of Deformation Mechanism 61
4.4.2. Evaluation Hypotheses Wet Sintering Theory 62
4.4.3. Influence of r_p on Latex Coalescence 68
4.4.4. Influence of r_p and *R.H.* on the *MFFT* 70
4.5. Conclusions 73
References 75

Chapter 5

The Process of Autohesion of Coalesced Latex Particles in Dried Thin Films of Acrylic Latices

5.1. Introduction 77

5.2. Autohesion Theories 78

5.2.1. Interfacial Contact and Bonding in Autohesion 78

5.2.2. Interdiffusion 80

5.2.2a. Self-diffusion Theories 80

5.2.2b. Experimental Evidence from the Literature 82

5.3. Experimental 83

5.3.1. Materials 83

5.3.2. Transmission Spectrophotometry 83

5.3.3. *TEM* 84

5.4. Results and Discussions 84

5.4.1. Swelling Behaviour of the Remaining Internal Interfacial Boundaries. 84

5.4.2. Internal Interfacial Boundaries Studied with *TEM* 87

5.5. Conclusions 89

References 89

Chapter 6

Influence of Core-shell Morphology on Latex Coalescence

6.1. Introduction 91

6.2. Synthesized Materials 93

6.2.1. Procedure Seeded Emulsion Polymerization 93

6.2.2. Procedure Shot-growth Emulsion Polymerization 94

6.3. Characterization Core-Shell Latices 95

6.3.1. Particle Size 95

6.3.2. Soap Titrations 97

6.3.3. *DSC-*T_g 98

6.3.4. Latex Coalescence 98

6.3.4a. Interparticle Interference 98

6.3.4b. Rayleigh Scattering 100

6.3.4c. *MFFT* Core-shell Latices. 101

6.3.3d. *DMTA* 102

6.4. Conclusions 103

References 104

Appendices 107

I : Rayleigh Scattering Model 2 107

II : Calculation of the Size of the Stabilizing Layer. 108

III : Indentation as a Function of the Volume Fraction of Spheres in a H.C.P.-Unit 109

IV : Theoretical Interparticle Interference Change for Isotropic and Bi-axial Deformation Mechanisms. 110

V : Rayleigh Light Scattering of Ellipsoids . 111

List of Symbols 113

Summary 117

Samenvatting 121

Dankwoord 125

In memoriam Prof.dr.ir H.C.A. van Beek 126

Curriculum Vitae 127

CHAPTER 1

INTRODUCTION

1.1. GENERAL INTRODUCTION

The study described in this thesis was performed as part of an innovation oriented research program funded by the Dutch government, called "Onderzoeks Stimuleringsprogramma Verf (OSV)" to support the paint industry in The Netherlands. The objective of the program was to introduce the scientific approach to help solving the normally very practical problems of the paint industry [1,2]. To get industrial attention for the program, the choice was made that all projects had to be focused on aqueous dispersion coatings. Because of the limited budget of the program only five projects could be supported, which already started in the period of 1986-1987. The five projects were carefully chosen in order to investigate the complete spectra of problems involved with aqueous dispersion coatings. The projects varied from the synthesising of aqueous dispersion coatings to the intrastructure of the coalesced polymer particles in thin films of dried dispersion coatings. Normally, industrial aqueous dispersion coatings consist of many components. This often leads to a very complicated macroscopic behaviour, where the influences of the different microscopical properties are not easily accessible for the interpretation of the macroscopic properties. Therefore, the research was done on less complicated systems, in which only basic components were varied to get a better understanding of the macroscopic properties of the dried coating from changes in microscopic properties like particle interactions (polymer particles, pigments and additives), latex morphology, latex coalescence and autohesion.

Evaluation of the research program OSV at a conference (The Netherlands, Rhenen, 21 March 1991 [3,4]) proved that the accomplished scientific results are of great importance for the better understanding of problems involved with aqueous dispersion coating. Therefore a new and much larger innovation oriented research program, Innovatie gericht Onderzoek Programma Verf (IOP-Verf), has been set up. This IOP-Verf program started in the beginning of 1992 with an initial budget of 5 million dollars for a period of two years [5].

1.2. THIS THESIS

This thesis concerns the study of the process of film formation of drying thin films of acrylic latices by means of turbidity measurements. Turbidity determines the extent of the attenuation of a light beam which passes the latex film. The turbidity of non-absorbing media is caused by scattering and interparticle interference. The aim of this study is to determine the factors that define the process of film formation of binder particles in drying aqueous dispersion coatings, based on acrylic polymers.

The film formation process of latices involves the physical processes that play important roles after the application of the latex to a surface until the complete drying and ageing of the applicated latex coating. The physical processes involved are for the water component diffusion and evaporation and for the polymer and the stabilizer component flocculation, coalescence and autohesion. Autohesion involves the processes by which the internal interfacial boundaries disappear between the deformed latex particles. Some of these physical processes are of very different nature and some will interact during the film formation process. Because of this multi-disciplinary character of the film formation process of latices it will be rather complicated to investigate the influences of the microscopical physical properties on the macroscopical behaviour of the dried coating.

This thesis will be focused on the process of coalescence and autohesion during the film formation process of a drying latex film, because very little is known about the mechanisms that operate during the coalescence and the autohesion process.

In order to study the coalescence process of the particles in drying films of very concentrated latices, it is necessary to determine the sizes and the spatial arrangement of the latex particles. In Chapter 2, a technique is described, which determines from the turbidity of a thin latex film, the particle size, interparticle displacements and stacking of the latex particles. The technique is based on the scattering and interparticle interference properties of concentrated thin latex films. The interparticle interference and scattering can be described with the multilayer interference theory and Rayleigh scattering theory respectively. Some experiments will be discussed, which support the hypotheses developed by the theory. These experiments were done on static systems, whereby the latices are fixed between two plane parallel quartz plates to exclude the influence of water evaporation. The results of these measurements were verified with other particle size measurements and imaging techniques, like *QELS*, SF_3, *TEM* and *SEM*.

Typical interference patterns measured during the film formation process, will be

discussed of latex films which were dried above and below the minimal film formation temperature (*MFFT*). In chapter 3 these specific interparticle interference patterns are subjected to a more detailed investigation. This results in detailed information about the regularity of the interparticle structure during the drying process of the latex film, the critical interparticle distance at which the flocculation process is initiated and the size of the stabilizer layer around the latex particles.

Theoretical descriptions of deformation and autohesion of the latex particles during the drying and ageing process of a thin latex film can be found in chapters 4 and 5. The coalescence theories are used to relate the turbidity behaviour of drying thin latex films with the (visco)elastic properties of the dried latex film, which were measured in a *DMTA*. The interparticle interference change in a drying latex film is related to the interparticle distance and displacement. When the latex particles coalesce the interparticle distances become smaller. This means that the change in interparticle interference from this point on is related to the indentation of the latex particles. From the typical behaviour of the interference patterns of drying latex films the mechanism by which the latex particles deform can be determined.

When the latex particles are completely coalesced the film becomes transparent. However, when this film is immersed into a *0.1 N HCl* solution, the remaining internal interfacial boundaries between the adherent binder particles will swell, which regenerates an interference pattern. The regenerated interference pattern is related to the size and number of the swollen interfacial boundaries. It is tried to relate the turbidity behaviour of swollen latex films with the autohesion theory. Experimental evidence will be demonstrated, which supports some of the hypotheses underlying various theories (see chapter 5). These preliminary measurements give a good description of the internal interfacial boundaries that remain in dried latex films.

In the literature *MFFT* measurements are often used to compare the film formation properties of different latices. This *MFFT* is defined as the drying temperature at which the drying latex film becomes homogeneous, transparent and crack free. The *MFFT* is determined by the visual interpretation of the transparency of dried films. The visual transparency is related to the concentration and the sizes of the remaining interstices in the dried latex film. Because the sizes of the interstices are related to the size and the extend of the deformation of the latex particles, it is evident that larger particles need to coalesce more than smaller particles to get evenly transparent latex films (see Chapter 4). It was found that the *MFFT* strongly depends on the wave-length when the transmittance of dried latex films is used to evaluate the *MFFT*.

Core-shell morphology in latices has been used to improve the latex coalescence and the elastic properties of the finally dried latex film. When the core consists of a hard polymer and the shell of a soft polymer, then it was expected that the latex coalescence will mainly be determined by the shell material, whereas the firmness of the finally dried latex film will depend on the elastic properties of core material in a continuous phase of shell material.

Chapter 6 is focused on the core-shell (PS-PBMA) characterization by turbidity measurements. Also other techniques are used, like *TEM, DSC, MFFT, QELS* and *Soap titration* to support the turbidity measurements and to get a better insight in the core-shell morphology of the two-staged polymerized latex particles. Combinations of the results of these techniques with the changing interparticle interference patterns during latex coalescence gave detailed information about the mechanism of coalescence of core-shell particles in relation to the (visco)elastic properties of the dried latex film.

References

1 Hofman-Caris, C.H.M., *Chemisch Weekblad*, **87(15)**, 154 (1991).
2 Nijveld, W.J., Ross, A.F., *Verf Kroniek* **57**, 424 (1984).
3 OSV Seminar, "Watergedragen Verven", Rhenen, The Netherlands, 1991.
4 OSV, *Verf Kroniek* **64**, 250 (1991).
5 Programma Voorbereidings Commissie IOP-verf, "Meerjarenplan voor het IOP-VERF", Civi Consultancy, Leidschendam, The Netherlands, 1991.

CHAPTER 2

INTRASTRUCTURE OF THIN FILMS OF ACRYLIC LATICES DETERMINED WITH TRANSMISSION SPECTROPHOTOMETRY.

This chapter relates the turbidity behaviour of thin latex films with physical properties of the latex. It is focussed on the intrastructure in films of concentrated acrylic dispersions. In concentrated latices the binder particles are arranged in closely packed structures, which cause coloured light patterns, due to Bragg diffraction [1-3,22]. Light waves travelling in the latex film are scattered at the internal structures of the spheres and the water voids. The pattern of the light transmission as a function of wave-length reveals the internal structure of the latex film. The influence of weight fraction, particle size, particle size distribution and film thickness on the transmission pattern has been investigated. The results are verified with other particle-size measurements and imaging techniques.

2.1. INTRODUCTION

In order to study the coalescence process of particles in drying concentrated acrylic dispersions, it is necessary to determine the particle sizes. Techniques by which particle sizes in the mesoscopic area (*50-500 nm*) can be measured are Transmission Electron Microscopy (*TEM*), Scanning Electron Microscopy (*SEM*), Sedimentation Field Flow Fractionation (SF_3), Quasi Elastic Light Scattering (*QELS*) [4] and Turbidity/ Transmission [5]. The main disadvantage of the first four techniques is the destruction of the latex structure as a result of the necessary complete drying or dilution of the latex.

In this study a transmission technique will be demonstrated. With this technique a transmission spectrum is measured, i.e. the transmission (T) of light through a thin latex layer is measured as a function of the wave-length (λ). This is a non-destructive technique by which latices can be characterized during the drying process. Much literature exists on the optical properties of latices. The literature that describes the optical properties of very concentrated aqueous latices is limited [1-3,5,16-22]. Recent work is concentrated on colloidal silica particles in benzene or cyclohexane

[22-27] and on diluted aqueous latices [27-31].

In non-absorbing media transmission of light is, in general, prevented to some extent by *scattering*. In media with a regular structure the transmission may also be prevented by *interparticle interference*, which is strongly dependent on the wave-length. In that case a sharp minimum in the transmission spectrum arises. An example of such a spectrum is shown in *Fig. 2.1*.

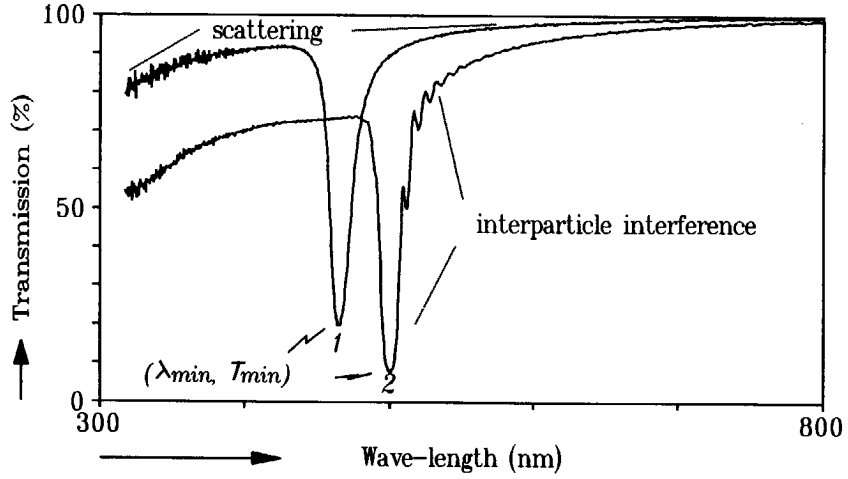

Fig. 2.1 Typical transmission spectra of latex (c9) films.
1 - V_f = 0.60 d_l = 13 μm, 2 - V_f = 0.45 d_l = 18 μm.

The interparticle interference is given by λ_{min}, T_{min}, from which the particle size and their mutual distance can be calculated, provided the packing structure of the latex is known. Spectrum (1) is that of a latex with a polymer volume fraction of 0.60 and spectrum (2) of 0.45. The increase of polymer concentration decreases the interparticle distance between the latex particles, so that the shift of the interparticle interference is related to the decrease of interparticle distance.

In order to obtain an interference pattern as shown in *Fig. 2.1*, the latex has to satisfy the following criteria :

a) narrow particle size distribution;

b) high volume fraction (V_f) of particles (to get a stable packing);

c) small film thickness (d_l) (low degree of scattering);

d) difference between refractive indices of solvent (n_s) and polymer (n_p).

In this study multilayer interference is used to characterize drying latex dispersions, and Rayleigh scattering to describe the ultimate drying of the

dispersions, where the scattering is caused by the water interstices between the deformed polymer particles in the nearly dry medium.

2.2. THEORY

Transmission is defined as $T = \frac{I_t}{I_o}$, where I_o is the intensity of the incident light, and I_t the intensity of the transmitted light. If the reduction in the transmission is caused by scattering and interference the experimental results of the section *2.5* can be described with the aid of :

(a) Fresnel's regular reflection theory [6];

(b) Multi-layer interference theory [7-10];

(c) Rayleigh and Mie's scattering theory [6,11,12].

The theoretical part of this study is focused first on transmission and reflection in a multilayered structure and secondly on light scattering by particles which are small compared to the wave-length.

2.2.1. Multilayer Interference

The transmission and reflection in a plane parallel transparent layer of thickness A and with an absolute refractive index n, is schematically shown in *Fig. 2.2.* It represents a polymer particle layer with a thickness A being directly proportional to the characteristic structure-length of the packed polymer particles in the latex.

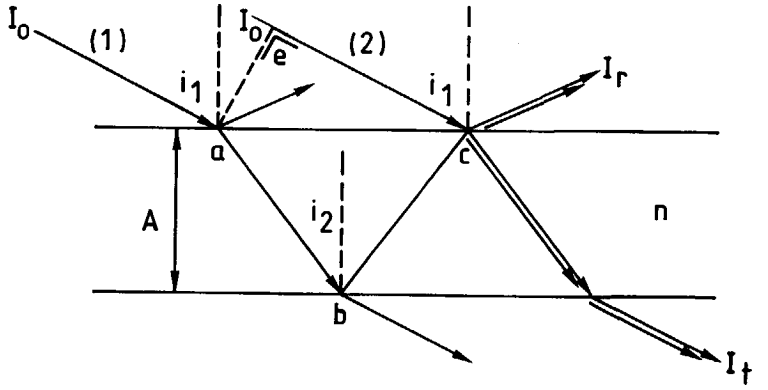

Fig. 2.2 Light interference in a plane parallel transparent layer.

As a result, light beam *1* will interfere with light beam *2* at point *c*. If the optical path-length difference equals $(\frac{1}{2}+k).\lambda$ $(k=0,1,2..)$, both beams are in opposite phase and the transmission will be minimal. In principle, the phase difference (ϕ) is given by :

$$\phi = \frac{2.\pi}{\lambda}.\left[2.n.[ab] - [ec]\right] = \frac{4.\pi.A}{\lambda}.\left[\frac{n}{\cos i_2} - \tan i_2.\sin i_2\right] \qquad (1)$$

Substituting Snellius'law (i.e. $\sin i_1 = n.\sin i_2$) into Eq.(1) we obtain:

$$\phi = \frac{4.\pi.A.n.\cos i_2}{\lambda} \qquad (2)$$

For a given plate thickness (A) minimal transmissions are obtained for:

$$\phi_{min} = (2.k+1).\pi \qquad k=0,1,2..$$

$$\lambda_{min} = \frac{4.A.n.\cos i_2}{2.k+1} \qquad k=0,1,2.. \qquad (3)$$

In *Fig. 2.3* part of a multilayer system is demonstrated schematically. It represents the lamellar phase of the latex, where polymer particle layers are separated by water layers. It consists of $2k+1$ layers of alternatively low and high refractive indices, sandwiched between two relatively thick glass plates.

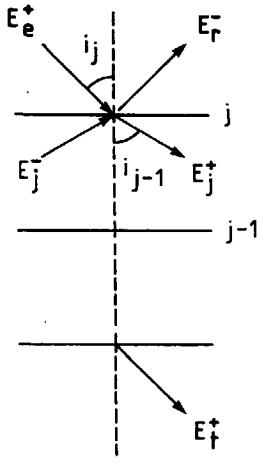

Fig. 2.3 Light interference in a multilayer system.

In the multilayer interference theory [7-10] a system transfer matrix (m_{ij}) is defined in the absence of absorbence :

$$\begin{bmatrix} E_e^+ + E_r^- \\ \mu_e\left(E_e^+ - E_r^-\right) \end{bmatrix} = \begin{bmatrix} m_{11} & m_{12} \\ m_{21} & m_{22} \end{bmatrix} * \begin{bmatrix} E_t^+ \\ \mu_t . E_t^+ \end{bmatrix} \tag{4}$$

where the system transfer matrix is the result of the multiplication of the transfer matrices of $(2k+1)$ layers :

$$\begin{bmatrix} m_{11} & m_{12} \\ m_{21} & m_{22} \end{bmatrix} = \prod_{j=1}^{2k+1} \begin{bmatrix} \cos \phi_j & \frac{i}{\mu_j} \sin \phi_j \\ i.\mu_j . \sin \phi_j & \cos \phi_j \end{bmatrix} \tag{5}$$

where :

E_e^+ = the electric field vector of incident light

E_r^- = the electric field vector of reflected light

E_t^+ = the electric field vector of transmitted light

$i = \sqrt{-1}$

ϕ_j = the phase shift for the *jth* layer :

$$\phi_j = \frac{2.\pi.n_j.d_j.\cos i_j}{\lambda} \tag{6}$$

where n_j = absolute refractive index of the *jth* layer

d_j = thickness of the *jth* layer.

i_j = angle of incidence of the *jth* layer

For S-polarized light :

$$\mu_j = n_j.\cos i_j \tag{7}$$

and for P-polarized light :

$$\mu_j = n_j / \cos i_j \tag{8}$$

Hence, for normal incidence $\mu_j = n_j$, whereas μ_t and μ_e are, for normal incidence, the refractive indices of the glass plates (n_g).

Eq. (4) can be rearranged to:

$$r = \frac{E_r^-}{E_e^+} = \frac{m_{11} - \mu_e^{-1}.\mu_t.m_{22} + \mu_t.m_{12} - \mu_e^{-1}.m_{21}}{m_{11} + \mu_e^{-1}.\mu_t.m_{22} + \mu_t.m_{12} + \mu_e^{-1}.m_{21}} \tag{9}$$

As the reflection coefficient is given by $R = r^2$, we obtain for the transmission coefficient of non absorbing media :

$$T = 1 - R = 1 - r^2 = 1 - \left(E_r^-/E_e^+\right)^2 = \left(E_t^+/\ E_e^+\right)^2 \tag{10}$$

If the thickness of the constituent polymer and water layers d_ℓ and d_h as well as their absolute refractive indices n_ℓ and n_h are known, then by combining Eqs. (4) and (5) and (10), we obtain a relationship between the number of layers $(2k+1)$ and the transmission or the reflection coefficient. For normal incidence $i_j=0$, $\mu_j=n_j$ and $\mu_e=\mu_t=n_q$. Moreover, inserting the special phase shifts $\phi_{min}=(2k+1).\frac{\pi}{2}$ $(k=0,1,2...)$ or, with $k=0$ so that $n_j.d_j = \frac{1}{4}.\lambda_{min}$, into Eq. (5), we obtain :

$$m_{11} = m_{22} = 0$$

$$m_{12} = i^{(2k+1)}.\left(\frac{n_h}{n_\ell}\right)^k.n_\ell^{-1} \qquad m_{21} = i^{(2k+1)}.\left(\frac{n_\ell}{n_h}\right)^k.n_\ell \tag{11}$$

Substituting Eq. (11) into Eq. (9) gives :

$$r = \frac{n_q^2.m_{12} - m_{21}}{n_q^2.m_{12} + m_{21}} = \frac{n_q^2. - \mathbf{n}_{eff}^2}{n_q^2. + \mathbf{n}_{eff}^2} \tag{12}$$

Where :

$$\mathbf{n}_{eff}^2 = \left(\frac{n_\ell}{n_h}\right)^{2.k}.n_\ell^2$$

which is called the effective index of refraction at normal incidence of the light beam.

Combining Eqs. (12) and (10) we obtain, after some rearrangement :

$$n_{eff}^2 = n_q^2 \cdot \frac{1-r}{1+r} = n_q^2 \cdot \frac{2-T-2\sqrt{1-T}}{T} \qquad (13)$$

Hence, the number of layers will be equal to :

$$2k = ln \left(\frac{n_q^2}{n_\ell^2} \cdot \frac{2-T-2\sqrt{1-T}}{T} \right) \Big/ ln \left(\frac{n_\ell}{n_h} \right) \qquad (14)$$

An example is given in *Table 2.1*, where the transmission, calculated with the aid of Eq. (14), is given for various numbers of layers ($n_q = 1.52$, $n_\ell = 1.33$, $n_h = 1.47$). The values of the measured transmission must be corrected for the outer boundaries reflections (air/glass and glass/air); these (Fresnel) reflections [6] are given by $R_r = \left((n_q - 1)/(n_q + 1)\right)^2$

Table 2.1 Influence of Number of Layers on T_{min}.

$2k+1$	0	1	3	5	15	25	35	55	75
T_{min}	0.993	0.983	0.947	0.896	0.534	0.234	0.097	0.014	0.002

2.2.2. Rayleigh Scattering

The attenuation of a light beam which passes a scattering medium, is defined by Lambert-Beer's relation [6,11] :

$$S = - d_l^{-1} . ln\ T \qquad (15)$$

where S is the scattering coefficient, and d_l the optical path-length in the sample. In concentrated latices multiple scattering occurs. Penders [27] and Jansen [25] stated that turbidity is not very sensitive to multiple scattering and that multiple scattering only changes the angular distribution of the scattered intensity. Therefore the turbidity may be calculated from the scattering theory of single-scattered light. A lineair plot of $ln\ T$ versus path-length will not exclude the presence of multiple scattering, but demonstrates only that multiple scattering (according to Lambert-Beer's Eq. 15) is not important. *Figure 2.4* shows an experiment, where $ln\ T$ is given as function of path-length (film thickness) and wave-length (latex c9 table 2.III). This figure shows linear relations, which means that multiple scattering is not important.

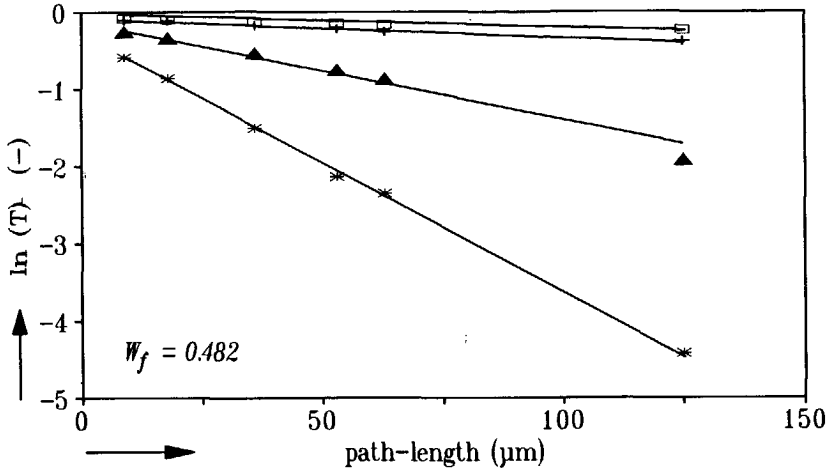

*Fig. 2.4 Influence of film-thickness/ wave-length on transmittance of latex (c9). □ = 700 nm, + = 600 nm, ▲ = 400 nm, * = 300 nm.*

Mie's theory yields a relationship between the scattering coefficient and the properties of a monodisperse sample of isotropic spherical particles [6,11-13]. For the conditions :

$$x < 0.8 \quad \text{and} \quad e_p > 3.r_p \tag{16}$$

where $x = 2.\pi.r_p/\lambda$

$2.e_p$ = interparticle distance

Mie's theory yields as a solution :

$$S = N_p.\pi.r_p^2.Q_{sca} \tag{17}$$

where $Q_{sca} = \frac{8}{3}.x^4.\left(\frac{m^2 - 1}{m^2 + 2}\right)^2$

$$N_p = \frac{V_f}{\frac{4}{3}.\pi.r_p^3} \quad (number\ of\ particles/m^3)$$

m = relative refractive index n_p/n_s

n_s = refractive index of solvent

On substituting Eq. (17) into Eq. (15) we obtain the well known Rayleigh scattering equation :

$$ln\ T_{model1} = \left[\frac{-32.\pi^4.r_p^3.V_f.d_l}{\lambda^4} \cdot \left[\frac{m^2-1}{m^2+2}\right]^2\right] \qquad (18)$$

This equation can only be used at low volume fractions of polymer particles, but the principle can also be applied at higher volume fractions. *Figure 2.5* shows a plot of $ln(\lambda)$ against $ln(-ln(T))$, which reveals the wave-length dependence of the overall transmission data of the latex c9 film (except for the interparticle interference minimum). The data are fitted with the least squares method and resulted in a slope of 4.0 ± 0.1. This means that the Rayleigh wave-length dependence to the power 4 can be used to describe the behaviour of this kind of latex.

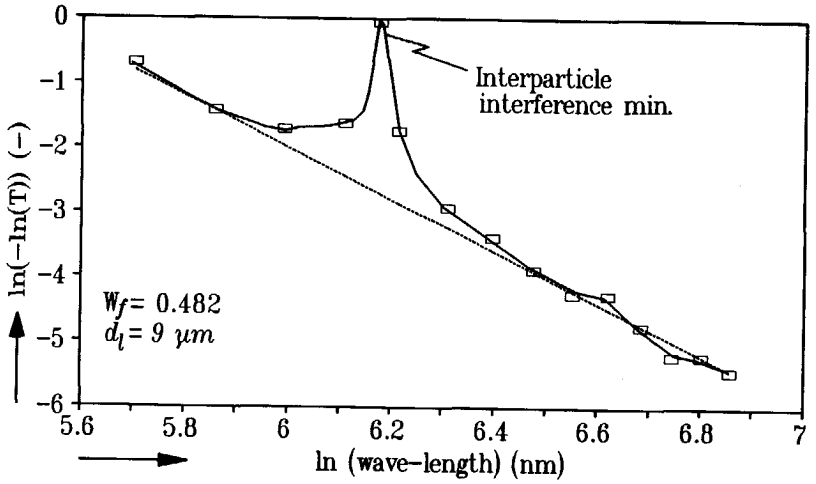

Fig. 2.5 Wave-length dependence of transmittance of thin latex(c9) films.
□ = *Experiment*, ···· = *Curve fit*

2.3. MODEL

The interference patterns are a consequence of the layered structure of the binder particles. The most common packing structures for regularly arranged spheres of uniform size are (*see Fig. 2.6*) : Hexagonal close packing (*h.c.p.*), face centered cubic packing

(*f.c.c.*), body centered cubic packing (*b.c.c.*), simple cubic packing (*s.c.p.*) and simple hexagonal packing (*s.h.p.*) with packing densities of 0.7405, 0.7405, 0.6802, 0.5236 and 0.6981 respectively [14,15]. The f.c.c. structure can be divided into two repeating units viz. hexagonal (*equal to h.c.p.*) and cubic packing.

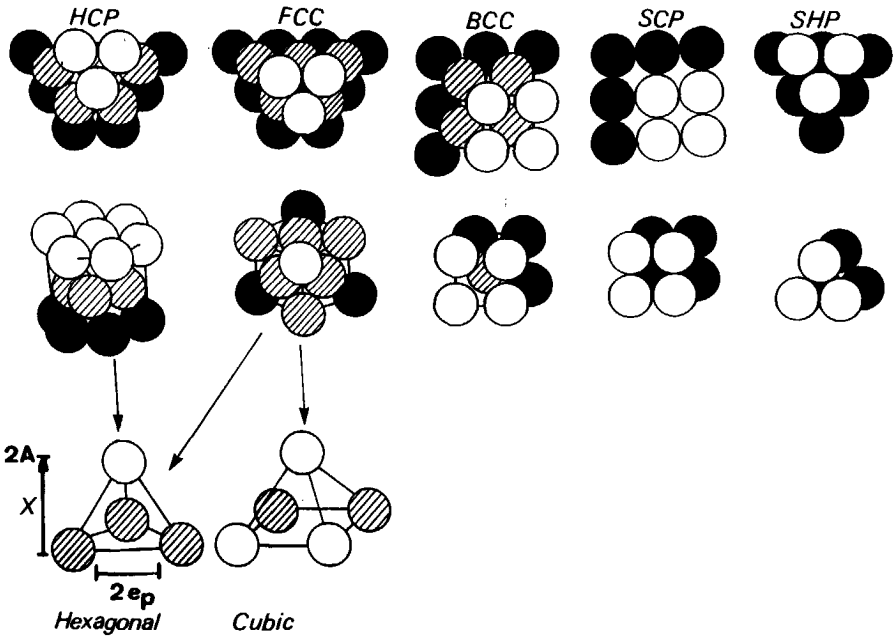

Fig. 2.6 Packing structures for regularly arranged spheres of uniform size.

2.3.1. The Particle Distance and Layer Distance

The relation between volume fraction (V_f), particle radius (r_p) and particle distance ($2.e_p$) is given by :

$$V_f = \frac{\pi . r_p^3}{C_1 . (r_p + e_p)^3} \tag{19}$$

where the geometric constant C_1 is given in *Table 2.II*, along with C_2 (Eq. 20) and C_3 (Eq. 25).

The experimental value of λ_{min} of the interference pattern depends on the optical layer thickness of the packing structure. So, λ_{min} is dependent on the distance between the sphere layers (A) perpendicular to the incident light beam (*Fig. 2.6*). For the

mentioned packing structures A will be given by :

$$A = C_2.(r_p + e_p) \tag{20}$$

where the geometric constant C_2 is given in *Table 2.II.*

Table 2.II Packing Structure Constants.

Structure	C_1	C_2	C_3
hexagonal	$3\sqrt{2}$	$\frac{1}{3}\sqrt{6}$	$2\sqrt{3}$
cubic	$3\sqrt{2}$	$\frac{1}{2}\sqrt{2}$	4
b.c.c.	3	$\frac{1}{2}$	4
s.c.p	6	1	4
s.h.p.	$4\frac{1}{2}$	$\frac{1}{2}\sqrt{3}$	$2\sqrt{3}$

2.3.2. The Average Refractive Index

For the calculation of λ_{min} with the aid of Eq. (3), the refractive index of the medium is needed. If we consider a system with N large molecules in a pure solvent, then it is usually assumed that the polarizability of the large molecules is related to the excess dielectric constant of the solution over that of the pure solvent (ε_{ps}), so that

$$(\varepsilon-\varepsilon_{ps}) = 4.\pi.\alpha_m.N/V = 4.\pi.\alpha_m.c \tag{21}$$

For dilute solutions, we obtain :

$$\alpha_m = \left(\frac{\delta\varepsilon}{\delta c}\right)/(4.\pi) \tag{22}$$

Since the optical dielectric constant ε is equal to the square of the solution refractive index, it is evident that n^2 is proportional to the polymer concentration. So that the average refractive index of a latex may be formulated as [10,32] :

$$n^2 = V_f.n_p^2 + (1 - V_f).n_s^2 = n_s^2 + V_f.(n_p^2 - n_s^2) \tag{23}$$

This solution, however, is only an approximation for high concentrations of polymer. Substituting Eqs. (19), (20) and (23) into Eq. (3), we obtain :

$$r_p = \frac{\left(\frac{1}{2} + k\right).\lambda_{min}}{2.C_2.\left(\frac{\pi}{C_1.V_f}\right)^{\frac{1}{3}}.n.\cos\left[\arcsin\left(\frac{\sin i_1}{n}\right)\right]} \tag{24}$$

The particle radius r_p can be calculated from λ_{min} and V_f for the different packing structures and the number of layers (Eq. (14), whereby in this case $\phi = \pi$ (k=0); $n_l/h_l = n_s/n_p$ and $T=T_{min}$) .

Because the wave-length of the light beam, at which interference occurs, is much bigger than the size of the polymer particles and the water interstices, the light beam will pass the latex film as it would be a homogeneous medium with small perturbations in optical density. These perturbations in a medium with a very regular structure can be viewed as a variation in refractive index alternating gradually between a relatively high and low value. A more sophisticated solution is needed to simulate the gradually alternating refractive index of the latex film. The basis of the solution is the value of the average refractive index (n_x) over the cross-section of the packing structure perpendicular to the incident light, in order to calculate λ_{min} and T_{min}. The volume fraction of spheres as function of the height x over a thickness Δx is given by (*see Fig. 2.6*) :

$$V_f(x,\Delta x) = \frac{\frac{1}{2}.\pi.\int_x^{x+\Delta x}\left(r_p^2 - x^2\right).dx}{\frac{1}{2}.C_3.\left(r_p + e_p\right)^2.\int_x^{x+\Delta x} dx} = \frac{\pi}{C_3.\left(r_p + e_p\right)^2}.\left(r_p^2 - x^2 - x\Delta x - \frac{1}{3}\Delta^2 x\right) \tag{25}$$

For the different structures the results for C_3 are given in *Table 2.II.* On letting Δx tend to zero, we obtain :

$$V_f(x) = \lim_{\Delta x \to 0} V_f(x,\Delta x) = \frac{\pi.\left(r_p^2 - x^2\right)}{C_3.\left(r_p + e_p\right)^2} \tag{26}$$

Substitution of Eq.(26) into Eq.(23) yields :

$$n_x^2 = n_s^2 + \frac{\pi.(r_p^2 - x^2)}{C_3.(r_p + e_p)^2}.(n_p^2 - n_s^2) \qquad (27)$$

Figure 2.7 shows the change of n_x across the hexagonal packing structure for various fractions (V_f). When this n_x-curve is approximated by two transitions in refractive index (two steps), then Eqs (3) and (12) can be used to calculate λ_{min} and T_{min}. However, when the n_x-curve is approximated by more transitions (multi steps), then the *n_x-curves* can be considered as representing a multilayered system. For each step the results need to be substituted in the interference matrix which will give the system transfer matrix over one layer Eq.(4). Then the transmission coefficient can be calculated from the multiplication of these system transfer matrices over the number of sphere layers. The calculations will be discussed in the section "Model results and discussions".

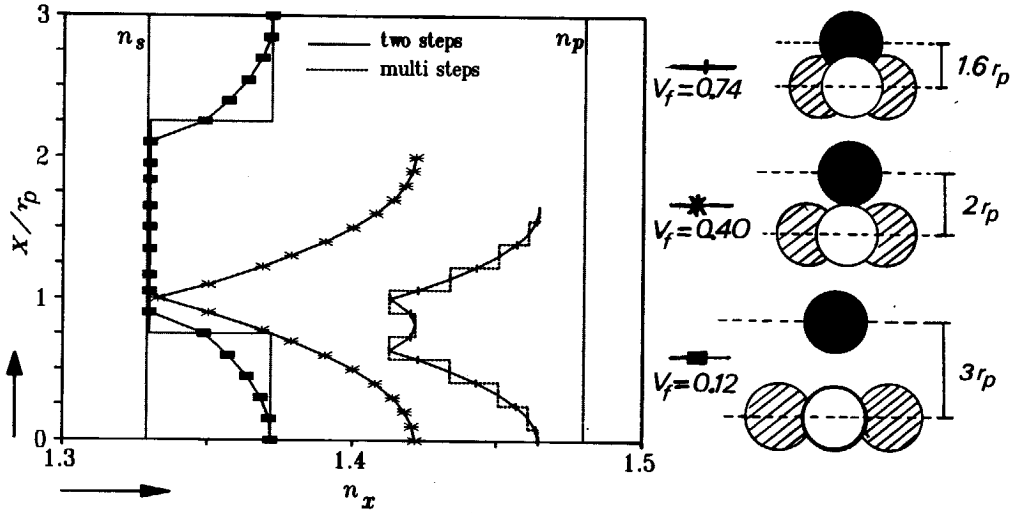

Fig. 2.7 Change of n_x over the hexagonal packing structure.

2.3.3. Rayleigh Scattering Models

In order to fit the experimental results with the Rayleigh scattering theory the following assumptions are made at high weight fractions: the water phase with polymer particles inverts into a polymer phase with water particles (inclusions), the number of inclusions is equal to the original number of particles (N_p) and the relative refraction index is defined as $m^* = n_s/n_p$.

We can distinguish two models, the first model is based on spherical inclusions with a characteristic radius corresponding to the length z in *Figure 2.8*, the second model is based on the projected area and perimeter, perpendicular to the incident light, of the water inclusions (*Fig. 2.9*).

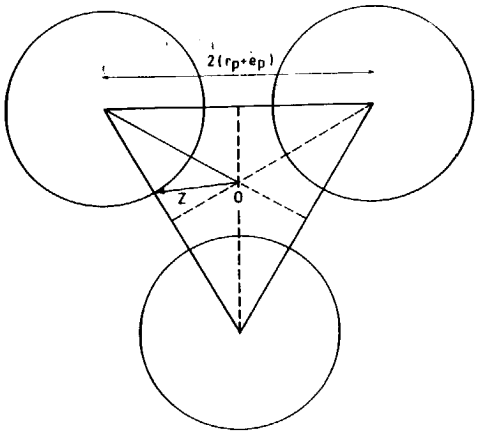

Fig. 2.8 The size (Z) of a water inclusion between three spheres.

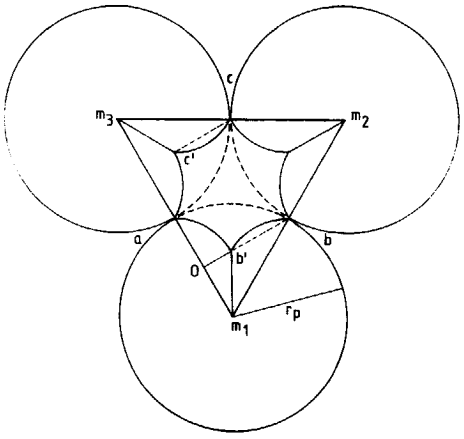

Fig. 2.9 Projection of a water inclusion in a hexagonal packing structure.

Model 1. The length z in *Fig. 2.8* is equal to :

$$z = \sqrt{\frac{1}{3}.(r_p + e_p)^2 + e_p^2} \tag{28}$$

This radius z seems to be arbitrarily chosen, but in comparison with experimental results it describes the transmission very well. Rewriting Eq.(17) with $r_p = z$ and $m = m^*$ and substituting this into Lambert-Beer's Eq. (15), we obtain :

$$ln\ T_{model1} = \left(\frac{-32.\pi^4.z^6.V_f.d_l}{r_p^3.\lambda^4} . \left(\frac{m^{*2}-1}{m^{*2}+2} \right)^2 \right) \tag{29}$$

The experimental results can be verified with a combination of the multilayer interference model and the Rayleigh scattering model (1). *Figure 2.10* shows the influence of volume fraction on the transmission spectra, calculated with these combined models. The change in refractive index over a sphere layer is approximated

with 20 steps. *Figure 2.10* shows :

a) the transmission increases, with increasing volume fraction of polymer because the size of the interstices decreases;

b) the transmission minimum shifts to a lower wave-length, because the interparticle distance decreases. The transmission minimum rises also, because the ratio between the maximum and minimum value of the alternating refractive index over the sphere layer decreases.

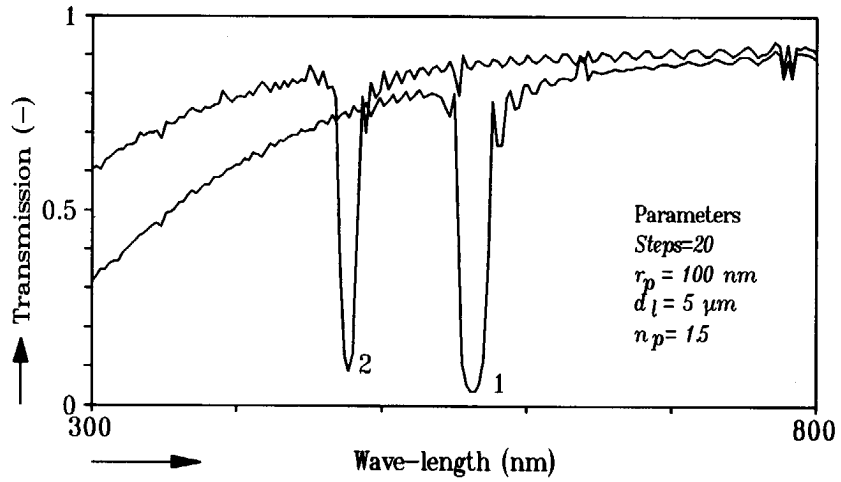

Fig. 2.10 Model calculations of transmission spectra.
1 - V_f = 0.40, 2 - V_f = 0.74.

Model 1 is based om the assumption that the water inclusions in the array of hexagonally packed latex particles are responsible for the scattering properties. The characteristic size z (Eq. 28) gives the effective size of the scatterer, but $^4/_3.\pi.z^3$ represents only $^1/_3$ of the total volume of water present in one inclusion. The Rayleigh-theory is based on the Lorentz-Eq. [12], where the polarizability of a scatterer depends on its volume. If the exact volume of the water inclusion is used, the theory does not describe the turbidity behaviour of the concentrated latex films. However, model 1 can describe the turbidity behaviour over a long range of concentrations.

Model 2, also based on eq. 17, where the scattering coefficient of spherical scatterers depends on the projected area ($\pi.r_p^2$) and the ratio of perimeter and wave-length ($2.\pi.r_p/\lambda$). This principle is applied to the water inclusions in an array of

hexagonally packed latex particles.

The triangular interstice between three spheres is given by "triangle" *abc* (*Fig. 2.9*). If a sphere is placed on top of these three spheres (hexagonally), this will give three interstices more. These interstices are congruent to triangle abc, however rotated around the axes m_1m_2, m_2m_3 or m_3m_1. The rotation factor is $1/3$, because the angle between the base $m_1m_2m_3$ and the sides of the pyramid is 70.5 degrees. In appendix *I* the calculations of perimeter and projected area are given. These calculations resulted in Eq. 30. The difference between model 1 and model 2 is very small and will be shown in the section Rayleigh Scattering models 2.5.3.

$$ln\ T_{model2} = \left(\frac{-2.A_i.\kappa_i^4.V_f.d_l}{\pi.r_p^3.\lambda^4} \cdot \left(\frac{m^{*2}-1}{m^{*2}+2} \right)^2 \right) \qquad (30)$$

where A_i is the area of the projected inclusion and κ_i the primeter.

2.4. EXPERIMENTAL

Thin latex layers of various thicknesses were obtained by fixation of the latex between two plane parallel quartz plates, separated by a spacer. The thickness of the spacer could be varied between 6 and 55 μm. The influence of weight fraction of binder, film thickness, particle size and particle size distribution and angle of incidence on the interference patterns were investigated.

2.4.1. Materials

The latices (*see Table 2.III*) were synthesized by DSM Resins Holland. The disperse phase of the c-series consists of copolymers and terpolymers of butyl acrylate (*BA*), methyl methacrylate (*MMA*) and methacrylic acid (*MAA*) in various compositions, whereas the copolymer in the ps1 latex consists of styrene and styrene sulfonic acid.

Most latices are stabilized by either sodium dodecyl benzene sulfonate (*SDBS*) or nonylphenol26 ethylene oxide (*NF26eo*). Dispersions c3 & ps1 are free of stabilizer (the emulsifier was kindly removed by Dr. R. Struis, State University Leiden, The Netherlands). The polymerizations were initiated by potassium peroxydisulfate. The composition and physical parameters of the latices are given in *Table 2.III*.

Table 2.III Composition and Physical Properties of the Latices.

Latex	*c4*	*c5*	*c8*	*c9*	*c10*	*c3*	*ps1*
MMA/BA/MAA (wt%)	*48/50/2*	*48/50/2*	*48/50/2*	*10/90/0*	*74/24/2*	*95/0/5*	---
SDBS	*0.4*	*0*	*0.4*	*1.0*	*0*	*0*	*0*
NF26eo	*0*	*0.7*	*0*	*0*	*0.9*	*0*	*0*
W_f*(-)*	*0.494*	*0.482*	*0.497*	*0.502*	*0.504*	---	---
pH	*2.2*	*2.1*	*2.3*	*2.1*	*2.6*	---	---
M.F.F.T. (^oC)	*14*	*14*	*12*	---	---	---	---
η *(mPa.s)*	*330*	*30*	*30*	*60*	*30*	---	---
r_p*(Malvern) (nm)*	*70*	*122*	*110*	*99*	*157*	*76*	*64*
T_g (^oC)	*7*	*7*	*7*	*-45*	*50*	*>100*	*>100*
ρ *(kg/m)*	*1120*	*1120*	*1120*	*1060*	*1153*	*1210*	*1045*
n_p	*1.482*	*1.482*	*1.482*	*1.477*	*1.486*	*1.490*	*1.60*

W_f = Weight fraction polymer; pH = -Log [H^+], M.F.F.T. = Minimal Film Formation Temperature; η = Viscosity latex; T_g = Glass transition temperature of the polymer; ρ = Density polymer; n_p = Refractive index polymer.

2.4.2. Influence of Weight Fraction on Transmission

Figures 2.11 and *2.12* show the influence of polymer weight fraction on the transmission spectrum. The transmission spectra are shown for a large number of samples of constant thickness (55 μm) and composed of latices c9 (*Fig. 2.11*) and c10 (*Fig. 2.12*). At first the transmission decreases with increasing polymer weight fraction (*Figs. 2.11a/2.12a*), but at a certain weight fraction the transmission increases again (*Figs. 2.11b/2.12b*). The initial decrease of the transmission can be explained by the increase of the scattering area with increasing polymer concentration. During the drying process phase inversion takes place, so that water becomes the dispersed phase. The simultaneous increase of the transmission is a result of the decrease of scattering area with decreasing water content.

From *Figs. (2.11b-8,9)* and *(2.12b-10,11)* it is clear that the interference is increasing. This is the consequence of a better arrangement of the polymer particles. An increasing weight fraction of polymer causes the transmission minimum to be shifted to lower wave-lengths (*Figs. 2.11c/2.12c*), as a consequence of the closer packing structure of the particles.

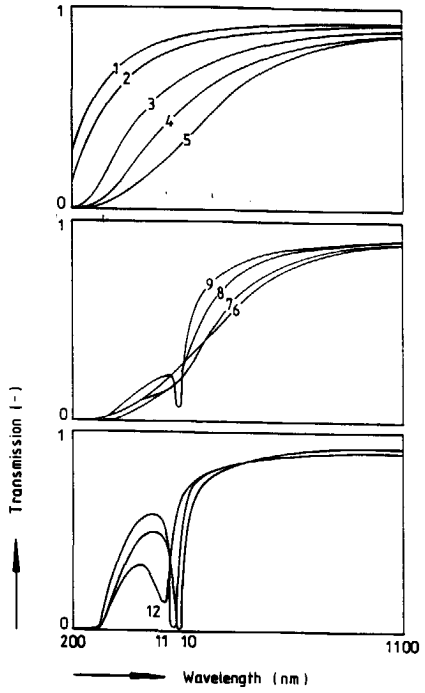

Fig. 2.11 Influence of W_f on the transmission spectrum of latex (c9): (a) 1=0.006, 2=0.010, 3=0.026, 4=0.054, 5=0.103; (b) 6=0.173, 7=0.285, 8=0.382, 9=0.430; (c) 10=0.475, 11=0.516, 12=0.587.

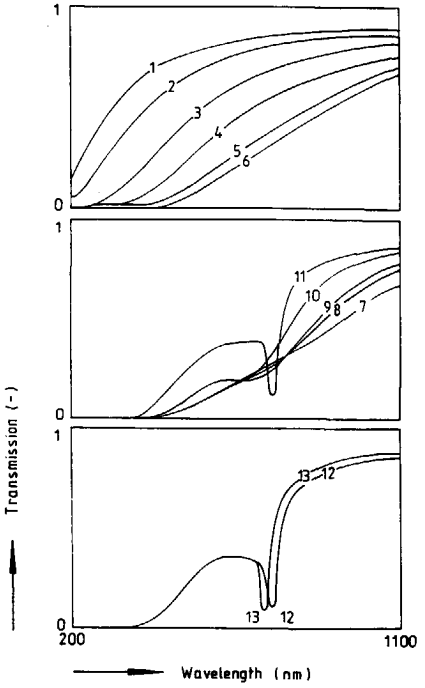

Fig. 2.12 Influence of W_f on the transmission spectrum of latex (c10): (a) 1=0.006, 2=0.011, 3=0.025, 4=0.054, 5=0.109, 6=0.162; (b) 7=0.217, 8=0.327, 9=0.382, 10=0.490, 11=0.540; (c) 12=0.546, 13=0.588.

2.4.3. Influence of Weight Fraction on λ_{min}

Fig. 2.13 demonstrates the influence of the polymer weight fraction on λ_{min}. In latices containing an emulsifier, a transmission minimum only appears at high weight fractions, in latices without emulsifier, however, it appears already at low weight fractions. Apparently the emulsifier shields off the electric double layer around the particles, so that a stable packing structure can be achieved only if the particles are forced to pack together, e.g., due to a high weight fraction. In the absence of an emulsifier the double layer will be relatively large [1], because of the highly charged surface of the polymer particles, due to the SO_4^- end groups of the polymer. As a result of the electrostatic repulsions, which are extended to several particle diameters, the

particles will be forced into a regular packing structure at much lower weight fractions. This is in agreement with measurements by Hiltner et al [2], who reported closely packed structures for weight fractions of *1 %*.

It also appears that λ_{min} strongly increases with particle size, hence, measurement of λ_{min} provides a method to determine the size of the particles.

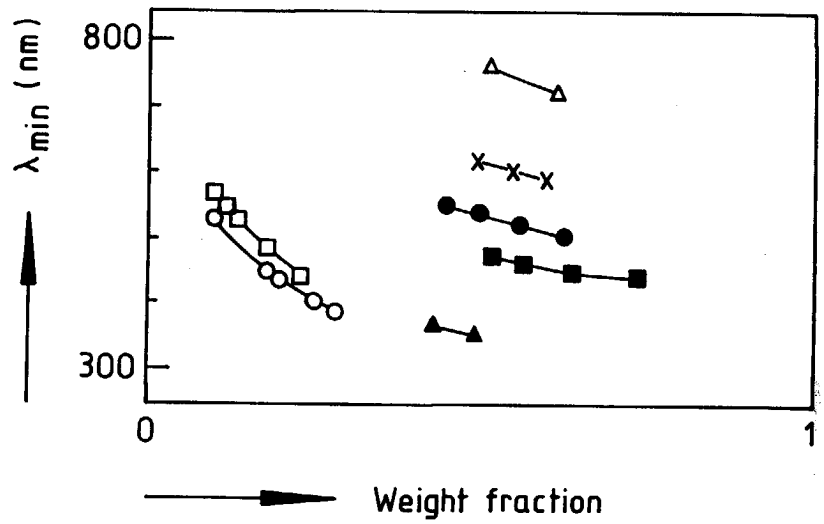

Fig. 2.13 Influence of W_f on λ_{min} : ▲ = c4, x = c5, ● = c8, ■ = c9, Δ = c10, □ = c3, O = ps1.

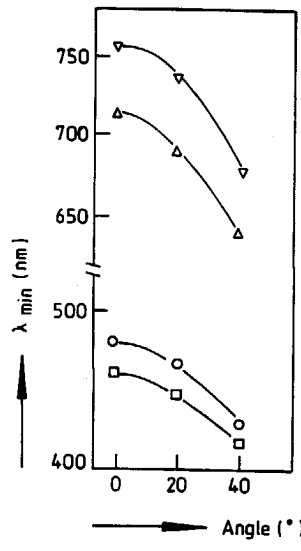

2.4.4. Influence of Angle of Incidence on λ_{min}

Figure 2.14 shows the angle of incidence of the light beam on λ_{min}. With increasing angle of incidence λ_{min} decreases (just as can be expected for an interference filter). This effect arises from the decrease in optical path length difference in the packing structure.

Fig. 2.14 Influence of the angle of incidence on λ_{min}:
Latex c10 ▽-W_f=0.51, Δ-W_f=0.61
Latex c9 O-W_f =0.52, □-W_f=0.56

2.4.5. Influence of Film Thickness on the Interference Pattern

Figure 2.15 demonstrates the influence of the layer thickness of the latex on the interference. The film thickness, which varied from 6 to 25 μm, has hardly any effect on λ_{min}, but a tremendous effect on the overall transmission and on T_{min}. With increasing film thickness the transmission and T_{min} decrease, which is due to the increase of the number of particles in the optical path, and to the increase of the number of regular particle layers.

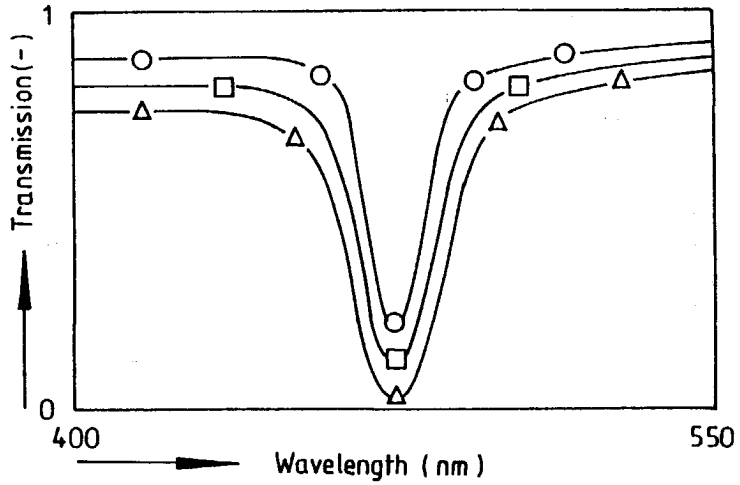

Fig. 2.15 Influence of film thickness on transmission spectrum of latex (c9) with : $W_f = 0.50$, o= 6 μm, □ = 12 μm, Δ = 25 μm.

2.4.6. Influence of Particle Distribution on the Interference Pattern

Figure 2.16 illustrates the influence of a binary particle size distribution on the interference pattern. The distributions were obtained by mixing latices c9 (r_p= *99 nm*) and c10 (r_p= *157 nm*) up to a particle number fraction of latex c10 of 0.048. The figure shows that the interference effect decreases and even disappears when the number fraction exceeds 5 %. This dramatic effect is due to the destructive effect on the packing structure by larger particles. The conclusion is that it might be possible to determine the particle size distribution from the interference pattern. However, more experiments are needed to find a useful relationship for such determinations. In any case, the extinction of the interference pattern might be used to determine the time needed for coalescence of the particles in a continuous drying experiment.

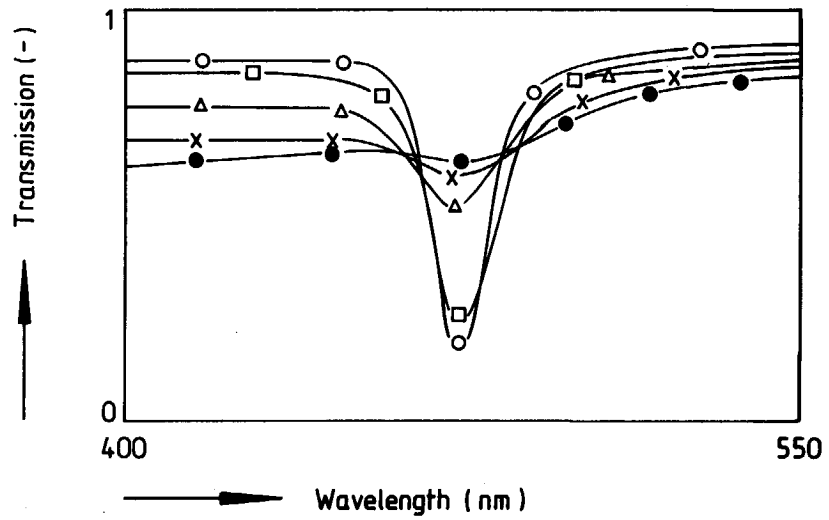

Fig. 2.16 Influence of a binary particle size distribution on the transmission spectrum. Particle number fraction (c10/c9): o = *0,* □ = *0.003,* Δ = *0.010,* x = *0.022,* • = *0.048.*

2.5. MODEL RESULTS AND DISCUSSIONS

2.5.1. The Particle Size

The particle sizes calculated from λ_{min} and their weight fraction, are shown in *Table 2.IV.* The calculated particle size depends strongly on the packing structure. Calculations have shown that the weight fraction does not affect the calculated particle radius.

In order to determine the packing structure of the samples, the calculated particle sizes are compared with the results of other particle size measuring and imaging techniques. The particle sizes calculated with the two step model and the multi step model are almost equal. *SEM* and *TEM* measurements can be performed only on latices with a high T_g. The *SEM* picture of latex c10 (*Fig. 2.17*) shows a very dense hexagonal like structure. The particle sizes according to hexagonal, *s.c.p.* and *s.h.p.* are close to the *SEM* and *TEM* results.

The particle sizes according to *QELS* depend on the absorbed water layer around the particle. The particle sizes of the hydrophilic acrylic particles, measured with *QELS* will have larger values compared to those measured with *SEM* and *TEM*, but in the case of the hydrophobic polystyrene particles they will have the same values.

Pore volume measurements on dried acrylic latex films with a high T_g showed a pore volume fraction of about 0.25. This is a value expected for hexagonal or cubic packing. On the one hand we came to the conclusion that the packing structure could be hexagonal, *s.c.p.* or *s.h.p.* and on the other hand hexagonal or cubic. Hence, it is not unrealistic to conclude that the packing structure of the drying dispersion is hexagonal, which can be *f.c.c.* or *h.c.p.* (*see Fig. 2.6*). In the following sections of model results this hexagonal packing is used in the calculations.

Table 2.IV Particle Sizes (nm) Determined with Different Techniques

Analysis technique	Latices						
	c4	c5	c8	c9	c10	c3	ps1
QELS-Malvern	70	122	110	99	157	76	--
Coulter	--	--	--	95	152	72	64
SF_3	--	--	--	--	138	--	--
TEM	--	--	--	--	125	59	58
SEM	--	--	--	--	139	--	64
Interference							
hexagonal	66	117	101	90	142	62	59
cubic	76	134	116	04	163	74	71
b.c.c.	97	170	147	33	207	93	88
s.c.p.	61	107	93	83	130	58	56
s.h.p.	63	112	97	86	135	59	56

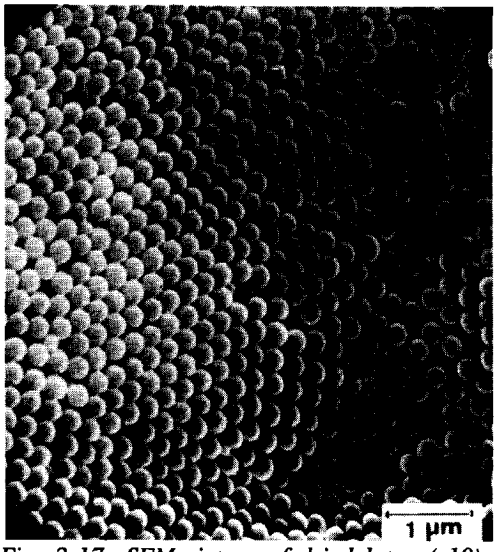

Fig. 2.17 SEM-picture of dried latex (c10).

2.5.2. Interparticle Interference

Influence of film thickness on transmission. From the transmission minimum the number of regularly packed layers of spheres can be calculated. In the model where the film is built up of lamellae of alternatively high and low refractive indices the number of layers is K_{lp} (Eq. 14), whereas in the model where the film is built up of a continuous phase with a periodically changing refractive index the number of layers is K_{cp}. The maximum possible number of layers is given by K_{max}, which is equal to the film thickness divided by the structure length (A) (Eq. 20). *Table 2.V* shows the results of K_{lp} and K_{cp} for the latices c9 and c10. The value of T_{min} is corrected for Rayleigh scattering and for regular reflections at the glass/air boundaries.

Table 2.V Number of Regularly Packed Sphere Layers

	Experimental			Multilayer		
Latex	d_l (μm)	λ_{min} (nm)	T_{min}	K_{max}	K_{lp}	K_{cp}
C9*	6	474	0.228	35	20	36
	12	474	0.132	71	24	44
	25	480	0.007	149	47	84
C10**	6	758	0.615	22	9	14
	12	758	0.322	44	12	20
	25	755	0.297	92	13	22

* *Latex C9* $W_f = 0.516$ $r_p = 90$ *nm;* ** *Latex C10* $W_f = 0.508$ $r_p = 142$ *nm.*

The number of layers K_{lp}, calculated with Eq. 14, is always smaller than K_{cp} as a consequence of the bigger difference in refractive indices. The number of regular layers increases with increasing film thickness, but not as much as the relative increase of K_{max}, which is proportional to the film thickness. Microscopic observations have shown that the regular layers start to build up from the glass interfaces. The maximal thickness of these regular sphere layers (K_{cp}) at the glass interfaces is about 7 and 3 μm for latices c9 and c10 respectively. This is in agreement with measurements by Luck et al [3], who report regular layers of about 6.6 μm for a 20 μm film. For thin films (6 μm) of latex c9 the number of layers K_{cp} is equal to the experimental value (K_{max}). The calculated number of layers reaches a maximum value for high film thicknesses. This means that the interference is only caused by the regular packed sphere layers close to the glass interface. The differences between K_{max} and K_{cp} depend on the particle size distribution (*see Fig. 2.16*) and the balance between the

attractive and electrostatically repulsive forces between the particles.

Influence of angle of incidence on λ_{min}. The theory predicts that λ_{min} depends on the angle of incidence and is proportional to *cos i (Eq. 3)*. The experiments also show (*see Fig. 2.14*) that λ_{min} decreases with increasing angle of incidence. The agreement between experiments and the model for the dependence on the angle of incidence is extremely good, see *Table 2.VI.*

Tabel 2.VI Influence of Angle of Incidence on λ_{min}.

Latex	Angle (degree)	λ_{min}(exp.) (nm)	λ_{min}(calculated) (nm)
c9*	0	476	478
	20	463	462
	40	428	426
c9**	0	458	458
	20	445	445
	40	412	409
c10+	0	753	756
	20	734	733
	40	676	674
c10++	0	717	720
	20	693	697
	40	639	640

* *Latex c9* $W_f = 0.516$; ** *Latex c9* $W_f = 0.561$; + *Latex c10* $W_f = 0.508$; ++ *Latex c10* $W_f = 0.610$.

2.5.3. Rayleigh Scattering Models

Comparisons of the results of the calculations of the Rayleigh-scattering, (Eqs. (18), (29) and (30)), and the experimental results are shown in *Figs. 2.18* and *2.19.* The transmission in these figures is adjusted for the glass/air interfaces and multilayer interference, so that the transmission is given by :

$$T = T_{scattering} * T_{interference} * T_{fresnel} \tag{31}$$

The experimental results for the latices c9 and c10 are in good agreement with Eq. (18) for $W_f \leq 0.10$ (*Figs. 2.18a and 2.19a*), whereas for $W_f \geq 0.30$ they are in good agreement with Eqs. (29) and (30) (*Figs. 2.18b and 2.19b*).

Apart from the important role of the interference in the transmission spectrum for volume fractions 0.528 and 0.588, Eqs. (29) and (30) still give an accurate description

of the scattering behaviour of the latex (*Figs. 2.18c and 2.19c*). It is surprising that Eq. (18) yields a relatively good fit to the experimental data, as this equation is only valid for $x<0.8$ (Eq. (19)), so for values of V_f smaller than 0.05. Eqs. (29) and (30), for water inclusions, are also valid only for $x<0.8$, which in this case means, volume fraction larger than 0.78. The ratio K_{lp}/K_{max} used in *Figs. 2.18c and 2.19c* are 0.2 and 0.16 respectively for 55 μm latex films.

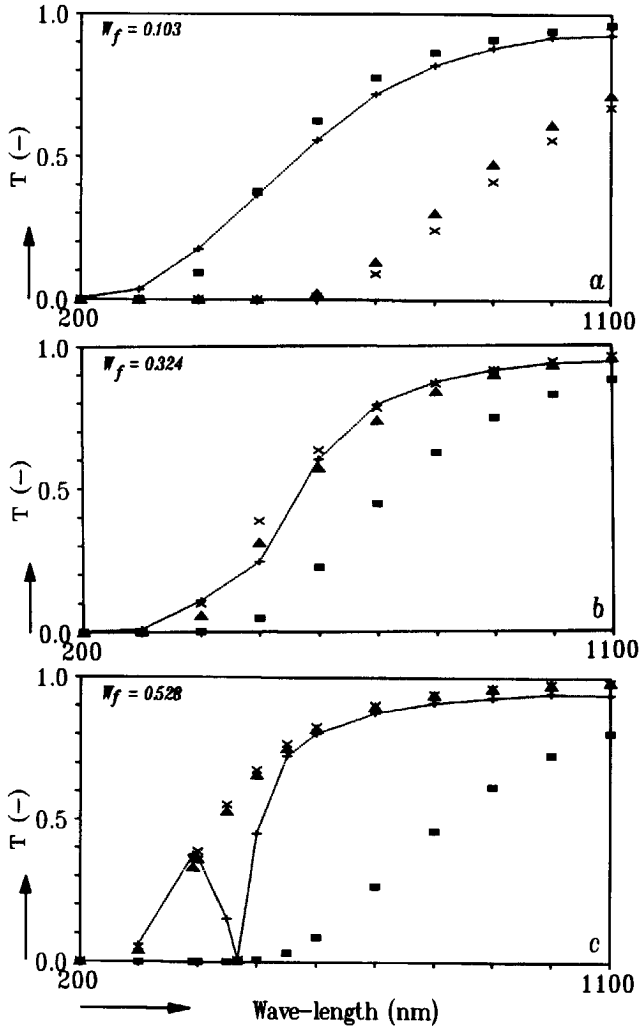

Fig. 2.18 Transmission spectra of latex (c9) compared with the Rayleigh scattering models

+ = Experimental, ■ = Ray.Scat.(Eq.[18]), ▲ = Model 1, x= Model 2.

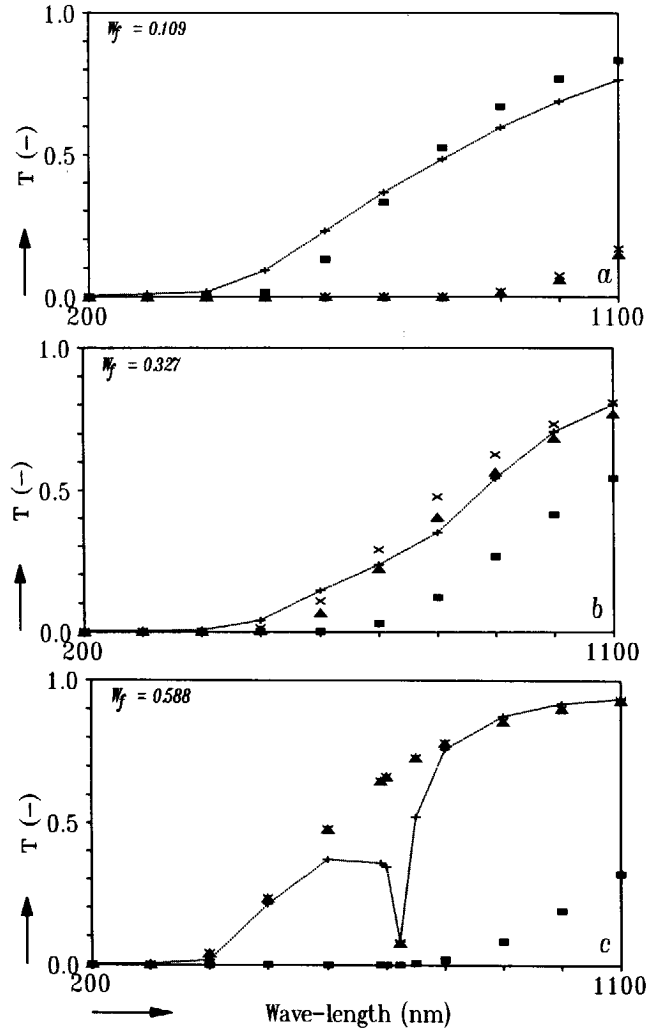

Fig. 2.19 Transmission spectra of latex (c10) compared with the Rayleigh scattering models

+ = Experimental, ■ = Ray.Scat.(Eq.[18]), ▲ = Model 1, x= Model 2.

2.6 CONCLUSIONS

The multilayer interference theory provides a method to characterize the geometrical parameters of the particles in a drying latex film. Besides λ_{min} and T_{min} the model only makes use of the physical parameters of the latex to calculate the particle

diameter and packing structure of the concentrated acrylic latex films.

The scattering behaviour of concentrated latices can be described with the "inverse" Rayleigh scattering equation based on the water inclusions in the packing structure. This empirical relation can be used to characterize the size of the water inclusions between the binder particles.

The interference pattern is very sensitive to the particle size distribution. The fading of the interference pattern can be used in drying experiments to find the time of flocculation or coalescence of the particles, because this disrupts the regular packing of sphere layers (Chapter 3). The calculated particle sizes for a hexagonal structure are in agreement with the results of *SEM* and *TEM* measurements.

The dependence of λ_{min} on the angle of incidence agrees extremely well with the model calculations.

The light scattering and multilayer interference theories give a good description of the behaviour of the internal displacements of polymer particles in concentrated acrylic latex films. This theory can be used to describe, from the change in the transmission spectrum, the film formation mechanism of a drying and ageing latex film.

References

1 Hiltner, P.A., Krieger, I.M., *J. Phys. Chem.* **73**, 2386 (1969).
2 Hiltner, P.A., Papir, Y.S., Krieger, I.M., *J. Phys. Chem.* **75**, 1881 (1971)
3 Luck, W, Klier, M., Wesslau, H., *Ber. Bunsen-Ges. Phys. Chem.* **67**, 75 and 84 (1963)
4 Dahmeke Barton, E, "Measurement of Suspended Particles by Quasi Elastic Light Scattering." Wiley, New York, 1983.
5 van Tent, A., te Nijenhuis, K., *in* "Proceedings XVIIth International Conference in Organic Coatings Science and Technology, Luzern, Switzerland, 1991," p. 317.
6 Kortüm, G.,"Reflexions-Spektroskopie." Springer-Verlag, Berlin, 1969.
7 Martin, L.C.,"Technical Optics." Sir Isaac Pitman, London, 1966.
8 Knittl, Z., "Optics of Thin Films." Wiley, London, 1976.
9 Levi, L., "Applied Optics," Vol. 2. Wiley, New York, 1980.
10 Born, M, "Principles of Optics, Electromagnetic Theory of Propagation, Interferenc and Diffraction of Light." Pergamon Press, Oxford, 1975.
11 van de Hulst, H.C., "Multiple Light Scattering." Academic Press, Amsterdam, 1980.
12 van de Hulst, H.C., "Light Scattering by Small Particles." Wiley, New York, 1957.
13 van de Hulst, H.C., "Optics of Spherical Particles." Duwaer & Sons, Amsterdam, 1946.
14 Tsimboukis, D.G., *Adv. Org. Coat. Sci. Technol. Ser.*, **4**, 189 (1982).
15 Atkins, P.W., "Physical Chemistry " Oxford Univ. Press, London, Second Ed., 1983.
16 Heller, W, Vassy, E., *J. Chem. Phys.* **14**, 565 & 566 (1946).
17 La Mer, V.K., *J. Phys. Colloid Chem.* **52**, 65 (1948).
18 Sinclair, D., La Mer, V.K., *Chem. Rev.* **44**, 245 (1949)
19 Kogelnik, H., *Bell Syst. Tech. J.* **18**, 2909 (1969).
20 Ottewill, R.H., *Prog. Colloid Polym. Sci.* **67**, 71 (1980).
21 Furusawa, K, Tobori, N., *J. Chem. Soc., Faraday Trans.* **84**, 4397 (1988).
22 Bragg, W.H., "The Crystalline State." Bell, London, 1933.
23 Vrij, A., Nieuwenhuis, E.A., Fijnaut, H.M., Agterof, W.G.M., *Colloid Stability,*

Faraday Discuss. Chem. Soc. **65**, 101 (1978).
24 Fijnaut, H.M., Pathmamanoharan, C., Nieuwenhuis, E.A., Vrij, A., *Chem. Phys. Lett.* **59**, 351 (1978).
25 Jansen, J.W., de Kruif, C.G., Vrij, A., *J. Colloid Interface Sci*, **114**, 492 (1986)
26 Philipse, A.P., Vrij, A.,*J. Chem. Phys.* **88**, 6459 (1988).
27 Penders, M.H.G.M., Vrij. A., *J. Chem. Phys.* **93**, 3704 (1990).
28 Gaylor, K., Snook, I., van Meggen, W., *J. Chem. Phys.* **75**, 1682 (1981).
29 Kubota, K., Hayashi, S., Mandai, H., *J. Colloid Polym. Sci.* **98**, 579 (1984).
30 Eliçabe, G.E., Garcia-Rubio, L.H., *J. Colloid Polym. Sci.* **129**, 192 (1989).
31 Broide, M.L., Cohen, R.J., *Phys. Rev. Lett.* **64**, 2026 (1990).
32 Berne, B.J., "Dynamic Light Scattering." Wiley, New York, 1976.

CHAPTER 3

THE FILM FORMATION PROCESS OF DRYING THIN FILMS OF ACRYLIC LATICES.

In this chapter the changing interparticle interference patterns during the drying process of latex films are investigated. These patterns are verified with the multilayer interference theory, described in chapter 2. This results in detailed information about the regularity of the interparticle structure during the drying process of the latex film, the critical interparticle distance at which the flocculation process is initiated and the size of the stabilizer layer around the latex particles. These measurements give a good description of the behaviour of the latex particles during the process of film formation of a latex film.

3.1. INTRODUCTION

The process of film formation of an acrylic latex film can be divided into six stages [1-4] (*Fig. 3.1*).

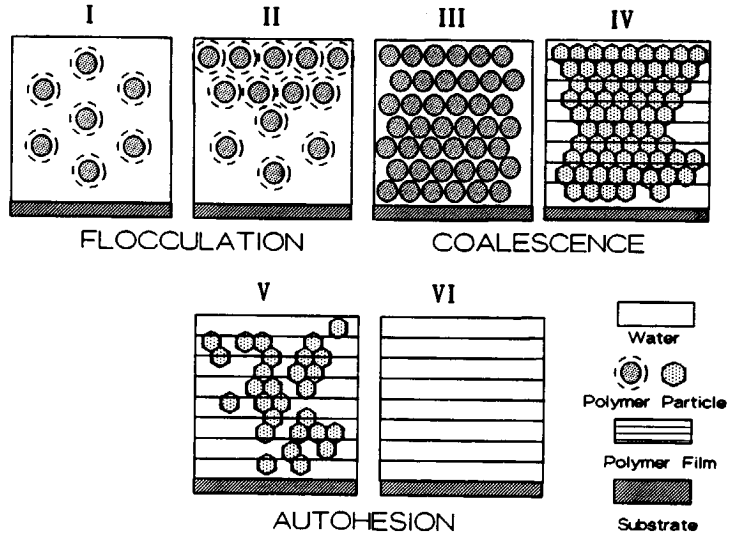

Fig. 3.1 Typical film formation behaviour of drying acrylic latices.

The first four stages describe the process of flocculation and coalescence and the last two stages describe the process of autohesion.

I: Evaporation of water from the bulk causes uniform shrinkage of the interparticle distance.

II: Percolation of water between the flocculated particles near the air/latex interface and eventually evaporation of water at the air/latex surface.

III: Dense packing of particles.

IV: Evaporation of water from the formed interstices between the densely packed immobile particles causes the particles to deform into a polyhedric structure;

V: Diffusion of water through the closed polymer film and autohesion of polymer particles (the particles lose there identity);

VI: Homogeneous polymer film.

The process of flocculation and coalescence of a drying acrylic latex film consists of the first four stages of *Fig. 3.1*. For drying temperatures above the Minimal Film Formation Temperature (*MFFT*) it was found that the latex particles deformed into a polyhedric structure but at drying temperatures far below the *MFFT* the latex particles did not deform and the remaining interstices were filled with air. These first four stages can be followed clearly from the changing transmission spectrum of a drying latex film. Examples of such experiments are shown in *Figs. 3.2* to *3.6*, where latex B4 films are dried below and above its *MFFT* (*see Table 3.1)*.

Figure 3.2 - The water evaporates from the bulk, resulting in an isotropic decrease of the interparticle distance (*stage I*). The shift of the interparticle interference minimum (λ_{min}, *spectra* $1 \longrightarrow 4$) is related to the decrease of the interparticle distance.

For the calculation of the interparticle distances in a drying latex film only the changes of λ_{min} are required, assuming that the latex particles are ideally packed (Chapters 2). But this is hardly the case when a latex film is just applicated to the glass surface. As a consequence of the evaporation of water at the air-latex surface a concentration difference develops across the latex film. It is possible to simulate these concentration differences with the multilayer interference model by, for instance, a slow increase of the interparticle distances across the latex film. The results of these simulations are shown in section *3.3.1b.*

Figure 3.3 - More evaporation of water causes the particles in the latex film to flocculate (*stage II)*. The transmission spectrum has now two minima, because the interparticle distance in the flocculated state is smaller than that in the dispersed state. From these λ_{min} values the interparticle distances can be calculated for the

dispersed state just before flocculation and in flocculated state (*see section 3.3.2).* The intensity of the lowest λ_{min} increases when the drying time advances, due to the evaporation of water the flocculated state is building up from the surface *(spectra 1 ⟶ 6).*

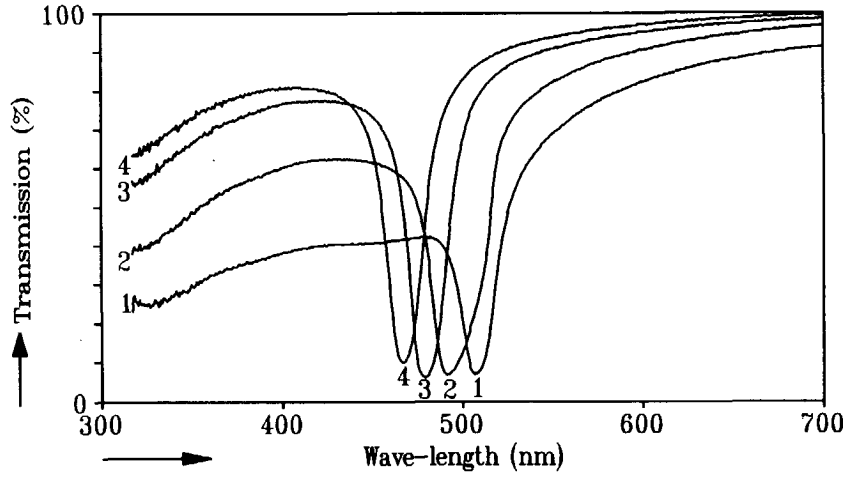

Fig. 3.2 Turbidity behaviour of a drying latex B4 film during the first stage of the film formation process.

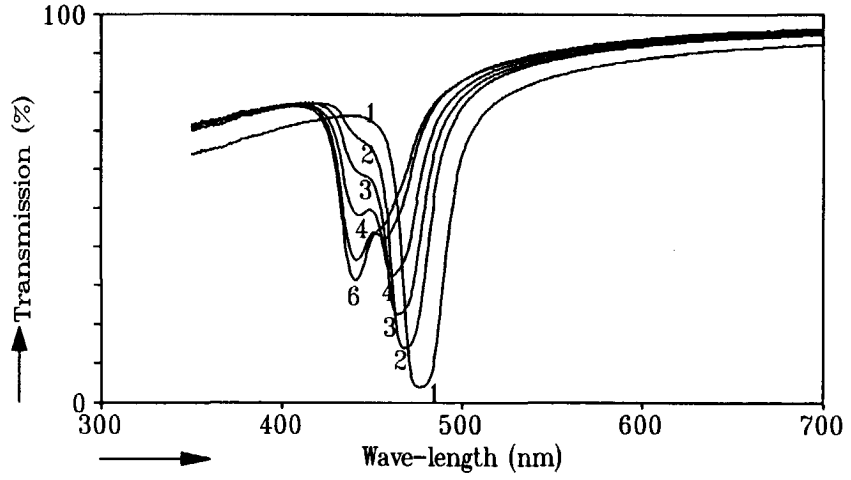

Fig. 3.3 Turbidity behaviour of a drying latex B4 film during the second stage of the film formation process.

Figure 3.4 - All particles are now flocculated *(spectrum 1, stage III)*, resulting in hexagonally closely packed latex particles. Because the latex is dried below the *MFFT* the latex particles can not deform, so that the interparticle distance stays constant when more water evaporates. This means that λ_{min} stays at the same wave-length (spectra 1 $\longrightarrow$ 6), where the value of λ_{min} *(444 nm)* corresponds to an interparticle distance of zero. In this stage the overall transmission decreases very fast due to the evaporation of water from the inclusions between the particles, by which air inclusions remain behind. The dried latex, that remains, looks like a crumbly/powder-like film.

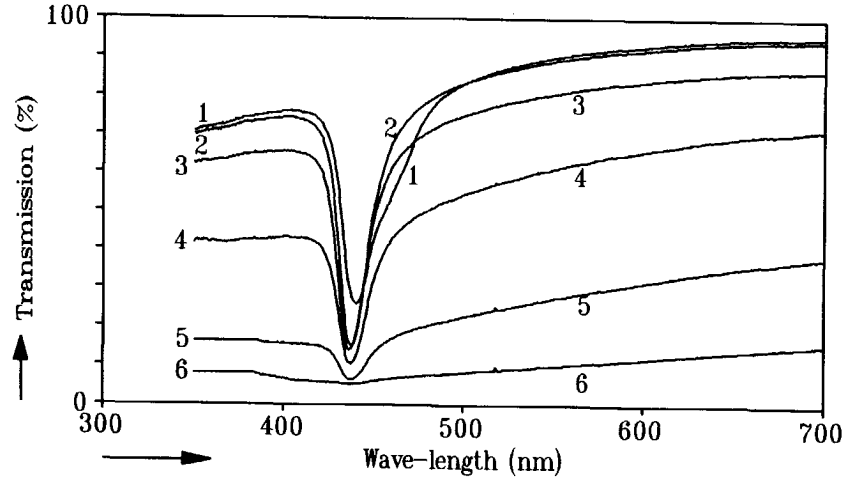

Fig. 3.4 Turbidity behaviour of a drying latex B4 film at a drying temperature below the MFFT.

Figure 3.5 - When this same latex is dried just below the *MFFT*, latex coalescence is initiated, so that λ_{min} decreases, when more water evaporates. However, when λ_{min} has reached a value of 370 nm *(spectrum 4)* the transmission drops *(spectrum 5)* and the λ_{min} does not change any more. This means that the deformation of the latex particles stops, because at this point the forces of resistance of particle deformation become bigger than the capillary forces. From the last value of λ_{min} it is possible to estimate how far the coalescence process has been progressed. Measuring this last λ_{min} as function of temperature reveals the elastic properties of the latex particles as function of temperature *(see chapter 4)*. The transmission decreases because the remaining interstices are filled with air. The overall transmission is higher than in the previous case, because the size of the air filled interstices are smaller.

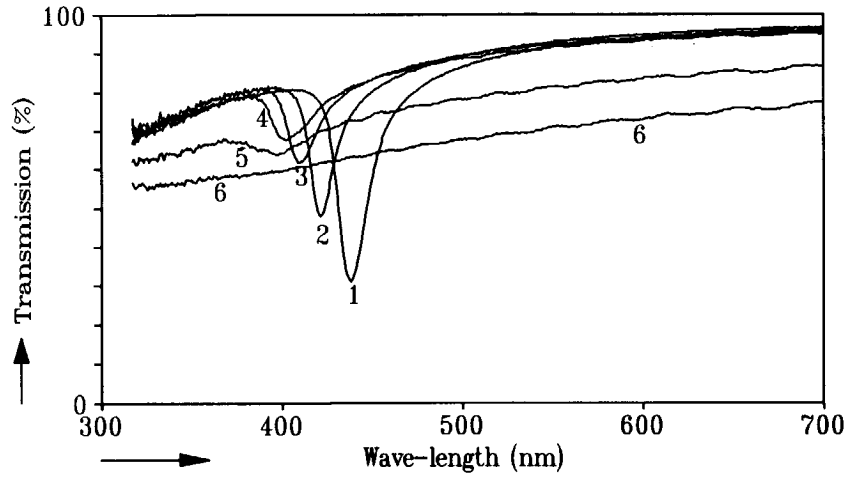

Fig. 3.5 Turbidity behaviour of a drying latex B4 film at a drying temperature just below the MFFT.

Figure 3.6 - At temperatures above the *MFFT* the latex particles can deform completely, so that the interparticle distance decreases further when more water evaporates (*spectra 1 → 6, stage IV*)). Thus when the particles make contact and deform, the changing interparticle interference patterns reveal the deformation time and the magnitude of the deformation. This behaviour reveals the deformation mechanism of the latex particles (*see chapter 4*). These results can be used to determine and improve the mechanisms that describe the process of coalescence.

The latex becomes transparent because the interstices disappear or become so small that they hardly scatter any light in the *UV-Vis* spectrum range. When this transparent latex film is immersed in a *0.1 N HCl* solution, the remaining internal interfacial boundaries will swell. This regenerates an interference pattern, which must be related to the size and number of the swollen interfaces. It is expected that during ageing of the latex film the amount of interfaces will decrease with time. So that changes in the number and the size of the remaining interfaces as function of drying and ageing process of the latex film could give some information about the autohesion process of the coalesced latex particles (*see chapter 5*).

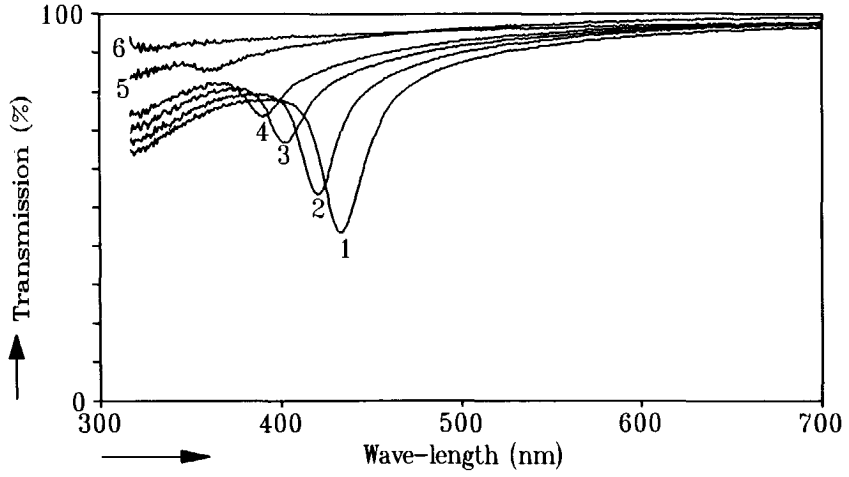

Fig. 3.6 Turbidity behaviour of a drying latex B4 film at a drying temperature above the MFFT.

3.2. EXPERIMENTAL

3.2.1. Materials

The latices that have been used for this study were made in a semi continue emulsion polymerization process. The binder of the latices consists of copolymer of Butyl Acrylate (*BA*) and Methyl Methacrylate (*MMA*) in a mass ratio of *35:65*. The emulsion polymerization took place under starved conditions, which means that the polymer composition is distributed uniformly over the particle. The physical parameters and chemical compositions are given in *Table 3.1.*

3.2.1a. Procedure Semi-continue Emulsion Polymerization

The semi continuous emulsion polymerization was carried out in a stirred tank reactor under nitrogen vapor. The polymerization consisted of three parts :

a) Inlay; The tank was filled with 300 *ml* water with some dissolved *SDBS*. The particle size of the synthesized latex is controlled by the amount of *SDBS* in the inlay when all other parameters are held constant during the emulsion polymerization process. Then the inlay is heated up to 80 ^{o}C.

b) Pre-mulsion; The pre-emulsion consisted of *280 g MMA*, *180 g BA*, *140 g* H_2O and *4.6 g*

SDBS (1 wt% of monomer). The pre-emulsion was stirred until a stable viscous emulsion was obtained.

c) Initiator; The initiator consisted of *1.5 g* $Na_2S_2O_8$ dissolved in *10 g* of water.

When the inlay reached a temperature of *80* ^oC the initiator was added to the reactor. After one minute the pre-emulsion was dosed to the reactor over a period of 3.5 hours (*starved conditions*). After that, the temperature was increased to *85* ^oC for a period of 1 hour (*to get 100 % conversion*). Then the reaction mixture (*Latex*) was cooled slowly to room temperature. The physical parameters and chemical compositions of the latices are given in *Table 3.1.*

Table 3.1 Composition and Physical Properties of the Latices.

Latices		*B4*	*B6*	
MMA/BA(wt%)		*65/35*	*65/35*	
SDBS	*(g/l)+*	*0.584*	*0.502*	
	(wt)++	*0.01*	*0.01*	
W_f	*(at 50 ^oC)*	*0.481*	*0.473*	*+ =Concentration in inlay*
MFFT	*(^oC)*	*25-28*	*29-31*	*++=Based on polymer content*
r_p	*(nm) (QELS)*	*103*	*132*	W_f *=Weigt fraction polymer*
	(Interference)	*94*	*119*	T_g *=Glass transition temperature*
T_g	*(^oC) Dry*	*32*	*35*	n_p *=Refractive index polymer*
	Wet	*28.5*	*30*	ρ *=Density polymer (Calculated)*
ρ	*(kg/m^3)*	*1145*	*1145*	* *=GPC (a significant polymer*
n_p		*1.482*	*1.482*	*fraction is non soluble in THF,*
$\bar{M}_n$	*(kg/mol)*	*>130**		*possibly due to crosslinking)*
$\bar{M}_w$	*(kg/mol)*	*>493**		

3.2.2. Equipment and Measurements

The acrylic latices were dried in a conditioned room, where the weight loss and transmission spectra were measured simultaneously (*Fig. 3.7*). The relative humidity (*R.H.*) and drying temperature in the conditioned room could be changed respectively between *10-90 %* and *0-50* ^oC. The weight loss of the drying latex film was measured every second with the aid of an analytical balance *(Mettler AM-100)*. The transmission spectra were measured with the aid of a diode-array spectrophotometer (*ORIEL-Instaspec II*). A transmission spectrum was measured every 5 seconds, where the measured transmission spectrum is the average of a collection of 4 spectra with a total scan

time of 0.32 s. The transmittance of the drying latex film was measured in the middle of the coated glass plate with a radius of *3 cm* and a scan radius of *300 μm*.

The problem with these drying experiments is the non-uniform drying behaviour of the latex films across the coated glass plate. The latex film dries with a circular drying front [5,6], starting at the edge of glass plate *(Fig. 3.8)*.

This means that the measured average weight fraction (W_a) as a function of time differs strongly from the weight fraction of the scanned area. Initial measurements showed that there were big differences in polymer concentration of the drying latex film across the coated glass plate *(Fig. 3.9)*.

This was done by washing the partly dried latex films with water, so that only the coalesced part of the latex film stayed on the glass plate. The weight fraction of the non-coalesced area (W_{nc}) will then be given by :

$$W_{nc} = \frac{W_f M_f - M_c}{M_t - M_c} \qquad (1)$$

where $W_f M_f$ is the total polymer weight brought on the glass plate at t=0, M_c is the weight of the polymer (coalesced latex) that stayed on the glass plate after washing with water and M_t is the total weight of the partly dried latex film at time t. *Figure 3.9* shows that the particle concentration of the non-coalesced area increases very slowly. This can be explained by the flocculation of the latex particles at the drying front, as a consequence some free water will be excluded, which will flow in the direction of the non-coalesced center (less resistance).

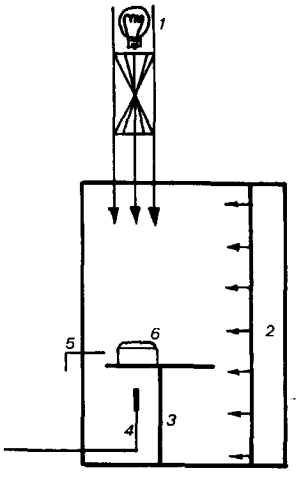

1) Halogen lamp, which focus a plane parallel light beam on the sample. 2) Temperature and R.H. controlled air current in conditioned room. 3) Plateau of the analytical balance (AM-100 Mettler). 4) Optical glass fiber, which directs the transmitted light of the sample to the diode array spectrophotometer (ORIEL Instaspec II). 5) Temperature and R.H. measurements 6) Sample, a latex coated quartz glass plate.

Fig. 3.7 Schematic representation of the experimental drying equipment.

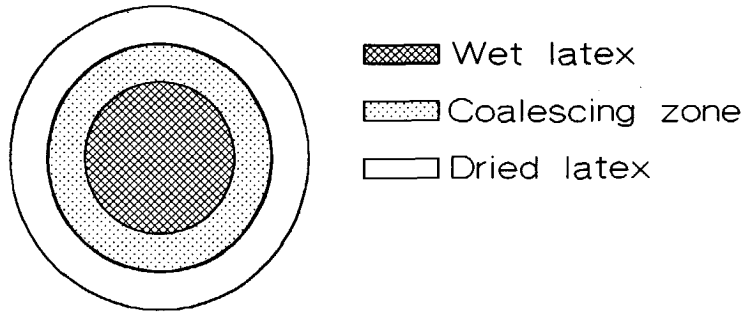

Fig. 3.8 Typical circular drying front of a thin latex film coated on a glass plate.

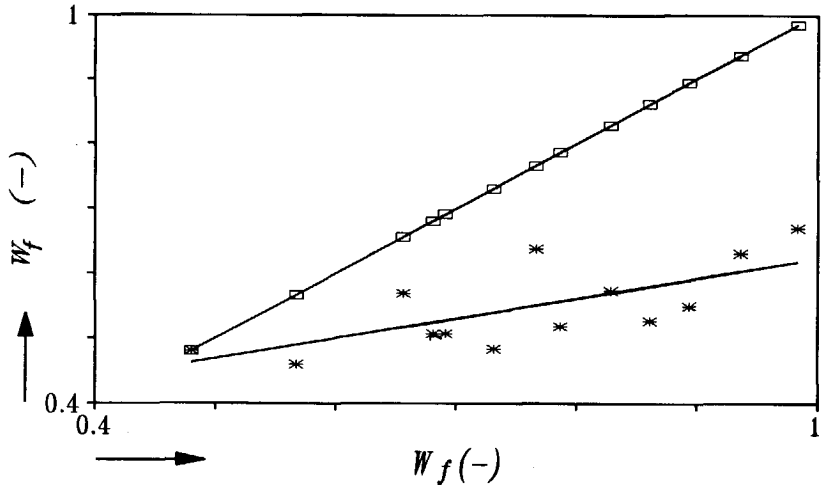

Fig. 3.9 Differences in polymer weight fraction of a drying latex film across the coated glass plate. □ - W_a, * - W_{nc}.

The volume fraction of the drying latex film in the detection zone (V_f) can be calculated from the interparticle interference data (*see chapter 2*). *Figure 3.10* shows an experiment where V_f is given as a function of drying time of a latex B4 film. The volume fraction patterns are very different. The volume fraction predicted from the interparticle interference data (V_i) increases slowly, until the drying front reaches the detection zone (*300 s.*); then the volume fraction increases very fast and equals 1 when the drying front passes the detection zone (*425 s.*). This means that the time needed for the coalescence of the particles is about *75 s* ($0.74 < V_f < 1$), which is much shorter than predicted by the average volume fraction (V_a), which is *300 s.* Because the time of coalescence is important for the relation of the (visco)elastic properties during latex coalescence and the *DMTA*-properties of dried latex films *(see chapter 4)*,

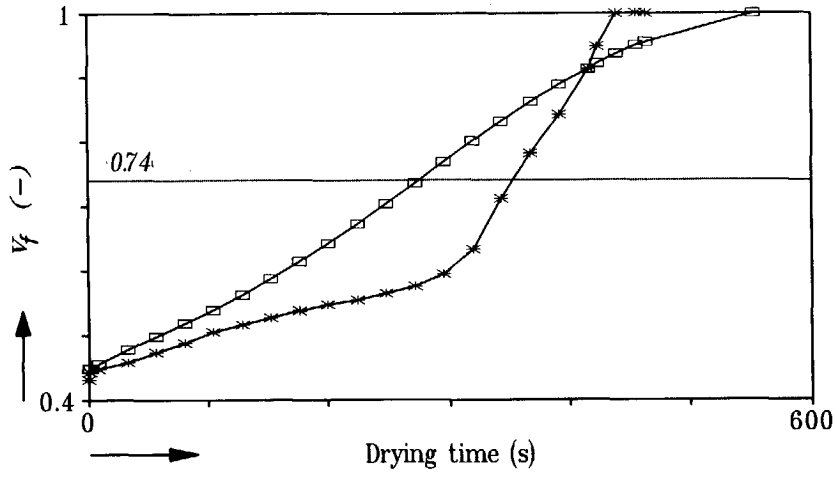

Fig. 3.10 Polymer volume fraction as function of drying time.
□ - V_a, * - V_i

the volume fraction as calculated from the interparticle interference is used for the description of the drying process of the latex films.

3.3 RESULTS AND DISCUSSIONS

This section gives a detailed study of the interparticle interference patterns of drying thin films of acrylic latices at different stages of the film formation process.

3.3.1 Regularity of the Interparticle Structure

In the beginning of the drying process, when the latex film is just brought onto the glass plate, secondary interparticle interference minima are present, as a consequence of a concentration difference across the latex film. Two types of interference patterns were measured of latex B4. In the first case (*Fig. 3.11a*) an interference minimum was found, which consisted of two minima, and in the second case (*Fig. 3.11b*) was found one primary and many secondary interparticle interference minima. When more water evaporates these secondary interference minima disappear and the primary interparticle interference minimum becomes more and more distinct *(Fig. 3.11c)*. This is a consequence of decrease of the concentration difference across the latex film and of the better arrangement of the latex particles in the packing structure, which increases the overall regularity of the interparticle structure.

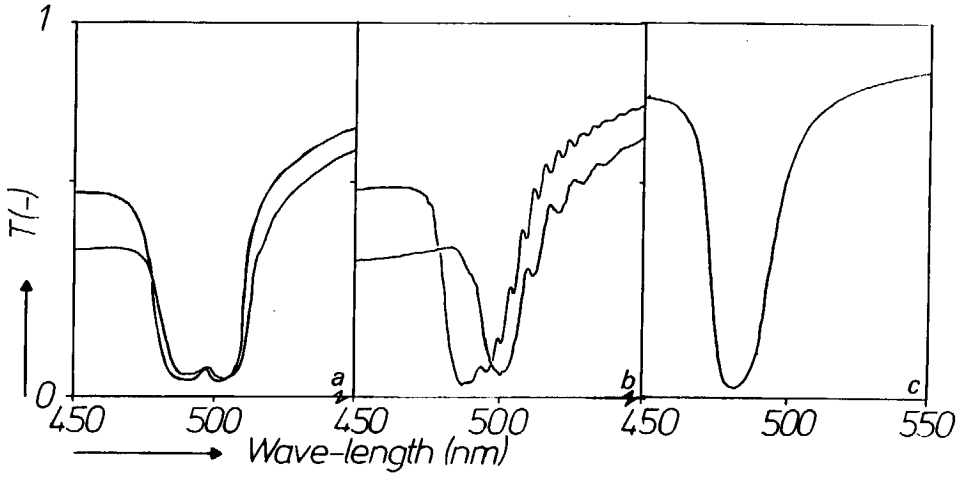

Fig. 3.11 Typical Interparticle interference patterns of the latex films in the early stage of the drying process.

*3.3.1*a *Secondary Interference Minima*

The secondary interparticle interference minima are also present in the computer calculation of the multilayer interference theory (*see Fig. 2.10*). For the model calculation the multilayer interference theory (*section 2.2.1 and 2.3.2*) and the Rayleigh scattering model 1 (*section 2.3.3*) were used. These theoretical secondary interference minima are caused by light interference over the latex film, so that the frequency of the secondary interference minima corresponds to the film thickness. *Figure 3.12* shows how the frequency of the secondary interference minima changes when the film thickness is changed from 5.1 to 15.2 μm (calculated). From the wave-length difference between the secondary interference minima the thickness of the latex film can be calculated with (*see section 2.2.1. Eq (3)*) :

$$d_l = \frac{p}{2.n_d} \cdot \left(\frac{\lambda_{k+p} \cdot \lambda_k}{\lambda_k - \lambda_{k+p}} \right) \qquad (2)$$

where p is the number of minima from λ_k to λ_{k+p} ($\lambda_{k+p} < \lambda_k$), n_d is the refractive index of the latex. It was found that the film thickness calculated from the secondary interference minima of respectively 5.5 and 15.9 μm corresponds very well with the film thickness used in the computer calculation of respectively 5.1 and 15.2 μm.

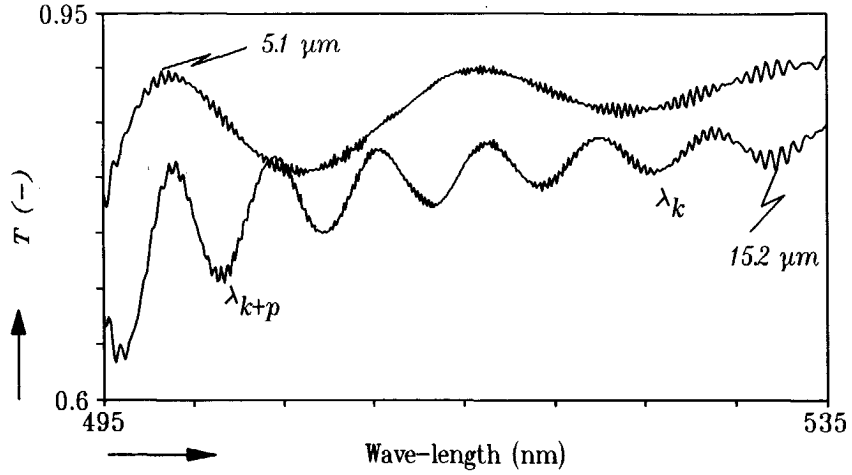

Fig. 3.12 Influence of the film thickness on the frequency of the secondary interparticle interference minima.

3.3.1b. Polymer Concentration Profiles

The decrease of the concentration difference and the increase of the regularity of the packing structure of a drying film can be described by two possible models depicted in *Fig. 3.13.* In the first model (*a*) the interparticle structure in the drying latex film at the air/latex surface consists of very regularly packed layers of particles, where the interparticle distances are constant, below these regularly packed layers the interparticle distances are gradually increasing towards the glass surface (t_1). By further evaporation of water the number of regularly packed layers increases (t_2 *to* t_3). When the interparticle distance across the latex film becomes constant (t_4), more evaporation of water causes a uniformly decrease of the interparticle distances throughout the latex film (t_5). In the second model (*b*) two interparticle distances are present (t_1, $A_{(x=d)}$ & $A_{(x=0)}$), where the number of regularly packed layers at the air-latex interface increases and at the glass interface decreases when more water evaporates (t_1 *to* t_3). The rest of the course is equal to that of the first model.

For these typical systems the average refractive index can be calculated across the latex film. The interparticle interference patterns can be calculated from the multilayer interference theory by approximating the alternating average refractive index with small decrements (*see section 2.4.2*). The scattering is described with Rayleigh scattering model 1. The results of the model calculations can be seen in *Fig. 3.14.*

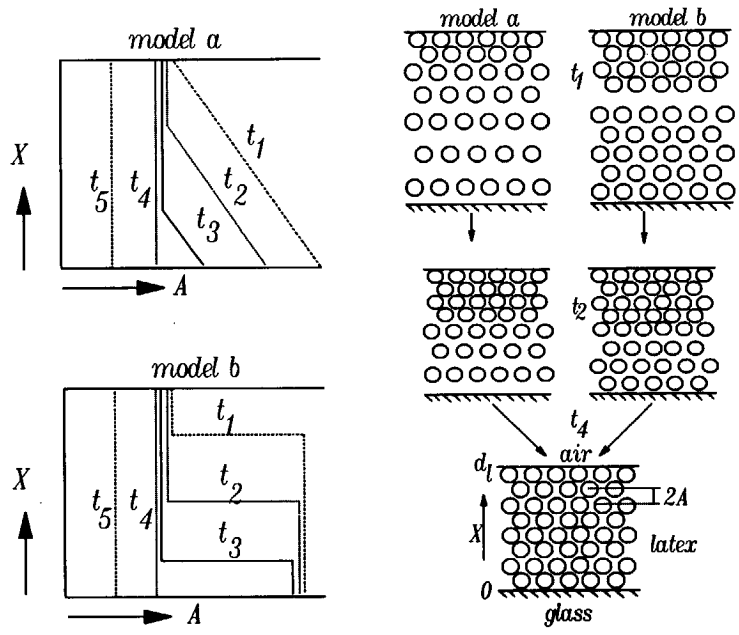

Fig. 3.13 Possible polymer particle concentration profiles across the latex film in the early stage of the drying process.

Figure 3.14a shows how the theoretical pattern should look like when no concentration difference exist across the drying latex film. This corresponds to the experimental situation depicted in *Fig. 3.11c*, where the regularity of the interparticle structure is maximal. However, the secondary interference minima disappear in the measured interparticle interference pattern, which contradicts the hypothesis of the increase of regularity of the interparticle structure.

Figure 3.14b shows the result of model *a*, where *50 %* of the film thickness has a constant interparticle distance and the other *50 %* has a difference in layer distance of *2.7 nm*. This results in a broader primary interference minimum and in secondary interference minima only at higher wave-lengths ($\lambda > \lambda_{min}$). This corresponds very well to the experimental situation depicted in *Fig. 3.11b*.

Figure 3.14c shows the result of model *b*, where two layer distances coexists both occupying *50 %* of the film thickness. This results in one primary interference minimum, which consists of two minima. This corresponds very well to the experimental situation depicted in *Fig. 3.11a*.

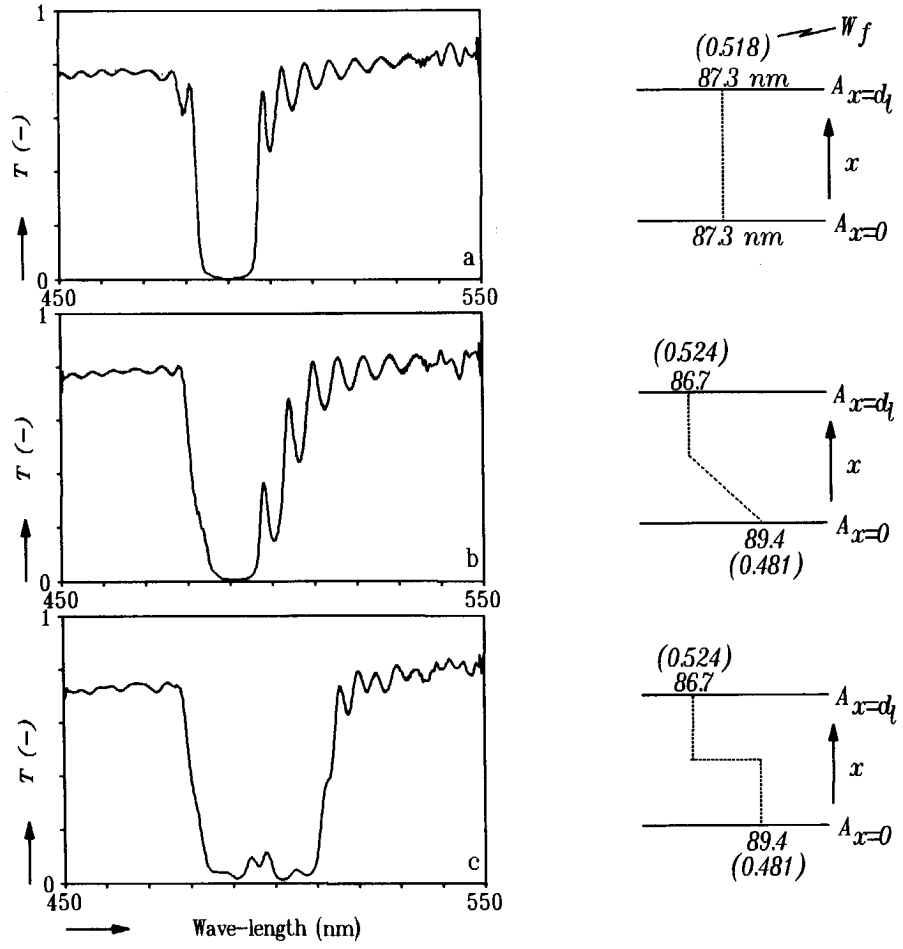

Fig. 3.14 The influence of the different particle concentration profiles on the computer calculations of the theoretical multilayer interparticle interference patterns.

The concentration differences discussed here, can give an accurate description of the experimental interference pattern caused by the latex film in the beginning of the drying process.

3.3.2 Critical Interparticle Distance

The latex particles in the drying latex will start to flocculate when they reach a critical interparticle distance. Because the interparticle distance in the flocculated state is smaller than that in the dispersed state, the transmission spectrum will show two interparticle interference minima (*Fig 3.15 spectrum no. 5 at 444 nm and 462 nm).* It appears that, with advancing drying time the intensity of the 444 *nm* interparticle interference minimum increases. This means that the flocculated state is build up from the latex-air surface into the film due to the water loss (*Fig. 3.15 spectra 1 → 8)*

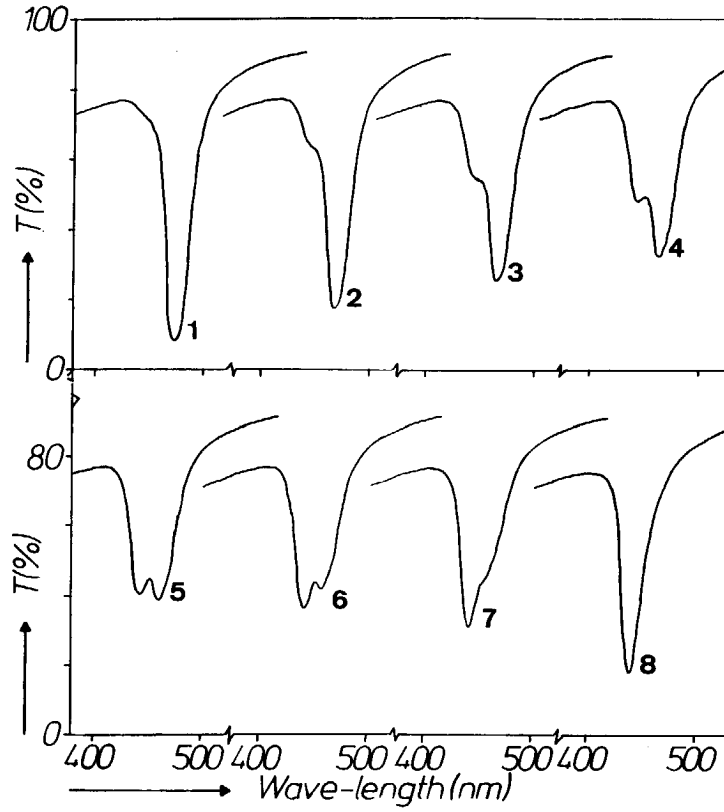

Fig. 3.15 The interparticle interference pattern change during the flocculation process of a drying latex (B4) film.

From the λ_{min} values the interparticle distances in the dispersed state can be calculated just before flocculation and in the flocculated state [*Chapter 2 Eqs. 3,19,20*]. For latex B4 we have found that the interparticle distance in the dispersed state is about 13 *nm* and in the flocculated state about *3 nm* (*Table 3.II*). For latex B6 the results were of the same order of magnitude.

Table 3.II Interparticle Interference Minimum Change During the Flocculation of the Latex Particles.

Latex	λ_{min}^{1} (nm)	λ_{min}^{2} (nm)	κ^{1} (nm)	κ^{2} (nm)
B4	462	444	13.2	2.8
B6	590	566	16.4	2.7

κ *interparticle distance*
1 before flocculation
2 after flocculation

3.3.3. Size of Stabilizer Layer around the Latex Particles

When the latex film is dried below the MFFT, the latex particles can not deform after they are flocculated. Therefore the interparticle interference minimum does not shift anymore when more water evaporates (*Fig. 3.16a spectra 1 → 7*). The overall transmission decreases very fast, because the water evaporates from the remaining interstices, by which these are filled with air. As a consequence the scattering intensity increases, because the relative refractive index (polymer/water→polymer/air) increases. However, when the film is almost completely dry, suddenly the transmittance increases very fast, which happens in a few seconds. Simultaneously the interparticle interference minimum has been shifted from *566 nm* to *531 nm (Fig. 3.16b spectra 7 → 15)*. This behaviour is completely reversible when the film is wetted and dried again. An explanation for this typical behaviour is the shrinking of the stabilizing layer (solved emusifier molecules) at the surface of the latex particles, due to the complete water loss of the drying latex film. This causes a decrease of the effective size of the latex particle and the scattering volume of the interstice between the latex particles. The λ_{min} shift of *31 nm* and *35m* for latices B4 and B6 respectively, can be explained by a stabilizer layer thickness of about *2-3 nm* (κ_{SDBS}, *see appendix II and Table 3.III*). This value is of the same order of magnitude as the length of the *SDBS*-molecule, which, when fully stretched is about *2 nm* long. When the film is wetted the emulgator will be dissolved again, which explains the reversible nature of this typical behaviour.

Table 3.III Thickness of Stabilizing Layer.

Latex	λ_{min}^{1} (nm)	λ_{min}^{2} (nm)	ΔA (nm)	κ_{SDBS} (nm)
B4	444	413	2.4	3.0
B6	566	531	2.1	2.6

1 = interstices filled with water; 2 = interstices filled with air.

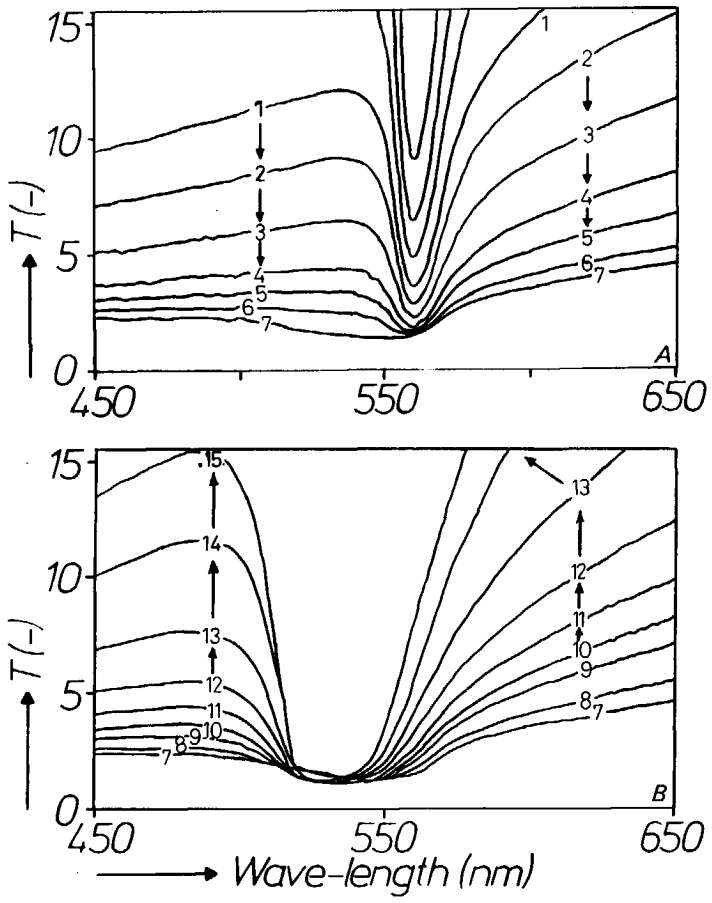

Fig 3.16 The interparticle interference pattern change of a drying latex (B6) film at the end of the drying process, when the film is almost dry.

3.4 CONCLUSIONS

The types of turbidity-measurements discussed in this chapter are a first attempt to investigate the mechanisms of film formation. These preliminary results demonstrate that turbidity-spectrophotometry could be a valuable tool for latex film research.

The changing interference pattern of a drying latex film reveals the interparticle

distances and displacements of the latex particles. It is found that the regularity of the internal interparticle structure of the latex particles increases in the beginning of the drying process. The increases of regularity of the interparticle structure can be simulated by different polymer concentrations profiles across the drying latex film.

The flocculation process can clearly be followed from the changes in the interparticle interference pattern. These changes reveal the critical interparticle distance at which the flocculation of the particles is initiated. It is found that the critical interparticle distance is about 14 % of the particle radius. After flocculation the particles are still separated by the stabilizer layer around the latex particles. It was found that the the size of this stabilizer layers around the latex particles is of the order of the size of a SDBS molecule (emulsifier).

References

1 Tent, A. van, Nijenhuis, K. te, "Proceedings XVIIth International Conference in Organic Coatings Science and Technology, Luzern, Switzerland, 1991," p. 317.
2 Redknap, *J. Oil. Chem. Assoc.* **49**, 1023 (1966).
3 Imoto, T, *Progress in Organic Coat.* **2**, 193 (1973/1974)
4 Leonardo, R.G., *J. Macromol. Chem., Macromol. Symp.* **35/36**, 389 (1990).
5 Hwa, J.C.H., *J. Polym. Sci.* **2**, 785 (1964).
6 Croll, S.G., *J. Coat. Techn.* **58**, 41 (1986).

CHAPTER 4

THE PROCESS OF COALESCENCE OF LATEX PARTICLES IN DRYING THIN FILMS OF ACRYLIC LATICES.

This chapter will focus on those theories that describe the deformation of the polymer particles during the drying process of thin films of acrylic latices. The coalescence theories are used to relate the turbidity behaviour of drying thin latex films with the viscoelastic properties of the dried latex films.

The changes in interparticle interference (see chapter 2, 3 and [1-7]) in a drying latex film are related to the changes in interparticle distance and displacement. When the latex particles coalesce the interparticle distance becomes smaller. This means that from this point on the change in interparticle interference is proportional to the indentation of the latex particles. From these measurements the mechanism by which the latex particles deform can be determined.

Turbidity measurements give a good description of the behaviour of the latex particles during the process of flocculation and coalescence and they can also be used to evaluate the *MFFT* of the latex. Investigated is the influence of drying temperature, humidity and particle size on latex coalescence and the *MFFT*.

4.1. INTRODUCTION

The process of flocculation and coalescence of a drying acrylic latex film consists of the first four stages of *Fig. 3.1.* For drying temperatures above the Minimal Film formation Temperature (*MFFT*), it was found that the latex particles deformed into a polyhedric structure, but at drying temperatures far below the *MFFT* the latex particles did not deform and the remaining interstices were filled with air.

In literature two possible mechanisms to describe the process of coalescence are proposed :

a: Dry sintering theory, (Frenkel [11], Dillon [12]). The concept of this theory is the formation of contact between polymer particles as a result of purely viscous flow. The driving force is the surface energy of the polymer.

b: Wet sintering theory, (Brown [13], Sheetz [14], Mason [15], Lamprecht [16], Menges

[17]). The concept of this theory is the application of Laplace's principle of capillary pressure to a system of three contiguous spheres, where the water surface tension is the driving force. Vanderhoff [18] proposed that the polymer/water interfacial tension is the driving force and that the Laplace principle must be applied to the radii of curvature between two coalescing spheres. The resulting contact pressure is used for the viscoelastic deformation of the particles, given by Hertz [19] or the JKR-contact theory [20,21].

This chapter gives a review of the coalescence theories known in literature and how the turbidity measurements can support these theories. Much has been written about latex coalescence [8-27], but only in the past several years a few non-destructive techniques (*Scanning Laser Acoustic Microscopy - SLAM* [28,29], *Dielectric measurements* [30,31] *and turbidity* [6,7,32,33]) have been developed to follow the coalescence process of the latex particles during the drying process.

4.2. LATEX COALESCENCE THEORIES

The MFFT of these latices lie around the T_g of the polymer. This means that all the film formation mechanisms take place around the T_g of the polymer. In this section the coalescence theories are divided into two categories and are evaluated at temperatures around the T_g.

4.2.1. Dry Sintering

In this model the polymer particles are deposited upon the surface, as the water evaporates, where they fuse into a film. For this model Dillon [12] has developed the following relationship for the coalescence of spheres caused by purely viscous flow (*Fig. 4.1)*:

$$\theta^2 = \frac{3.\gamma.t}{2.\pi.\eta.r_p} \qquad (1)$$

where θ is the coalescing angle, γ the polymer-air interfacial tension , η the viscosity of the polymer, r_p the sphere radius and t the time..

In chapter 2 we have concluded that the latex particles lie in a hexagonal packing (*h.c.p. or f.c.c.*). In this matrix of packed particles the complete deformation is a fact when θ is *30* ^oC. The time needed to get complete deformation by purely viscous flow will than be about 2.10^6 *s*, assuming a polymer/air interfacial tension value of

the order of *0.03 N/m*, a viscosity at T_g of about 10^{12} *Pa.s* and a particle radius of *100 nm*. Normally the the coalescence process takes place in the order of minutes, which is much faster than predicted by Eq. 1. However, the polymer particles in latices are not purely viscous. The polymer is mainly elastic, with a high viscous component. Even for cross-linked rubber latices, which are completely elastic, coalescence still occurs. The interfaces between these particles are often still visible after coalescence [21,34-39]. This is in contradiction with the viscous deformation theory as pointed out by Brown [13].

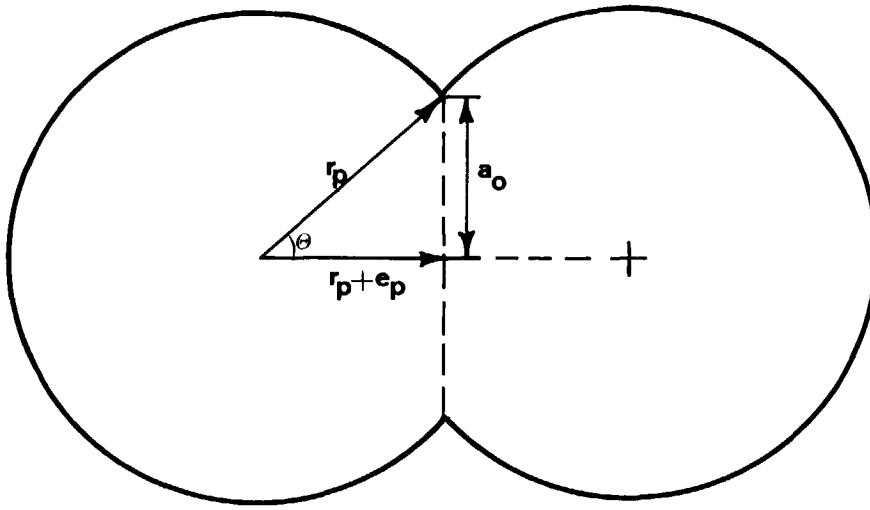

Fig. 4.1 Dry Sintering, coalescence of between two contacting latex particles as a result of purely viscous flow.

4.2.2. Wet Sintering

In the wet sintering theories the deformation of the polymer particles is thought to be caused by the capillary pressure. This deformation is a function of Youngs' elastic modulus and the coalescing time. To get complete coalescence, the capillary forces must be bigger than the forces of resistance of particle deformation. If the particles have been deformed completely, the cohesive energy between them prevents their separation as the cohesive forces at least counterbalance the internal forces build up during the time of the coalescence process. The resulting cohesive strength is a function of contact area, relaxation and the interaction energy of the surfaces.

4.2.2a) Capillary Forces [13-18]

The wet sintering model, which makes use of the capillary pressure as a driving force for the deformation of the polymer particles, was first developed by Brown.

Brown [13] used the capillary pressure which is caused by the possible capillary (*Fig. 4.2a*) between three spheres. The radius of the capillary is given by :

$$r_c = \frac{2}{3}.\sqrt{3}.(r_p+e_p) - r_p \tag{2}$$

where r_c is the radius of the capillary, r_p is the radius of the sphere, and $2.e_p$ is the interparticle distance ($e_p > 0$) or indentation ($e_p < 0$) of the spheres.

The relationship between the packing volume fraction of spheres (V_f) and the deformation is given for a hexagonal close packing (*appendix III*) by :

$$r_p+e_p = \left(\frac{\pi}{3.\sqrt{2}.V_f}\right)^{\frac{1}{3}}.r_p \tag{3}$$

The compressive pressure due to the curvature of the water in the surface of this capillary is given by the Laplace equation and is :

$$P_c \approx 2.\frac{\gamma_{\ell/a}}{r_c} \tag{4}$$

where $\gamma_{\ell/a}$ is the air-water(+additives) surface tension.

Brown postulated that this pressure acts over the compression area with radius a_o, which results in a deformation force given by :

$$F_B = P_c.\pi.a_o^2 \tag{5}$$

Sheetz [14], on the other hand, postulated that the capillary pressure acts over the capillary area, which is divided into a shearing force F_s and normal force F_n in a capillary (*Fig. 4.2b*) :

$$F_s = P_c.\pi.r_c^2.\cos\Phi \quad \text{and} \quad F_n = P_c.\pi.r_c^2.\sin\Phi \tag{6}$$

where Φ is the contact angle between water and polymer, which is determined by Young's equation. This means that F_s exerts a compression force on the matrix particles, whereas F_n tends to pull the wall of the capillary (particles) towards the centre.

Vanderhoff [18] and Menges [17] used the polymer-water interfacial tension as driving force. Their schematic representation of the coalescence of two spheres is given in *Fig. 4.2c*, where r_1 is the radii of curvature, r_2 is the radius of the compression segment and θ is the coalescing angle. The resulting pressure is given by :

$$P_V = \gamma_{p/\ell} \cdot \left(\frac{1}{r_1} - \frac{1}{r_2} + \frac{2}{r_p} \right) \tag{7}$$

Vanderhoff's model, which calculates r_1 and r_2, is based on the mass balance in the contact/compression region (for more details see his original article [18]).

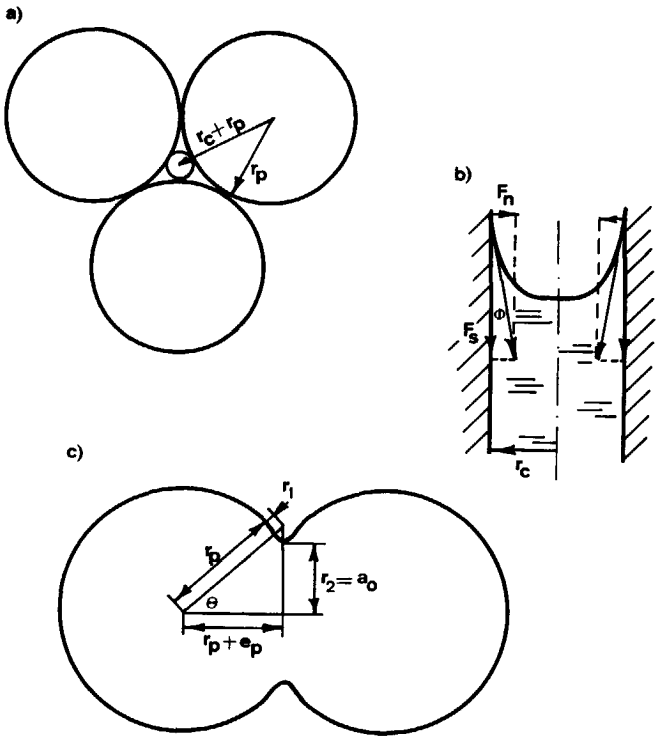

Fig. 4.2 Wet Sintering,

a) Brown's capillary pressure between three contiguous latex particles.

b) Sheetz' normal and perpendicular capillary forces acting over the matrix of latex particles.

c) Vanderhoff's deformation model.

4.2.2b Deformation Forces of Viscoelastic Bodies.

Hertz theory [19-21]. The contact between two smooth elastic bodies is given by the approximate theory of Hertz. For two spheres of radius r_1 and r_2 , which are pressed together under a load F_0 (e.g. the capillary force), the radius a_0 of the circle of contact is given by (*Fig. 4.3*):

$$a_0^3 = K^{-1}.R.F_0 \tag{8}$$

where K is a constant consisting of elastic constants of the material of each sphere and R is a function of r_1 and r_2:

$$K^{-1} = \frac{3}{4}.\left[\frac{1-\nu_1^2}{E_1} + \frac{1-\nu_2^2}{E_2}\right] \text{ , and } R = \left[\frac{r_1.r_2}{r_1+r_2}\right] \tag{9}$$

where ν is the Poisson ratio and E the Young's modulus of each material. At zero load the contact area is zero. The compression of the contact region, results in the approach of the two spheres by a distance $2.e_p$:

$$e_p \cong -2.\frac{a_0^2}{R} = -2.K^{-2/3}.F_0^{2/3}.R^{-1/3} \tag{10}$$

Johson-Kendall-Roberts-theory [20,21,27]. The JKR-contact theory takes also into account the attractive surface forces which operate between the solid spheres, so that it describes the equilibrium between two elastic spheres under a combination of body forces and surface forces. These 'additional' contact forces become important when the external load reduces towards zero. The basis of this theory is the Hertz equation, which is modified to take into account the cohesion/adhesion energy γ (*Fig. 4.3)* :

$$a_1^3 = K^{-1}.R.\left[F_0 + 3.\gamma.\pi.R + \sqrt{\left(6.\gamma.\pi.R.F_0 + \left(3.\gamma.\pi.R\right)^2\right)}\right] \tag{11}$$

So far we have dealt with the fundamental aspects of deformation of two contacting spherical bodies to a normal load c.q. capillary force. We have to bear in mind that these models of coalescence only describe contacts between pairs of particles. If these theories are extended for latex coalescence the large deformations can only be approximated and the influence of multiple contacts have to be considered in the analysis. For latex coalescence there are two possible mechanisms, viz. isotropic deformation or bi-axial deformation [40] (*Fig. 4.4).*

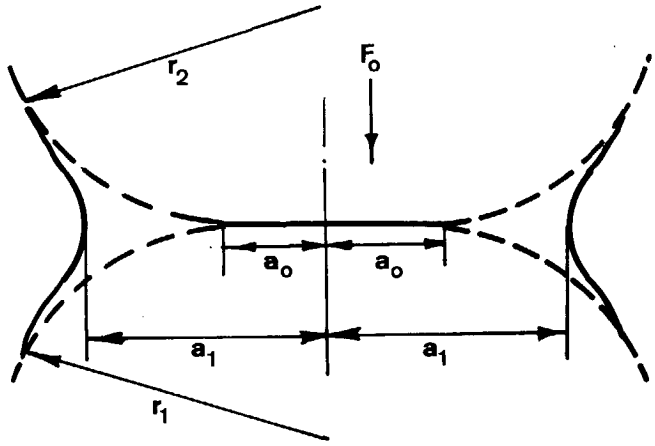

Fig. 4.3 Contact mechanics of elastic latex particles by Hertz (----) and JKR (——).

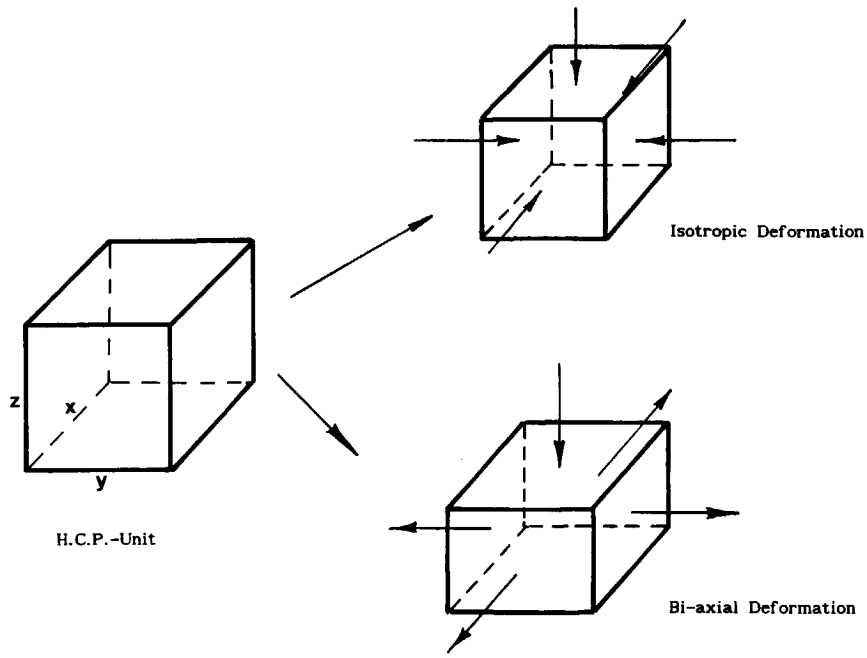

Fig. 4.4 Schematic representation of isotropic and bi-axial deformation mechanism.

4.2.2c Latex Coalescence

The indentation *($-e_p$)* of the isotropically coalescing latex particles as a function of volume fraction is given by *(see appendix III)*.

$$e_p = \left(\left(\frac{\pi}{3\sqrt{2}.V_f} \right)^{\frac{1}{3}} - 1 \right) . r_p \qquad (12)$$

A triangular shaped interstice is formed when the latex particles just touch *(see Fig. 4.5a)*. When the latex particles deform the shape of the interstice changes *(Fig. 4.5b)* as a function of indentation according to the Vanderhoff's deformation model. When the deformed particles have reached a packing volume fraction of *88 %*, the interstice between the coalesced latex particles becomes circular *(Fig. 4.2c)*. Further deformation causes the separate contact areas to interact. When this effect is neglected and the deformation is simply extended, then the interstices will be closed when the packing volume fraction reaches *93 %*, at which the capillary forces (from $\gamma_{\ell/a}$) become zero. During this deformation the contact area between the coalescing latex particles will change from a circular into a rectangular shape, due to the interacting contact areas. The corresponding maximum indentation of the coalescing latex particles has a value of *0.095* r_p *(V_f=1, Eq. 12)*.

The indentation *($-e_p^*$)* of the bi-axially coalescing latex particles as function of volume fraction is also given by *(see appendix III)* :

$$e_p^* = \left(\sqrt{\frac{\pi^2}{27.V_f^2}} + \frac{1}{3} - 1 \right) . r_p \qquad (13)$$

In this case the separate contact areas begin to interact when a packing volume fraction of *81 %* has been reached. When this effect is also neglected and the deformation is simply extended, then the maximum indentation will have a value of *0.165* r_p *(V_f=1, Eq. 13)*. During this deformation the contact area between the latex particles will also change from a circular into a rectangular shape. The formed polyhedric structure will be honeycomb shaped for the isotropically, as well as for the bi-axially deformed latex particles. In the case of bi-axially deformed particles the honeycomb structure is somewhat flattened. The projected size of the honeycomb structure (benzene ring, as seen by *SEM* [34-39]) will be in the case of bi-axial deformation about *10 %* bigger than in the case of isotropic deformation.

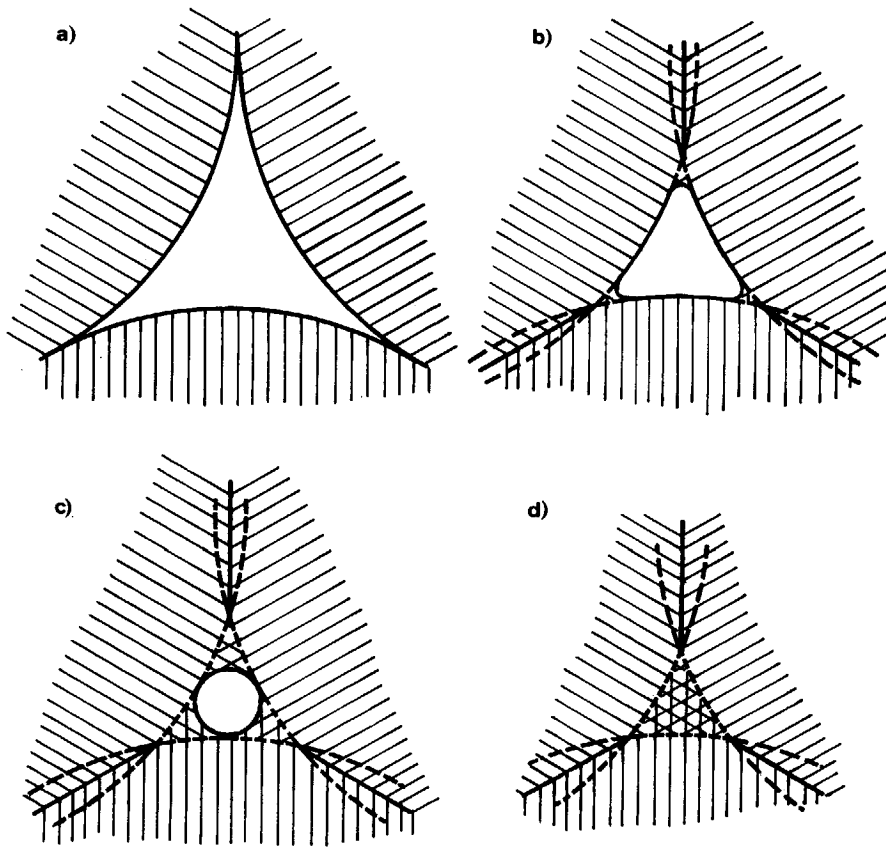

Fig. 4.5 Visualization of the change of the triangular interstice between three contiguous coalescing latex particles.

a) No deformation $V_f = 0.7405$ *and* $e_p = 0$.

b) $V_f = 0.80$ *and* $e_p/r_p = 0.025$.

c) The interstice becomes spherical and the separate contact areas begin to interact at $V_f = 0.88$ *and* $e_p/r_p = 0.056$.

d) When the influence of the interacting contact areas is neglected then the interstice will be closed at $V_f = 0.945$ *and* $e_p/r_p = 0.078$.

Figure 4.6 shows how the indentations of the contacting particles change as a function of the packing volume fraction of the isotropic and bi-axial deformation mechanisms.

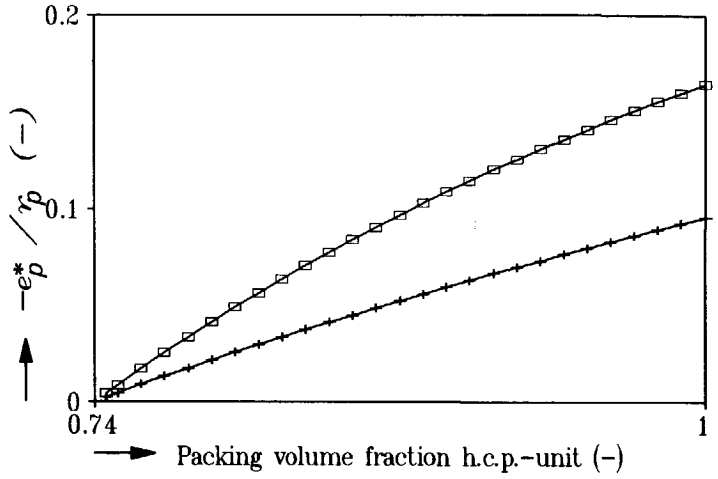

Fig. 4.6 The expected indentation as function of packing volume fraction for respectively the bi-axial (□) and the isotropic (+) deformation model.

Many theoretical combinations of the capillary forces and deformation forces are possible to evaluate latex coalescence. Three of these combinations will be discussed in the *section 4.4.2.*

4.3 EXPERIMENTAL

4.3.1. Materials

The latices that have been used for this study are made in a semi continue emulsion polymerization process. The binder of the latices consists of copolymer of Butyl Acrylate (*BA*) and Methyl Methacrylate (*MMA*) in a mass ratio of *35:65*. The emulsion polymerization took place under starved conditions, which means that the polymer composition is distributed uniformly over the particle. The physical parameters and chemical compositions are given in *Table 3.1.*

4.3.2. Equipment

The process of coalescence of drying thin films of latices was investigated with

transmission spectrophotometry. Therefore the acrylic latices were dried in a conditioned room, where the weight loss and transmission spectra were measured simultaneously (*see Fig. 3.3)*. The transmittance of the drying latex film was measured in the middle of the coated glass plate with a radius of *3 cm* and a scan radius of *300 μm*. The weight loss of the drying latex film was measured every second with the aid of an analytical balance *(Mettler AM-100)*. The transmission spectra were measured with the aid of a diode-array spectrophotometer (*ORIEL-Instaspec II*).

4.4. RESULTS AND DISCUSSIONS

This section shows how to relate the film formation mechanisms with the scattering properties of the drying latex film. Some experimental evidence will be discussed here, which supports some of the hypotheses developed in the foregoing sections.

4.4.1. Determination of Deformation Mechanism.

This is done by measuring transmission spectra and water loss of a drying latex film coated on a quartz glass plate. The measured spectra reveal the interparticle interference (λ_{min}) as a function of volume fraction of polymer. *Fig. 4.7* shows the results of such an experiment, where the interparticle interference (λ_{min}) is given as a function of the volume fraction of a drying latex B4 film above its *MFFT*. The plot can be divided roughly into two parts. First, evaporation of water causes the interparticle distance to decrease uniformly, as a consequence λ_{min} shifts to lower wave-lengths. Secondly, further evaporation causes the latex particles to pack into *h.c.p.* structure. From this point on latex coalescence starts. The shift of λ_{min} is now proportional to the indentation of the latex particles. The theoretical relations between λ_{min}, indentation and volume fraction for the two deformation mechanisms are given by *(see appendix IV):*

isotropic deformation

$$V_f = \frac{128}{27}.\pi.\sqrt{3}.\left[\frac{r_p.n_d}{\lambda_{min}}\right]^3 \qquad (14)$$

bi-axial deformation

$$V_f = \frac{4}{9}.\pi.\sqrt{3}.\left(\frac{r_p.n_d}{\lambda_{min}}\right) \qquad (15)$$

where n_d is the refractive index of the latex. The theoretically expected dependence of λ_{min} on the volume fraction of the isotropic and the bi-axial deformation mechanisms differ considerably. The results are also given in *Fig. 4.7.* It shows clearly that the bi-axial deformation mechanism describes the experimental data very well. So it is not unrealistic to conclude that the latex particles during latex coalescence of latex B4 are bi-axially deformed.

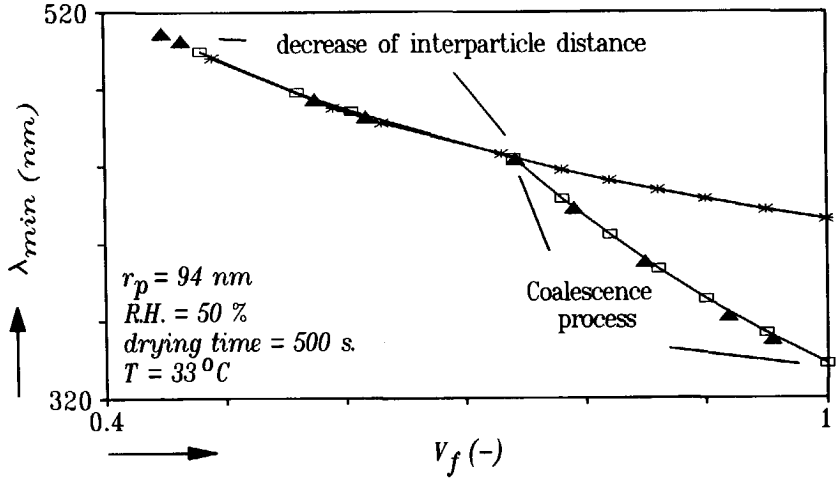

Fig. 4.7 The interparticle interference (λ_{min}) change of a drying latex B4 film as function of volume fraction polymer.
▲ - Experimental, ▫ - Bi-axial def., ✱ - Isotropic def. .

4.4.2. Evaluation Hypotheses Wet Sintering Theory

Latex films that are dried just below the *MFFT*, deform partly. The extend of this deformation depends on the temperature and drying time (which is a function of film thickness d_l and relative humidity *R.H.*). This latex looks like a crumbly, powder-like white film, when it becomes completely dry. When this film is carefully rewetted with water the interparticle interference reappears and can be measured. *Fig. 4.8* shows the results of dried latex B6 films over a temperature range of *20* to *50* ^oC. When the

particles of latex B6 did not deform, λ_{min} has a value of *560 nm*. From *Fig. 4.8* it follows that no deformation takes place below drying temperatures of *20 °C*. Above *20 °C* the latex particles begin to deform, first slowly, but in the region of the *MFFT* very fast. The last λ_{min} below the *MFFT* is found at *498 nm*, which corresponds to a packing volume fraction of *84 %* (Eq. 15). Higher volume fractions (lower λ_{min}) could not be found at these temperatures. This would mean that the capillary forces are always bigger than the forces resisting the deformation of the particles for packing densities above *84 %*, so that complete deformation follows.

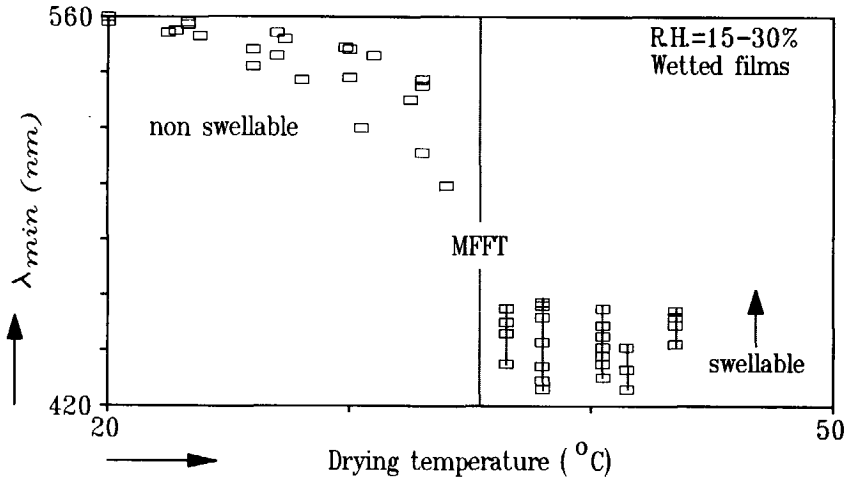

Fig. 4.8 The interparticle interference (λ_{min}) of rewetted dried latex B6 films as function of the drying temperature.

Above the *MFFT* the latex particles have deformed completely. The resulting transparent latex film will swell when immersed into water, as a consequence of internal interfacial boundaries still present between the deformed latex particles. During this immersion process λ_{min} shifts from *426* to maximal *460 nm* (λ_{min}=*460 nm* corresponds to a packing volume fraction of *90 %*, Eq. 15).

Figure 4.9 shows the calculated indentation ($-e_p^*/r_p$) of the coalesced latex particles as a function of the drying temperature. Substituting these data in the following wet sintering models, the theoretical dependence of the maximum Young's modulus (*E*) of the polymer particles, for which coalescence is possible, as a function of temperature can be determined during latex coalescence. The following three wet sintering models give a good synopsis of the behaviour of the capillary and deformation forces proposed in literature.

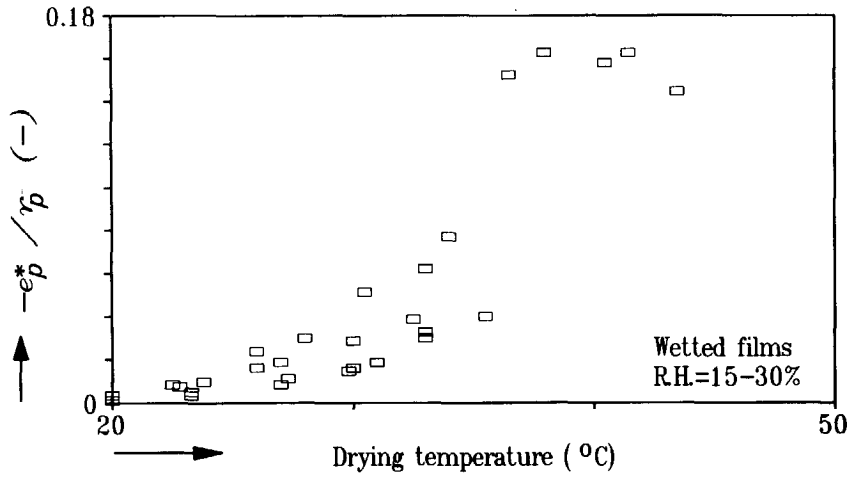

Fig. 4.9 The expected indentation ($-e_p^*/r_p$) of the latex B6 particles, according to the bi-axial deformation model, as function of the drying temperature.

1) Brown capillary pressure / Hertz-contact theory (Eqs. 2,4,5,8-10).

$$E_{B/H} = \frac{3}{2}.\pi.\frac{(1-\nu^2)}{a_o}.\frac{r_p}{r_c}.\gamma_{\ell/a} \tag{16}$$

Where $a_o \cong \sqrt{-r_p.e_p^*}$, which has been found by Hertz and which is only valid for small indentations and r_c is for the bi-axially deformation mechanism independent of e_p^* so that $r_c = 0.155.r_p$.

2) Sheetz capillary pressure / Hertz-contact theory (Eqs. 2,4,6,8-10)

$$E_{S/H} = \frac{3}{2}.\pi.\frac{(1-\nu^2)}{a_o^3}.r_p.r_c.\gamma_{\ell/a}.\sin\theta.\cos\Phi \tag{17}$$

Where $a_o \cong \sqrt{-2.r_p.e_p^*}$, which is the relation used by the dry sintering theory. This model can explain the bi-axial deformation mechanism, by postulating that a compression force (F_s) acts on the matrix of particles and that a normal force (F_n) tends to pull the particles towards the centre of the packed particles. In *Fig. 4.10* is depicted the schematics of the forces acting on a latex particle in a h.c.p. matrix. The normal forces will try to pull the particles at positions a,b,c and d in the direction of the

centre of the h.c.p.-unit, on the contrary the compression forces will try to push the particles at positions a,b and c away from the centre. When F_S' becomes equal to F_n then the positions of centres of the latex particles in the x-y-plane are not changed during latex coalescence, only the positions in z-direction changes. F_S' is equal to F_n when the Young-contact angle (Φ) is of the order of $\approx 52^o$ *(equal to* θ*)*. The net compressive force to deform the latex particles will then be of the order of $F_S.\sin\theta$.

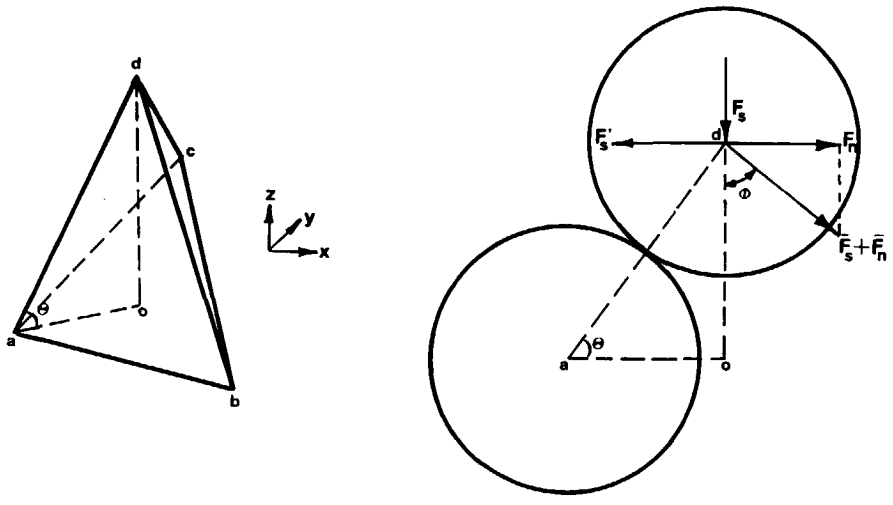

Fig. 4.10 Schematic representation of Sheetz' capillary forces on a latex particle in a h.c.p.-unit.

3) Vanderhoff / JKR-contact theory (Eqs. 7,9,11)

$$F_V = \pi.a_o^2.\gamma_{p/\ell}.\left(\frac{1}{r1} - \frac{1}{r2} + \frac{2}{r_p}\right) \tag{18}$$

$$E_{V/JKR} = \frac{3}{4}\frac{(1-\nu^2)}{a_o^3}.r_p.\left[F_V + \frac{3}{2}.\gamma.\pi.r_p + \sqrt{\left[3.\gamma.\pi.r_p.F_V + \left(\frac{3}{2}.\gamma.\pi.r_p\right)^2\right]}\right] \tag{19}$$

Where $r_1 = a_o \approx \sqrt{-4.r_p.e_p^*}$ and $\gamma = 2.\gamma_{p/a}$ *(Cohesive energy)*

Figure 4.11 shows the theoretical results of the maximum admissible values of the Young modulus for a given packing volume fraction and e_p^* for the bi-axial deformation mechanism. For these model calculations the next parameters were used :

- Radius of polymer particle *119 nm* (Latex B6);
- Polymer/air interfacial tension $\gamma_{p/a}$ of our latex lies in the range of *0.03 N/m*. The water/air interfacial tension for latices lies in the range *0.03-0.07 N/m*. When the concentration increases due to evaporation of water the Polymer/air interfacial tension will decrease due to the presence of surface active agents, so that for $\gamma_{\ell/a}$ the minimum value of *0.03 N/m* is chosen. It has also been found that the Polymer/water interfacial tension $\gamma_{p/\ell}$ in the presence of surface active agents lies in the range of *0-0.01* [14]. This means that Young-contact angle (Φ) is expected to lie between 0^o and 48^o.
- Poisson's ratio $\nu=0.4$.

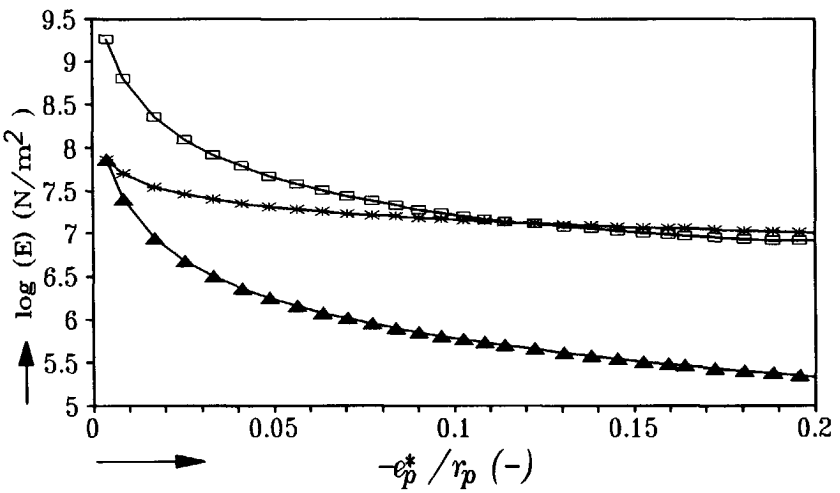

Fig. 4.11 Results of model calculations of the Young-modulus (E) as a function of indentation (e_p^*/r_p).
□ *-Vanderhoff/JKR (Eq. 19),* * *-Brown/Hertz (Eq. 16),* ▲ *-Sheetz/Hertz (Eq. 17).*

The combination of *Figs. 4.9* and *4.11* then gives the expected theoretical Young modulus-temperature plot of the latex particles during latex coalescence (*Fig. 4.12*). This theoretical modulus-(time)-temperature plot has been verified with the *DMTA* results of the completely coalesced dried latex films. The *DMTA* results taken correspond to the coalescing time of the latex particles. The coalescing time in this experiment is about 100 s, which corresponds to a frequency of *0.01 Hz*. The *DMTA* results at *0.01 Hz* of dried latex B6 films is also shown in *Fig. 4.12*.

Figure 4.12 shows that the calculated just admissible Young's modulus-temperature plots from the interparticle interference data are shifted substantially to lower

temperatures (about *5-10 ^{o}C*), with regard to the *DMTA* results of the dried latex film. This effect can be explained by the influence of water on the glass transition temperature. The influence of water on T_g was determined in a *DSC* by measuring the T_g of liquid latex and of the dried latex film. We found that the T_g of the dried latex film is about *5 ^{o}C* higher than that of the latex itself (*see Table 3.1*). It is well known that absorbed water [41] and relative humidity [42,43] lower the Young's elastic modulus of acrylic polymers.

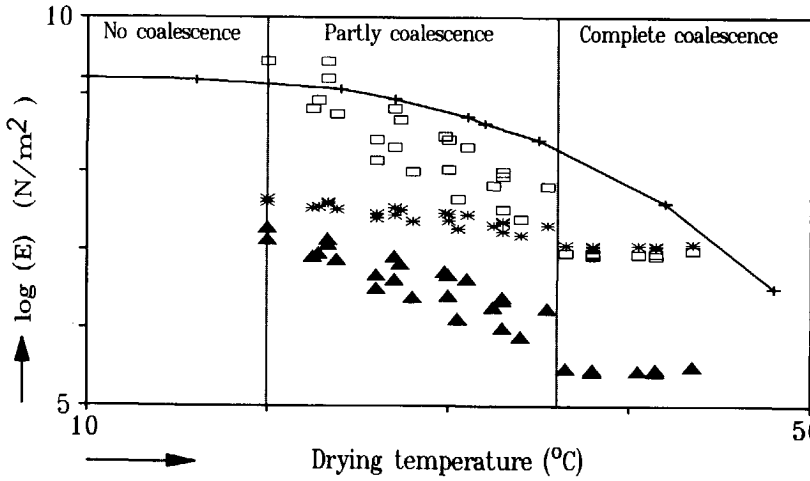

Fig. 4.12 Comparison of the theoretical expected Young-modulus-temperature plot of the latex B6 particles during latex coalescence with a 0.01 Hz DMTA plot of a completely coalesced dry latex b6 film. □ -Vanderhoff/JKR (Eq. 19), ✳-Brown/Hertz (Eq. 16), ▲ -Sheetz/Hertz (Eq. 17), + -0.01 Hz DMTA

Smith et al. [43] observed that the glass transition temperature of *PMMA* slides decreases *20 ^{o}C* at high humidities. They could predict the glass transition temperature of the acrylic polymer as function of the water absorption. They used for the 'glass transition temperature' of water a value of *104 K*. It has been observed [8,33,38] also that the film formation properties of drying hydrophilic latices were improved by higher humidities, while those of hydrophobic latices were not improved.

In view of this, the Vanderhoff/JKR model gives the best relation between the macroscopic viscoelastic properties (*DMTA*) and the calculated viscoelastic properties during the coalescence process of the latex particles. This kind of results was also found by Kendall [15] for polystyrene latices. The only shortcoming of the Vanderhoff model is that it is difficult to explain by which mechanism the latex particles bi-

axially deform. Only the model of Sheetz can give a satisfactory explanation for the bi-axial deformation mechanism, but the magnitude of the capillary force is not high enough for latex coalescence. Perhaps a combination of the two theories is possible, where Sheetz model only describes interparticle contact in the z-direction of the h.c.p.-unit and prevents interparticle contact in the x-y-direction (*see Fig. 4.10*). In the case that interparticle contact is established the Vanderhoff model will be able to describe further deformation of the latex particles. In the next two sections more experiments will be shown, where the influence of particle size and relative humidity on latex coalescence and the *MFFT* are investigated.

4.4.3. Influence of r_p on Latex Coalescence.

Latex films that are dried just below the *MFFT*, deform partly. The extent of this deformation depends on temperature and drying time (which is a function of film thickness and *R.H.*). The latex looks like a crumble powder-like white film, when it becomes completely dry. When this film is carefully rewetted with water, the interparticle interference reappears and can be measured. *Figure 4.13* shows these results for dried latex B4 and B6 films over a temperature range of *5* to *35* ^{o}C at a *R.H.* of *70 %* .

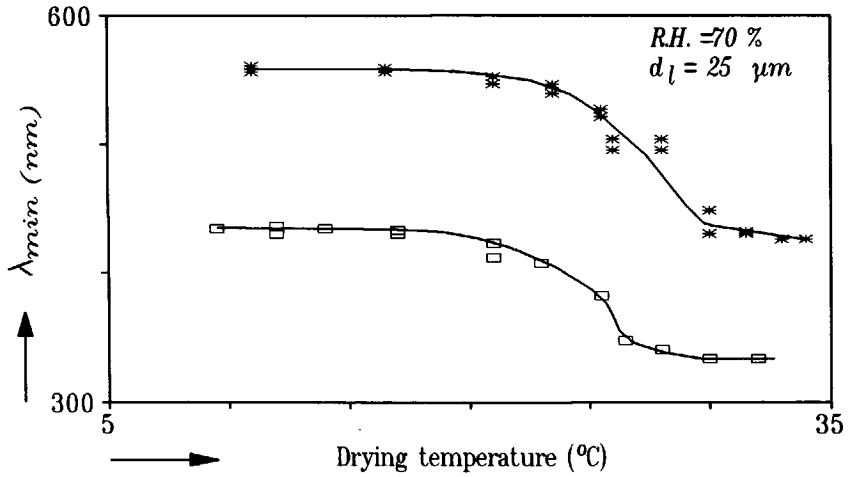

Fig. 4.13 The influence of the drying temperature on the interparticle interference (λ_{min}) of the rewetted dried latex B4 (□) and B6 (✱) films.

When the particles of latices B4 and B6 do not deform, λ_{min} will have experimental values of *438 nm* and *560 nm* respectively. From the λ_{min} values the indentation of the

latex particles as a function of drying temperature can be calculated from the bi-axial deformation model (Eq. 15). *Figure 4.14* shows the calculated indentation ($-e_p^*/r_p$) of the coalesced latex particles as a function of the drying temperature. It appears that the latex B4 particles deform at lower temperatures, with respect to those of the latex B6, but the deformation behaviour of latex B4 and B6 is almost the same. The difference is about *5 °C* , which corresponds accurately to the higher T_g of latex B6. That latex B6 has a higher T_g than latex B4 is surprisingly because the chemical composition and synthesizing method were the same. For both latices it appears that on reaching an indentation $-e_p^*/r_p$ of *0.09* (V_f=*0.85*), complete deformation of the latex particles follows (*see section 4.4.2.*). This means that from this point on the forces of resistance of particle deformation become lower than the capillary forces.

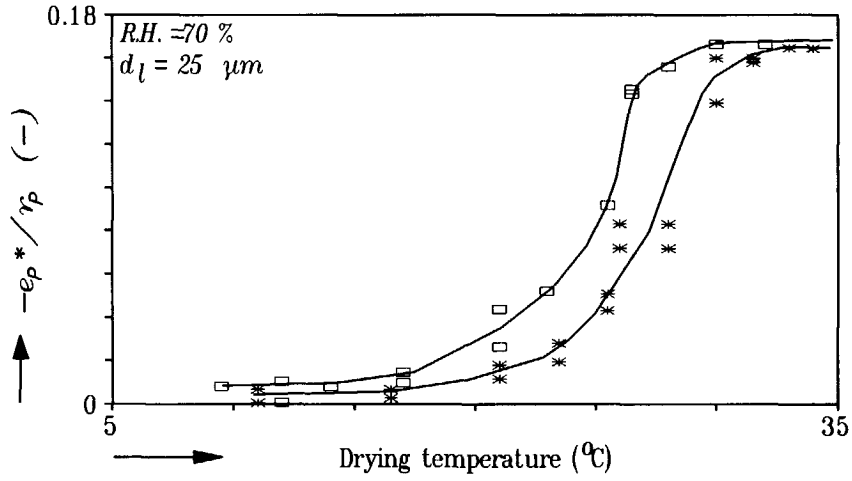

Fig. 4.14 Influence of the drying temperature on the indentation ($-e_p^*/r_p$) of the particles in dried films of latices B4 (□) and B6 (✱).

The latices B4 and B6 are coalescing completely at respectively *26 °C* and *30 °C*. The resulting transparent latex films will swell when immersed in water, as a consequence of the intact internal interfacial boundaries between the deformed latex particles. During this immersion process λ_{min} shifts in the case of latex B6 from *426* to maximal *460 nm* (*See Fig. 4.15;* λ_{min}=*460 nm* corresponds to a packing volume fraction of *0.9*). This phenomena will be discussed in more detail in chapter 5.

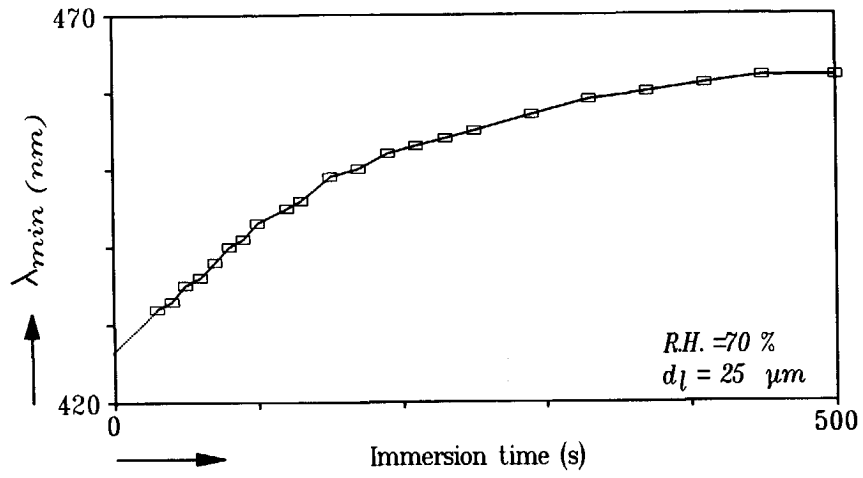

Fig. 4.15 Typical immersion pattern of a dried latex B6 film.

4.4.4. Influence of r_p and R.H. on the MFFT

Figure 4.16 shows how the transmittance, at wave-lengths of *275 nm* and *500 nm*, of dried latex B4 films changes as a function of the drying temperature. This plot can be divided into three regions, namely :

I) In the first region the latex particles are not deformed. This results in a crumbly/powder-like film;

II) In the second region the latex particles are deformed partly. This results in a latex film with cracks;

III) In the third region the latex particles have deformed completely. This results in a homogeneous, transparent polymer film.

The *MFFT* of a latex is equal to the drying temperature at which the drying latex film becomes homogeneous, transparent and crack free. Therefore the temperature between the second and third region is called the *MFFT* of the latex B4, which is in this case *26* ^oC.

Normally the minimum film formation temperature is determined by using a messing bar over which a temperature gradient is established, in this case from *0* to *50* ^oC. The bar is then coated with a *50 μm* thick latex film. The *MFFT* is determined by visual interpretation of the transparency of the dried latex film. Visually, the dried latex B4 film becomes transparent and crack free at a drying temperature of about *23* ^oC. The visual wave-length optimum of the human eye is about *500 nm*.

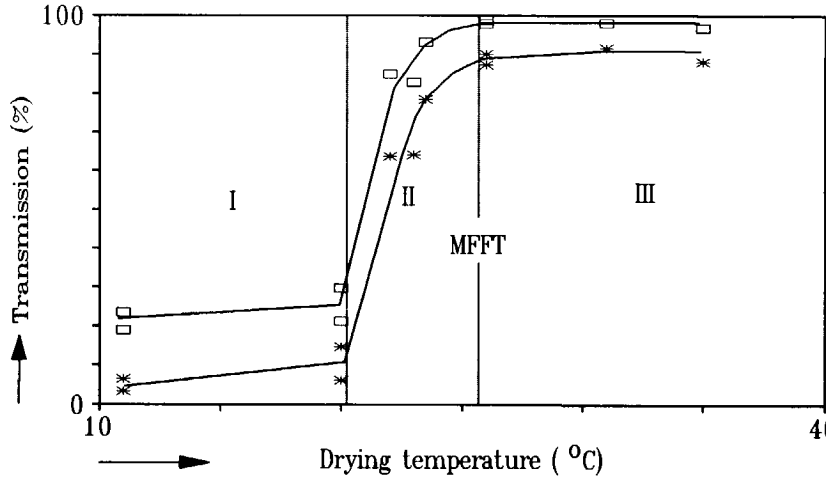

Fig. 4.16 The transmittance of dried latex B4 films, at wave-lengths of 275 nm (✳) and 500 nm (□), is given as function of the drying temperature.

Therefore the visual *MFFT* corresponds to the drying temperature of the dried latex film, where it has a transparency of about *90 %* at a wave-length of *500 nm*. The *MFFT* will increase here with *3 °C*, when the *90 %* transparency criterion is used at a wave-length of *275 nm*.

The scattering (Rayleigh) of almost completely deformed latex particles is caused by the remaining interstices, pores [7]. The size and volume of these interstices depend on the size of the latex particles and the extent of the deformation. *Figure 4.17* shows the calculated transmission spectra of dried latex films with particle sizes varying from *50* to *400 nm*. The dried latex films have a pore-volume of *3 %*, which corresponds to *99 %* deformation of latex particles (*see appendix 5, where the volume of absorbed water has been replaced by the pore-volume*). The transmittance of these latex films decreases fast in the visual wave-length range when the particle size increases. This means that the extent of the deformation of bigger latex particles must be higher than those of smaller latex particles to form evenly transparent latex films. Therefore if the latex coalescence of different latices is characterized by comparing their *MFFT's*, it is necessary that the minimal film formation temperatures are determined at a constant ratio of particle radius and wave-length.

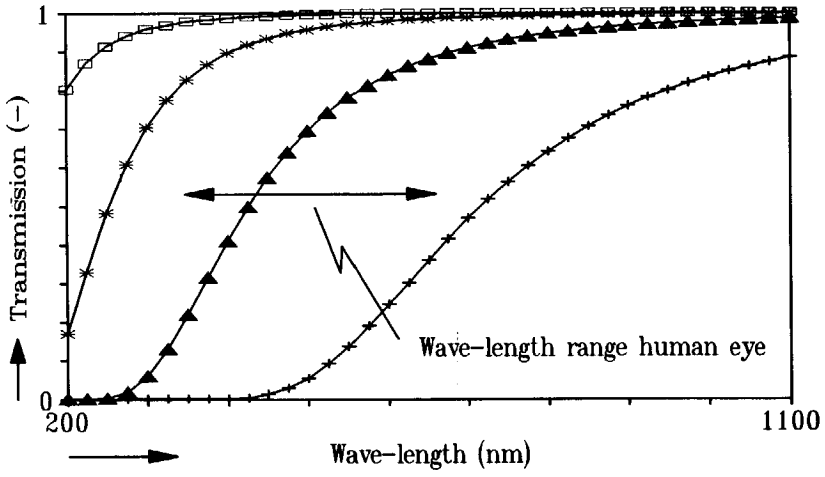

Fig. 4.17 Influence of particle size on the transmission spectra of evenly deformed latex particles (99 %).
□ - r_p = 50 nm, ✱- r_p = 100 nm, ▲ - r_p = 200 nm, + - r_p = 400 nm.

Figure 4.18 shows the influence of the humidity and particle radius on the *MFFT* of the latices B4 and B6. This plot shows that when the humidity decreases the *MFFT* increases. The *MFFT*'s of latices B4 and B6 shift *8 ^oC* and 14 ^oC respectively when the *R.H* decreases from *90* to *10 %*. This increase of the *MFFT* is caused by the decreasing drying time of the latex films at lower *R.H.*; as a consequence the time of coalescence of the latex particles decreases proportionally. In section *4.4.2.* we have found that the *MFFT* corresponds to the *DMTA-T_g* at a frequency reciprocal to the coalescing time. In this case the drying time is decreased by a factor of 10, so that the *DMTA-T_g* increases about *5-10 ^oC*. The latex with the bigger particles (B6) have higher *MFFT*'s than those with the smaller particles (B4). This effect can be explained by the *5 ^oC* higher T_g of latex B6. The conclusion is that the latex B4 particles coalesce at a low humidity much more easily than the latex B6 particles, because the *MFFT* of latex B4 shifts less than that of latex B6, when the humidity decreases from *90* to *10 %*.

Some recent articles make use of the *MFFT* to investigate latex coalescence [44,45]. There it was found that the *MFFT* increases with increasing particle size. Moreover, blending latices of small particles with those of big particles also reduces the *MFFT*'s (*of r_1:r_2=7.3*). This was explained by assuming that bigger latex particles have more resistance against coalescence. This explanation is not fully true, because the *MFFT* was determined by visual interpretation of the transparency of dried latex films. This

means that the *MFFT* of latices with small particles is always lower than that of latices with big particles, because the visual wave-length range of the human eye is limited and constant.

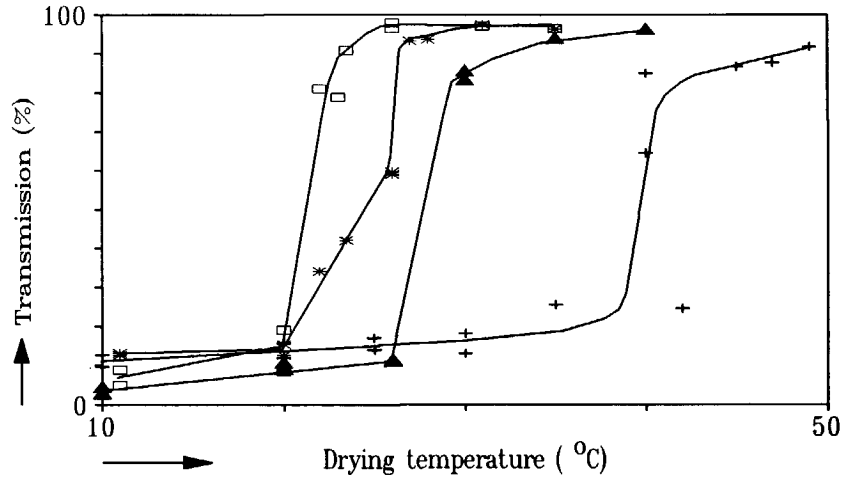

Fig. 4.18 Influence of particle size and relative humidity on the MFFT.
□ - *latex B4 90 % R.H.* λ = *400 nm,* * - *latex B6 90 % R.H.* λ = *500 nm,*
▲ - *latex B4 10 % R.H.* λ = *400 nm,* + - *latex B6 10 % R.H.* λ = *400 nm.*

These blending results can be explained by the fact that lager latex particles disrupt the packing matrix of the small latex particles *(chapter 2)*. This results in bigger interstices, which scatter much more light, so that the *MFFT* increases. It was reported that on adding no more then *0.8 number %* larger particles (*75 wt %*) to the latex with the smaller particles, the *MFFT* of the blend became almost equal to that of the latex with the larger particles.

4.5. CONCLUSIONS

The process of coalescence of latices can be followed accurately by measuring the change in the transmission spectrum during the drying process of a thin latex film. These changes give detailed information of the displacements and deformations of the latex particles during the drying process. This information will be needed to understand the influences of additives and morphology on the film formation process of industrially synthesized latices.

From the change of the interparticle interference of drying latex films it has been found that the latex particles are deformed during the process of coalescence by a bi-

axial mechanism. The wet sintering model of Sheetz gives a satisfactory explanation of the bi-axial deformation mechanism, but the magnitude of his capillary force is not high enough for latex coalescence. Therefore the Sheets model predicts only connectly interparticle contact between latex particles in the z-direction of the *h.c.p.*-unit. When good interparticle contact is established the deformation of the latex particles is then caused by the interfacial contact forces resulting from the radii of curvature between them (Vanderhoff model).

The Vanderhoff/JKR wet sintering model gives the best agreement between the macroscopic viscoelastic properties (*DMTA*) and the calculated viscoelastic properties during the coalescence process of the latex particles. In testing this model, the influence of absorbed water and relative humidity is taken into account, because they lower the viscoelastic properties of our acrylic polymers.

By measuring the interparticle interference of rewetted dried latex films, the deformation behaviour of the latex particles as a function of drying temperature can be investigated. It is found that, when $-e_p^*/r_p$ has been reached a value of *0.09* (V_f=*0.85*), complete deformation of the latex particles follows. This means that from this point on the forces of resistance of particle deformation become lower than the capillary forces. It probably also means that in this temperature range the Young's elastic modulus of the polymer decreases very fast and or the interaction of the separate contact areas, which have been neglected in the wet sintering model, causes a sudden increase of the capillary forces. The sudden increase of the capillary forces must then come from the radii of curvature formed between the interacting contact areas, which will be much smaller than the radii of curvature of the contact areas it self.

The *MFFT* of latices can be determined accurately by using turbidity measurements of dried latex films as a function of drying temperature. The *MFFT* can be used to investigate latex coalescence of different latices by relating their *MFFT*'s, provided the *MFFT*'s used are determined at a constant ratio of particle radius and wave-length.

It is found that the *R.H.* is affecting the *MFFT* of our latices B4 and B6. It was shown that the *MFFT* lowers *8* and *14* ^oC for latices B4 and B6 respectively when the *R.H.* was increased from *10 %* to *90 %*. This effect can be explained by the increasing drying time (coalescing time) of the latex films. Further more, we have found that at very low *R.H.* the latex B4 particles coalesces much more easily than the bigger latex B6 particles.

References

1 Luck, W, Klier, M., Wesslau, H., *Ber. Bunsen-Ges. Phys. Chem.* **67**, 75 (1963).
2 Luck, W, Klier, M., Wesslau, H., *Ber. Bunsen-Ges. Phys. Chem.* **67**, 84 (1963).
3 Hiltner, P.A., Krieger, I.M., *J. Phys. Chem.* **73**, 2386 (1969).
4 Hiltner, P.A., Papir, Y.S., Krieger, I.M., *J. Phys. Chem.* **75**, 1881 (1971).
5 Furusawa, K, Tobori, N., Hachisu, S., *J. Chem. Soc., Faraday Trans.* **84**, 4397 (1988).
6 Tent, A. van, Nijenhuis, K. te, *J. Colloid Interface Sci.* **150**, 97 (1992)
7 Tent, A. van, Nijenhuis, K. te, "Proceedings XVIIth International Conference in Organic Coatings Science and Technology, Luzern, Switzerland, 1991," p. 317.
8 Redknap, *J. Oil. Chem. Assoc.* **49**, 1023 (1966).
9 Imoto, T, *Progress in Organic Coat.* **2**, 193 (1973/1974)
10 Leonardo, R.G., *J. Macromol. Chem., Macromol. Symp.* **35/36**, 389 (1990).
11 Frenkel, J., *J. Phys. (USSR)*, **9**, 385 (1945).
12 Dillon, R.E., Matheson, L.A., Bradford, E.B., *J. Colloid Sci.* **6**, 108 (1951).
13 Brown, G.L., *J. Polym. Sci.* **12**, 423 (1956).
14 Sheetz, D.P., *J. Appl. Polym. Sci.* **9**, 3759 (1965).
15 Mason, G, *Br. Polym. J.* **5**, 101 (1973).
16 Lamprecht, J, *J. Colloid Polym. Sci* **258**, 960 (1980).
17 Menges, G, Schulze-Kadelbach, R., Reichstein, H., Thebing, U., Schmitz, J., *Reol. Acta* **19**, 633 (1980).
18 Vanderhoff, J.W., Tarkowski, H.L., Jenkins, M.C., Bradford, E.B., *J. Macromol. Chem.* **1**, 361 (1966).
19 Hertz, H, *J. für Reine und Angew. Math.* **92**, 156 (1881).
20 Johnson, K.L., Kendall, K., Roberts, A.D., *Proc. R. Soc. Lond. A.* **324**, 301 (1971).
21 Kendall, K, Padget, J.C., *Int. J. Adhesion and Adhesives* **7**, 149 (1982).
22 Anand, J.N., Karam, H.J., *J. Adhesion* **1** , 16 (1969).
23 Anand, J.N., Balwinski, R.Z., *J. Adhesion* **1** , 24 (1969).
24 Anand, J.N., *J. Colloid Interface Sci.* **31** , 196 (1969).
25 Anand, J.N., Dipzinski, L., *J. Adhesion* **2** , 16 (1970).
26 Anand, J.N., *J. Adhesion* **5** , 265 (1973).
27 Savkoor, A.R., "Dry Adhesive Friction of Elastomers," Doctoral Thesis, Delft, 1987
28 Myers, R.R., Schultz, R.K., *J. Appl. Polym. Sci.* **8**, 755 (1964).
29 Chiang, C.P., Rehfeldt, T.K., *J. Coat. Techn.* **58**, 27 (1986).
30 Henry, F., Cansall, F., Guillaume, J.L., Pichot, C., *Coll. Polym. Sci.* **267**, 167 (1989).
31 Sauer, B.B., Stock R.S., Lim, K., Ray, W.H., *J. Appl. Polym. Sci.* **39**, 2419 (1990).
32 Anwari, F, et.al. *J. Coat. Techn.* **62**, 43 (1990).
33 Court, F.H. de la, "Proceedings Xth Fatipec Congress," 1970, p.293.
34 Henson, W., Tabor, D.A., Bradford, E.B., *Ind. Eng. Chem.* **45**, 735 (1953).
35 Isaacs, P.K., *J. Macromol. Chem.* **1**, 163 (1966).
36 Bradford, E.B., Vanderhoff, J.W., *J. Macromol. Chem.* **1**, 335 (1966).
37 Bradford, E.B., Vanderhoff, J.W., *J. Macromol. Sci.-Phys.* **B6**, 671 (1972).
38 El-Asser, M.S., Robertson, A.A., *J. Paint Techn.* **47**, 50 (1975).
39 Roulstone, B.J. Wilkinson, M.C., Hearn, J., Wilson, A.J., *Polym. International* **24**, 87 (1991)
40 Bierwagen, G.P., *J. Coat. Techn.* **51**, 117 (1979).
41 Brodnyan, J.G., Konen, T., *J. Appl. Polym. Sci.* **8**, 687 (1964).
42 Evans, M.E., "Treatise on Coatings. Vol. II part 1"
43 Smith, L.S.A., Schmitz, V., *Polymer* **29**, 1871 (1988).
44 Eckersley, S.T., Rudin, A., *J. Coat. Techn.* **62**, 89 (1990).
45 Jenson, D.P., Morgan, L.W., *J. Appl. Polym. Sci.* **42**, 2845 (1991).

CHAPTER 5

THE PROCESS OF AUTOHESION OF COALESCED LATEX PARTICLES IN DRIED THIN FILMS OF ACRYLIC LATICES.

This chapter will focus on the phenomena that describe the autohesion of the coalesced polymer particles in dried thin films of acrylic latices. When the latex particles are completely coalesced the film becomes transparent. However, when this film is immersed into a *0.1 N HCl* solution, the remaining internal interfacial boundaries between the adherent binder particles will swell, which regenerates an interference pattern. The regenerated interference pattern is directly related to the size and number of the swollen interfacial boundaries. It is tried to relate the turbidity behaviour of swollen latex films with the autohesion theory. Experimental evidence will be given, which supports some of the hypotheses predicted by the theory.

The internal interfacial boundaries between coalesced latex particles were also studied with *TEM*. The *TEM*-photographs revealed the shape of the formed contact area between the coalesced latex particles.

These preliminary measurements give a good description of the internal interfacial boundaries that remain in dried latex films.

5.1. INTRODUCTION

For drying temperatures above the *MFFT* it was found that the latex particles deform into a polyhedric structure. This can be followed clearly from the changing transmission spectrum of a drying latex film (chapter 3). The autohesion process describes the process which causes the individually coalesced latex particles to lose there identity.

In the literature two possible mechanisms to describe the process of autohesion are proposed :

a: Interfacial contact and binding in autohesion, (Anand [1-5], Savkoor [6]). This theory was developped for the case of polymers in a highly viscous state. The rate of contact formation is controlled by the shape of the surfaces in contact, the viscoelastic properties of the polymer and the contact pressure (Hertz). The

establishment of molecular interaction between the surfaces, which have been brought into contact, is treated with a Lennard-Jones potential.

b: Interdiffusion, (Voyutskii [7-10], Bueche [11-13], Skewis [14] and recent articles [15-26]). This theory describes the diffusion of polymer chains across the interfacial boundary of two layers of polymer, which have been brought into contact. The formed transition layer increases the molecular contact area which increases the adhesive strength of the junction.

Over the past several years in the literature much attention has been paid on the process of autohesion, because it has become possible to examine the autohesion at molecular level with *Small Angle Neutron Scattering-SANS* [17-20], *Direct non-radiative Energy Transfer-DET* [21,26] and *marker displacements* [16,25]. The issue here is whether the polymer molecules within each particle in fact diffuse across the particle interfacial boundary during film formation. Early studies by electron microscopy [27-32] have demonstrated that the film formed initially has a honeycomb-like structure. In some cases, the particle interfaces disappeared with time, but in other cases, the interfaces persisted for months or longer. If the interfaces represent the contact areas between the deformed latex particles then it is not unrealistic to conclude that interparticle diffusion takes place or that an intermolecular polymer interface is formed in the former case but not in the latter.

5.2. AUTOHESION THEORIES

As long as all the water has not been evaporated the deformation energy, which generally will be needed for the deformation of the coalescing polymer particles, will be supplied by the cohesive energy and the capillary energy. When all the water has been evaporated the latex coalescence will be almost complete and only the cohesive energy remains. Diffusion of polymer chains over the contact area [7-26] and/or the forming rate of the intermolecular interface by viscous flow decrease the cohesive free energy. The cohesive energy is a function of the mobility of the main chain and the contact time and also of the cohesive energy between the diffused polymer and the bulk polymer.

5.2.1. Interfacial Contact and Bonding in Autohesion [1-6]

When the particles finally have deformed completely, the occurring internal stresses will try to relax. The particles will stay together when the $|$*cohesive energy*$|$ is

higher then the |*stress energy*|. The cohesion energy is obtained from the surface free energy. The energy needed to create two new identical polymer surfaces is called cohesive energy and is given by :

$$\Delta G = 2.\gamma_1 \tag{1}$$

Where γ_1 is the interfacial energy (J/m^2) between the polymer and the surrounding medium. The force-separation relation of the interaction between macroscopic solids can be described by the *3-9* Lennard-Jones potential (*Fig. 5.1*). This potential can be expressed by the force per unit area of the interacting surfaces :

$$F(z) = \frac{A_h}{6.\pi.z_0^3}.\left[\left(\frac{z_0}{z}\right)^3 - \left(\frac{z_0}{z}\right)^9\right] \quad (N/m^2) \tag{2}$$

where A_h is the Hamaker's constant, z_0 is the separation of the surfaces, where the interaction energy is minimal. The work W(z,∞) is the specific work of adhesion per unit area, which must be exerted to separate the two different surfaces 1 and 2. Hence,

$$W(z_0,\infty) = \gamma_1 + \gamma_2 - \gamma_{12} = -\int_{z_0}^{\infty} F(z)\, dz = \frac{A_h}{16.\pi.z_0^2} \tag{3}$$

The force of attraction between two surfaces attains its maximum at $1.2*z_0$ (See *Fig. 5.1*).

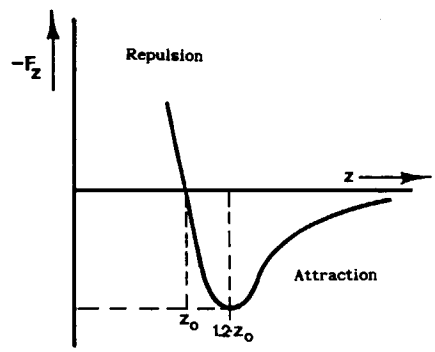

Fig. 5.1 Representation of a 3-9 Lennard-Jones force-separation relation between interacting macroscopic solids.

The attractive force per unit area can be calculated with the Lennard-Jones Eq.(2). For that purpose the values of the intermolecular spacing and Hamaker's constant must be known. The Hamaker's constant A_h depends on many molecular parameters [33]. From the refractive index, molecular weight and density of the polymer the value of the Hamakers constant can be estimated, which results in $A_h \approx 2.10^{-20}$ *J* for our *65:35 MMA/BA* copolymer latex. With the Hamaker's constant and the surface energy of the polymer the intermolecular spacing can be calculated, which results in $z_0 \approx 0.22$ *nm*.

Substituting these values into the Lennard-Jones Eq. (2) results in an attractive force per unit area of about 3.10^7 N/m^2. This calculated value of the attractive force corresponds very well to the value of the cohesive strength of *PMMA* listed in the Polymer Handbook (4.10^7 to 11.10^7 N/m^2).

The particles will rebound when the particles are not sufficiently attracted or bonded to resist the internal stresses, as a consequence cracks will be initiated in the drying latex film. These cracks propagate under the release of internal stresses, until the cohesion energy matches the stress energy. For pure elastic deformations the internal stresses of the particles equals the Young's elastic modulus of polymer [34,35].

The results of a latex coalescence experiment can be seen in *Fig. 4.12*, in which the just admissible Young's elastic modulus (Vanderhoff/JKR model) of the latex particles as function of drying temperature is given. From it, the Young's elastic modulus of the latex particles can be determined when the dried latex film becomes homogeneous and crack free. In this case the Young's elastic modulus lies between 1.10^7 and 6.10^7 N/m^2. This means that when the Young's elastic modulus of the latex particles becomes of the order of the calculated attractive force (3.10^7 N/m^2) no more cracks will be initiated in the drying latex film.

5.2.2. Interdiffusion

When the particles deform a polymer interfacial contact area will be formed. Polymer chains or segments will try to cross the interface, resulting in an increase of cohesive strength. To get a good cohesional strength between the deformed latex particles it is assumed that a penetration depth of a few chain segments ($\kappa \approx 1$ *nm*) is necessary.

5.2.2a. Self-diffusion Theories

Bueche and co-workers [11-14] have found a simple relationship between self-diffusion

constant and the bulk viscosity data for polymer molecules at temperatures at T_g and above, which resulted in :

$$\mathbb{D}.\eta = \frac{\rho.R.T}{36}.\frac{<r^2>}{M} \tag{4}$$

where $<r^2>$ is the average square of the end-to-end polymer chain distance, ρ the density of the polymer and M the molecular weight. The diffusion constant can also be used to calculate the diffusion length from the segmental mobility of the freely orienting chain segments, which is given by :

$$\kappa_p = \sqrt{2.\mathbb{D}.t} \tag{5}$$

where κ_p is the distance (m) of the movement of the centre of a molecule over a time interval of t (s). Bueche's Eqs. 4 and 5 make it possible to estimate the magnitude of the self-diffusion constant and the rate of autohesion. The average square of the end-to-end polymer chain distance is given by [39]:

$$<r^2>/(2.N.l^2) = C \tag{6}$$

where C is a constant, l is the length of a C-C-unit and N is number of monomers in a polymer chain.

The values for C, N and l corresponding to latex B4 are respectively *6.9*, *4482* and *0.154 nm* [39]. The viscosity of polymers at T_g is about 10^{12} *Pa.s* [35]. Substituting these values into Eq. 4, yields for $\mathbb{D}$ a value of $2.4\ 10^{-25}$ m^2/s. To get a good cohesional strength between the deformed latex particles it is assumed that a penetration depth of a few chain segments ($\kappa_p \approx 1$ *nm*) is necessary. The calculated time needed for this penetration will than be about 2.10^6 *s*.

More recently is the theory of reptation proposed by De Gennes, which describes the one-dimensional translational motion of a chain in the presence of fixed obstacles, due to the propagation of kinks along its length [25,40-42]. The time (τ_r) required for the chain to disengage from its original conformation by reptation increases as M^3, and is given by :

$$\tau_r = N.\ell^2/(3.\pi^2.\mathbb{D}^*) \tag{7}$$

where ℓ is the segment length and $\mathbb{D}^*$ is the self-diffusion constant based on reptation.

There have been some experiments performed to measure the molecular weight dependence of $\mathbb{D}^*$. Skewis [14] measured the displacement (κ) as function of time, temperature and molecular weight. He found that there were no major differences of self-diffusion constants between different types of linear polymers of comparable molecular weights *($T-T_g=Constant$)*. He and others [15-26] found that $\mathbb{D}^*$ scales as N^{-2}.

Green [16] used marker displacements measurements to measure the Polymer(A)-Polymer(B) interdiffusion. He found that the marker displacement is related to the self-diffusion constant of the polymer with the lowest molecular weight and is given by :

$$\kappa_m = C\sqrt{\mathbb{D}^*.t} \tag{8}$$

This technique depends on the net mass transport across the interface. When the polymer molecular weight of polymer (A) and (B) are equal, the net mass transport is zero and no marker movement is perceptible, so that C becomes 0. Otherwise, when the molecular weight of polymer (A) is much lower than that of polymer (B), then polymer (A) will diffuse into polymer (B) and C becomes 0.48. Reiter [25] found, with the same technique, that the polymer with the low molecular weight diffuses across the interface after an induction period close to the reptation time (τ_r) of the polymer. This means that actual interdiffusion starts after an inhibition close to the reptation time. Reiter measured for a *PS* polymer with a molecular weight close to our polymer (B4, 493 *kg/mol)* by using the N^{-2} dependence, a self-diffusion constant of $3.5\ 10^{-23}\ m^2/s$ and a reptation time of $1.6\ 10^6\ s$ at a temperature around the T_g of *PS*.

De Gennes pointed out that in the beginning of the diffusion process only those molecules that have a chain end at the interface, can diffuse across this interface. Only after a period equal to the the reptation time the other molecules have the possibility to cross the interfaces. This means that the process of autohesion by interdiffusion for our high molecular weight latices is only important for temperatures far above T_g or for ageing times in the order of weeks at temperatures around T_g ($t > \tau_r$).

5.2.2b. Experimental Evidence from the Literature

Many papers have been published on the interdiffusion of polymer molecules or segments between two contacting latex particles [1-26]. The observed kind of behaviour of interdiffusion show many contradictions with regard to the tack strength. For instance, Skewis [14] observed that tacked natural rubber strips instantaneously have a

tack strength equal to the tensile strength, which could not be related to the measured diffusion rate of 10^{-17} m^2/s. This does not mean that diffusion does not take place at all. Voyutskii [10] unambiguously showed that interdiffusion really plays an important role in the formation of adhesive joints between contacting particles. He postulated that interdiffusion increases the molecular contact area, which will lead to an increase of the tack strength. He also observed that the tack strength increased when the contact pressure was increased. However, this effect can not be explained by interdiffusion, because with increasing pressure the T_g of polymers increases about *0.024 K/atm* [34]. In antithesis with Voyutskii's theory, Anand [5] postulated that interdiffusion can only take place when the surfaces are brought together, so that intermolecular (cohesion) forces can play an important role. The contribution of interdiffusion to the adhesion (tack) strength seems insignificant, because diffusion at the interface only results in a rearrangement of molecules. Anand stated that the rate of contact formation (tack) will primarily depend on the degree of contact between the surfaces, which mainly depends on viscosity and contact pressure of the contacting sheets.

Which of these theories describes the tack phenomena well, will depend on the contribution of entanglements to the cohesion strength of the bulk polymer. If this contribution is large Voyutskii's theory describes the tack phenomena well enough, otherwise Anand's theory should be used. However, the question still remains whether these theories describe the autohesion process (how the latex particles lose there identity) of our acrylic latices.

5.3. EXPERIMENTAL

5.3.1 Materials

The latices B4 and B6 were synthesized in a semi-continue emulsion polymerization process. The binder of the latices consists of a copolymer of Butyl Acrylate (*BA*) and Methyl Methacrylate (*MMA*) in a mass ratio of *35:65*. All latices used are stabilized by Sodium Dodecyl Benzene Sulfonate (*SDBS*). The polymerizations were initiated by sodium peroxydisulfate. The physical parameters and chemical compositions of the latices are given in *Table 3.1.*

5.3.2 Transmission Spectrophotometry

The process of autohesion of dried thin films of latices was investigated with

transmission spectrophotometry. Therefore thin films of the acrylic latices were dried in a conditioned room above their *MFFT* on *55 μm* thick *PMMA*-sheets *(30*15 cm)*. After a certain drying and ageing period the coated *PMMA*-sheets were cut into identically round plates of *4 cm* in diameter, which are immersed into a *0.1 N HCl* solution. The transmission spectrum of the swollen coated plates were measured with the aid of a spectrophotometer *(Shimadzu UV-160)*. The amount of water absorption is found by measuring the weight of the swollen and dried plates with the aid of an analytical balance *(Mettler AM-100)*.

5.3.3. TEM

The TEM photographs were made of very diluted latices dried on grids at room temperature.

5.4 RESULTS AND DISCUSSIONS

5.4.1. Swelling Behaviour of the Remaining Internal Interfacial Boundaries.

The dried latex films become transparent when they are dried above the *MFFT*. The sizes of the possible remaining interfaces are so small that they will hardly scatter any light in the region of the visible light. When these films are immersed into an aqueous *0.1 N HCl* solution, the remaining interfaces will swell. This regenerates the scattering properties, which reveal the number and size of the remaining interfaces. The idea is that when interdiffusion (Voyutskii) or the rate of formation of molecular interaction (Anand) take place, the number of interfaces decreases so that the regenerated scattering properties will change. Then the decrease of interfaces with time is a possible measure for the interdiffusion rate of the polymers or the rate of formation the intermolecular interfaces, as a result of viscous flow.

To describe the scattering properties of swollen latex films, the multilayer interference theory and Rayleigh's scattering theory, based on ellipsoid-like swollen interfacial boundaries, have been used (see appendices IV and V). *Figure 5.2* shows how theoretically the transmittance should behave as function of the volume fraction immersed *HCl*-solution *(immersion pattern)* for different fractions of remaining interfaces (N_f). The immersion pattern declines more rapidly when the number of interfaces decreases, because the same amount of absorbed water will now be divided over less remaining interfaces, which results in bigger pores.

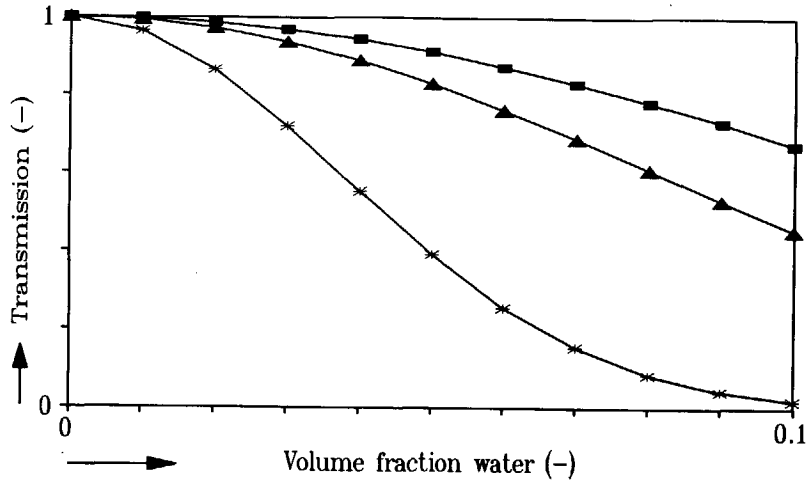

Fig. 5.2 Theoretical immersion patterns of dried latex B4 films with the Rayleigh scattering theory based on the remaining fraction of swollen ellipsoid-like internal interfacial boundaries.
■ - N_f = 1, ▲ - N_f = 0.5, ✱ - N_f = 0.1 .

Figure 5.3 shows how the transmittance changes of *1* and respectively *24* hours aged latex B4 films, when they are immersed into an aqueous *0.1 N HCl*-solution. The films were dried and aged at a temperature of *35 °C*. The transmittance data are taken at *400 nm* and the film thickness is normalized to *80 μm* with the Lambert-Beer's relationship. The immersion pattern is fitted with the Rayleigh's scattering model for elliptically shaped swollen internal interfacial interfaces (*see appendix V*). It shows that both of the experiments can be fitted with a fraction of remaining interfaces (N_f) of 1. This means that all the interfaces between the deformed latex particles are intact and that autohesion of the dried latex film was *not improved* over a period of *24* hours.

Figure 5.4 shows a plot of *ln* (n_d/λ_{min}) against *ln* (V_f), which reveals the dependence of the interparticle interference on the packing volume fraction. The data is fitted with the least squares root method, which resulted in a slope of 0.93. Theoretically, if the swelling is three-dimensional (*isotropic*) a slope of $^1/_3$ would be expected, and if the swelling is in one direction a slope of *1*. The figure clearly shows that the unidirectional swelling gives an accurate description of the swelling behaviour of latex B4. This unidirectional swelling behaviour is equal to the bi-axial deformation behaviour of the latex particles.

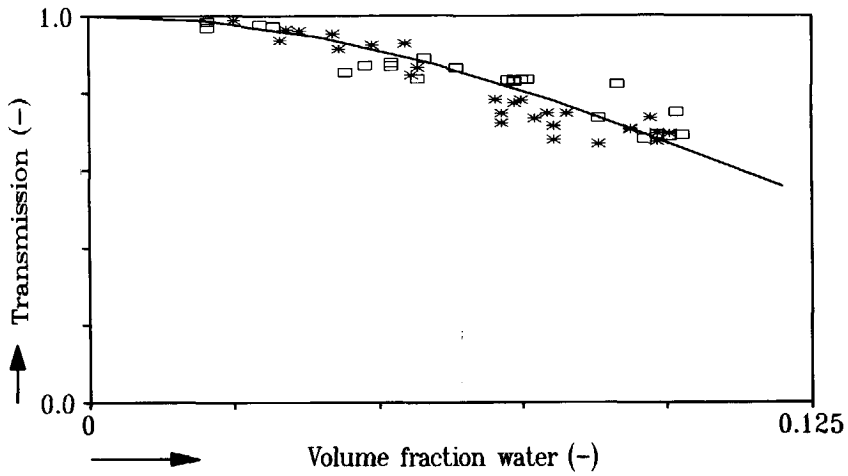

Fig. 5.3 The immersion patterns of 1 and 24 hours dried latex B4 films at 35 °C. ✳- drying time 1 hour, □ - drying time 24 hours, —— - Ray. scat. model ellipt. swollen interstices with N_f = 1.

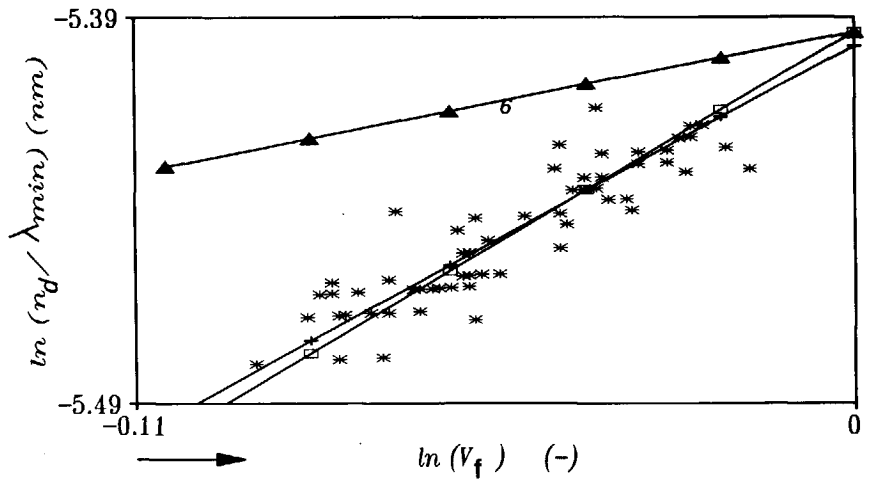

Fig. 5.4 The interparticle interference (n_d/λ_{min}) change of immersed dried latex B4 film as function of volume fraction absorbed water. ✳ - immersion experiments, □ - bi-axial swelling, ▲ - isotropic swelling, + - linear regression.

5.4.2. Internal Interfacial Boundaries Studied with TEM

In this section the interfacial boundaries between coalescing latex particles are shown in detail in a *TEM*-photograph. This photograph revealed dark elliptical shapes at the interfacial contact area of the coalesced latex particles, which were interpreted as emulsifier molecules concentrated around the area of contact.

Some early studies [27-32,36] done with *SEM* and *TEM* techniques suggested that the initially formed latex film has a polyhedric structure and that commonly these interfacial boundaries disappeared with time. *Figure 5.5* shows a *TEM*-picture of the internal interfacial boundaries between coalescing latex particles of latex c8 (*see Table 2.III*). The hexagonally packed latex particles in the middle of the picture are coalesced partly and the individually particles are still visible by the sharp dark stripes at there contact areas. The question is if these dark stripes represent the interfacial boundaries between the latex particles. If the interfacial boundaries in the *TEM*-photograph are studied in more detail, we can make out that the dark stripes are elliptically ring-shaped (Because the photograph is a projection of the latex particles, the elliptical ring-shape is caused by the projection of the contact area under a different angle). This would mean that the elliptical dark stripes are caused by the material at the perimeter of the contact area, otherwise the elliptical shape would be completely dark. The only explanation we could think of is that the emulsifier molecules, which are present at the surfaces of the contacting latex particles, are forced to the perimeter of the contact area during latex coalescence. This results in a high emulsifier concentration at the perimeter, which causes the dark stripes between the latex particles in the *TEM*-picture.

This means that during latex coalescence the emulsifier at the surfaces of the latex particles is collected at the edges of the formed polyhedrical structure. This results in internal interfacial boundaries situated at the edges of the polyhedric structure of the coalesced latex particles, which prevents complete polymer-polymer interfacial contact. These boundaries will swell easily in water, because of the high content of the hydrophilic emulsifier. In the previous section it was found that these internal boundaries did not disappear with time. This means that emulsifier remains in the latex film, even after an ageing time of *24* hours. This also means that the internal interfacial boundaries can only disappear when the emulsifier molecules disappear by migration or oxidation [37,38], and that they do not disappear by the polymer-polymer interfacial contact formation or polymer interdiffusion phenomena.

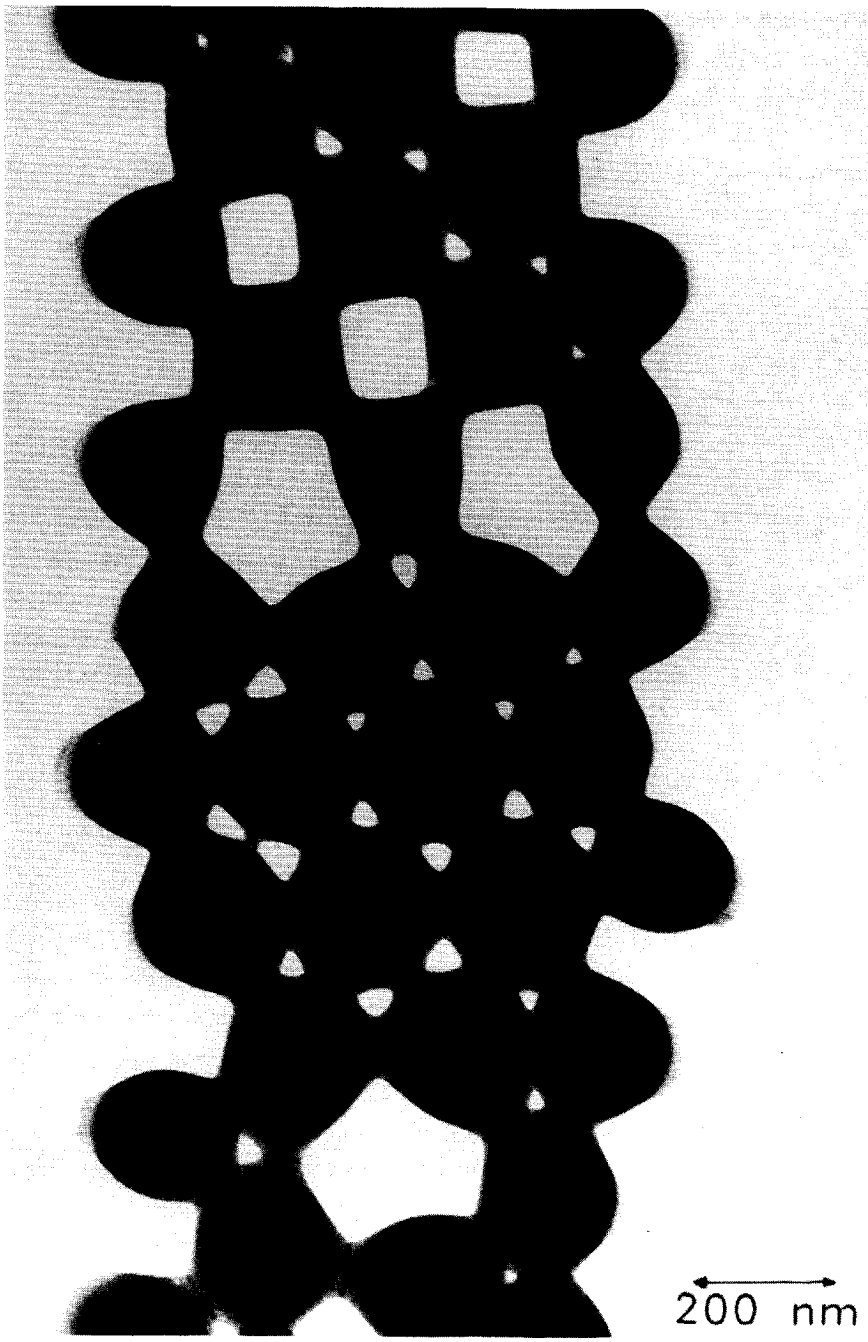

Fig. 5.5 TEM-photograph of coalesced latex particles

5.5. CONCLUSIONS

The swelling behaviour of dried and aged latex films is unidirectional. The unidirectional swelling behaviour is equal to the bi-axial deformation behaviour of the latex particles. The immersion pattern (transmittance versus amount of absorbed water) can be described accurately with Rayleigh's scattering theory for ellipsoid-like swollen internal interfacial boundaries.

The emulsifier at the surfaces of the latex particles is collected at the edges of the formed polyhedrical structure during latex coalescence. This causes internal interfacial boundaries, because good polymer-polymer interfacial contact is prevented.

The resulting transparent latex film of completely coalesced latex particles will swell when immersed into water, due to the high emulsifier content in the remaining internal interfacial boundaries. The possible disappearance of these internal boundaries, caused by the disappearance of the emulsifier molecules during ageing, increases the autohesion of the dried latex film. This means that interdiffusion of the polymer molecules over the interfacial boundary or that the rate of formation of molecular interaction not responsible are for the autohesion process of a dried latex film. It has been found that the fraction of remaining internal interfacial boundaries does not decrease with time and that the latex film absorbs maximal *10 %* of water. This means that emulsifier remains in the dried latex film and the adhesion between the deformed latex particles prevents that more than *10 %* water can be absorbed.

Hence, it is not unrealistic to conclude that the autohesion process (by which the latex particles lose there identity) is determined mainly by the disappearance of the emulsifier molecules from the dried latex film. Wherever any of the internal interfacial boundaries should disappear polymer-polymer contact will be established, so that polymer-polymer intermolecular contact formation and/or polymer interdiffusion phenomena can take over to increase the overall strength of the dried latex film. However, the question still remains whether the intermolecular contact formation and/or polymer interdiffusion phenomena play an important role in the film formation process of latex films.

References

1 Anand, J.N., Karam, H.J., *J. Adhesion* **1** , 16 (1969).
2 Anand, J.N., Balwinski, R.Z., *J. Adhesion* **1** , 24 (1969).
3 Anand, J.N., *J. Colloid Interface Sci.* **31** , 196 (1969).
4 Anand, J.N., Dipzinski, L., *J. Adhesion* **2** , 16 (1970).
5 Anand, J.N., *J. Adhesion* **5** , 265 (1973).
6 Savkoor, A.R., "Dry Adhesive Friction of Elastomers," Doctoral Thesis, Delft, 1987

7 Voyutskii, S.S., Margolina, Yu.L., *Rubber Chem. Techn.* **30**, 531 (1957).
8 Voyutskii, S.S., Shtarkh, B.V., *Rubber Chem. Techn.* **30**, 548 (1957).
9 Voyutskii, S.S., Vakula, V.L., *J. Appl. Polym. Sci.* **7**, 475 (1963).
10 Voyutskii, S.S., *J. Adhesion* **3**, 69 (1971).
11 Bueche, F, Cashin, W.M., Debye, P., *J. Chem. Phys.* **20**, 1956 (1952).
12 Bueche, F, *J. Chem. Phys.* **20**, 1959 (1952).
13 Vinogradov, G.V., Malkin, A.Ya., "Rheology of Polymers," Springer Verlag, New York 1980, p. 153-167.
14 Skewis, J.D., *Rub. Chem. Techn.*, 217 (1966).
15 Gent, A.N., Vondráçek, P., *J. Appl. Polym. Sci.* **27**, 4357 (1982).
16 Green, P.F., Palmström, C.J., Mayer, J.W., Kramer, E.J., *Macromolecules* **18**, 501, (1985).
17 Hahn, K., Ley, G., Schuller, H., Oberthür, R., *J. Colloid Polym. Sci* **264**, 1092 (1986).
18 Hahn, K., Ley, G., Oberthür, R., *J. Colloid Polym. Sci.* **266**, 631 (1988).
19 Linné, M.A., Klein, A., Miller, G.A., Sperling, L.H., Wignall, G.D., *J. Macromol. Sci.-Phys. Ed.* **B27**, 217 (1988).
20 Stamm, M., Brautmeier, D., Reiter, G., Foster, M., Hüttenbach, S., *SPE Antec* **36**, 825 (1990).
21 Wang, Y., Winnik, M.A., *Macromolecules* **23**, 4731 (1990)
22 Hess, W., Nägele, G., Akcasu, A.Z., *J. Polym. Sci. Polym. Phys. Ed.* **28**, 2233 (1990).
23 Saeki, S., Tsubokawa, M., Yamanaka, J., Yamaguchi, T., *Polymer* **31**, 2338 (1990).
24 Davis, P.J., Pinder, D.N., *Macromolecules* **23**, 5176 (1990).
25 Reiter, G., Hüttenbach, S., Foster, M., Stamm, M., *Macromolecules* **24**, 1179 (1991).
26 Wang, Y., Zhao, C., Mitchell, A.W., *J. Chem. Phys.* **95**, 2143 (1991).
27 Henson, W., Tabor, D.A., Bradford, E.B., *Ind. Eng. Chem.* **45**, 735 (1953).
28 Isaacs, P.K., *J. Macromol. Chem.* **1**, 163 (1966).
29 Bradford, E.B., Vanderhoff, J.W., *J. Macromol. Chem.* **1**, 335 (1966).
30 Bradford, E.B., Vanderhoff, J.W., *J. Macromol. Sci.-Phys.* **B6**, 671 (1972).
31 El-Asser, M.S., Robertson, A.A., *J. Paint Techn.* **47**, 50 (1975).
32 Roulstone, B.J. Wilkinson, M.C., Hearn, J., Wilson, A.J., *Polym. International* **24**, 87 (1991)
33 Hiemenz, P.C., "Principles of Colloid and Surface Chemistry," M. Dekker Inc., New York, 1986, p. 611-676.
34 Ferry, J.D, "Viscoelastic Properties of Polymers." Wiley, New York, 1961.
35 Nielsen E.L., "Mechanical Properties of Polymers and Composites." M. Dekker, Inc. New York, 1974.
36 Jenson, D.P., Morgan, L.W., *J. Appl. Polym. Sci.* **42**, 2845 (1991).
37 Zhao, C.L., Holl, Y., Pith, T., Lambla, M., *Colloid Polym. Sci.* **265**, 823 (1987).
38 Zhao, C.L., Dobler, F., Holl, Y., Pith, T., Lambla, M., *J. Colloid Interface. Sci.* **128**, 437 (1989).
39 Flory, P.J., "Statistical Mechanics of Chain Molecules " Wiley, New York, 1969.
40 De Gennes, P.G., *J. Chem. Phys.* **52**, 572 (1971).
41 Klein, J., *Macromolecules* **5**, 852 (1978).
42 Klein, J., *Macromolecules* **14**, 460 (1981).

CHAPTER 6

INFLUENCE OF CORE-SHELL MORPHOLOGY ON LATEX COALESCENCE

Core-shell morphology in latices has been used to improve the latex coalescence and the elastic properties of the finally dried latex film. If the core consists of a hard polymer and the shell of a soft polymer, then latex coalescence will mainly be determined by the shell material and the firmness of the finally dried latex film depends on elastic properties of a matrix of core material in a continuous phase of shell material. This would mean that latex coalescence is not affected by the core material. So, cheap polymer materials or other fillers in the core can be introduced without affecting the film formation process of the latices.

The core-shell morphology has been characterized with *DSC*, *MFFT*, *turbidity measurements* and if possible with *TEM*. Also soap titrations were used to determine the chemical composition on the surface of the core-shell polymer particles. These initial measurements have shown that core-shell polymer particles can be made of *PS* and *PBMA* respectively. However, the coalescence properties could not be related to a shell with pure *PBMA*. There are indications that the shell material did not consist of *100 % PBMA*. Further we found that the core is affecting the coalescence of the core-shell latex particles when the thickness of the shell is thin, because the visual *MFFT* of these latices decreases when the thickness of the shell increases. The *MFFT* as a function of the gross chemical composition of core and shell polymer coincidently corresponds to the theoretical copolymer T_g *(Fox)*, in the range of $0 < PS < 55$ *vol%* .

6.1. INTRODUCTION

This study was done in cooperation with the DSM-Resins company in The Netherlands, which had as a goal to synthesize and characterize a core-shell latex. The synthesizing methods used are seeded emulsion polymerization and shot-growth emulsion polymerization. The morphology of two-staged latex particles has been extensively studied by *SEM/TEM* techniques [1-16], but also other techniques were used, like *Soap titration* [17-19], *MFFT* [20-22], *DSC/DMTA* [23-27], *SANS* [28,29] and *turbidity measurements* [30-34]. This chapter will mainly focus on the core-shell characterization

by turbidity measurements. The techniques *TEM, DSC, MFFT, QELS* and *Soap titration* are only used to support the results found from the turbidity behaviour of drying core-shell latices.

The transmission spectrum (*UV-Vis*) is measured during the drying process of a thin film of latex. The changing scattering properties of the drying latex film reveal the internal displacements of the polymer particles [*chapter 2*,31,32]. When the particles flocculate or make contact and deform the changing scattering properties reveal the deformation time and the extend of the deformation from which the elasticity of the particles can be calculated [*chapter 4*]. This typical deformation behaviour can give information about the morphology of the core-shell particle. The coalescence process of drying core-shell latices can be divided into three regions, viz. (*Fig. 6.1*):

a) In the first region the core-shell latex particles are not deformed. This results in a crumble/powder-like film.
b) In the second region the core-shell latex particles are deformed partly;
c) In the third region the core-shell latex particles have deformed completely. The resulting latex film consists of a matrix of core material in a continuous phase of shell material.

The finally dried latex film is transparent when the refractive indices of the core and shell material are the same, but when the refractive indices are different the transmittance in the *UV-Vis* region depend on the amount of Rayleigh scattering. The amount of scattering depend on the core size and interparticle distance (shell size) in relation to the wave-length of the incident light.

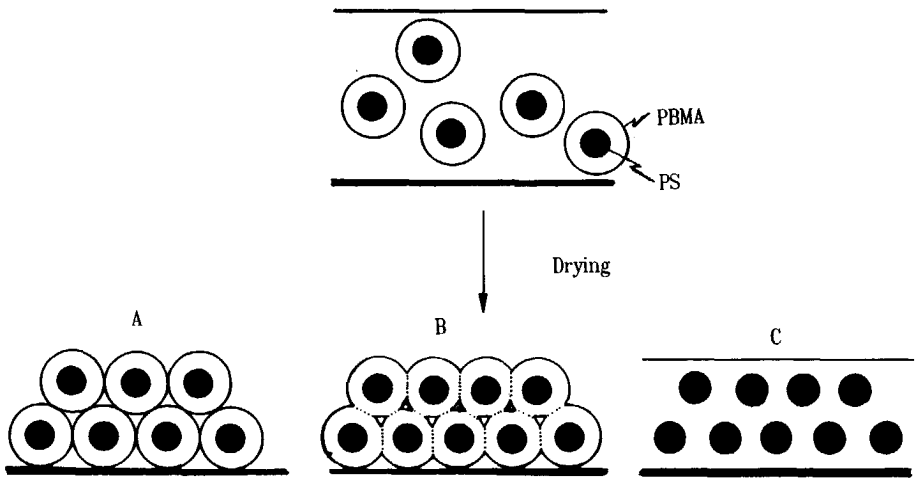

Fig. 6.1 The coalescence process of core-shell latices.

6.2. SYNTHESIZED MATERIALS

From the literature survey, the following conclusions were drawn to get a good core-shell morphology from seeded emulsion polymerization and shot-growth emulsion polymerization. In a two-stage polymerization of monomer II in the presence of polymer seed I we get a core-shell morphology [15], when polymer II is miscible with polymer I and when polymer II has equal or higher hydrophilicity than polymer I, then polymer II-rich outside layers will be formed. When the seed-latex is crosslinked, more grafting between polymer I and polymer II occurs due to the better overcoating of polymer II [8]. Seeded emulsion polymerization yields a lower percentage of grafting than shot-growth emulsion polymerization [9,10].

The latices used in this study, were synthesized in a semi continuous emulsion polymerization process. The polymerizations were carried out in a 1000 *cc* temperature controlled tank-reactor, equipped with a reflux condenser, nitrogen inlet, stirrer and pre-emulsion inlet. Seeded and shot-growth emulsion polymerization was carried out to overcoat *PS* and crosslinked *PS* with *PBMA*. The crosslink density of the *PS*-seed and the *PBMA* content were varied. The conversions were between *92* and *99 %*. These synthesized concentrated latices show normally very beautiful coloured light patterns, due to interparticle interference. These light patterns will disappear when other particles of a different sizes are added [32]. So if these light patterns disappear during seeded or shot growth emulsion polymerization, then it is most likely that there has been a secondary nucleation of a new crop of stable particles. In some cases this occurred, but these latices were not used.

6.2.1. Procedure Seeded Emulsion Polymerization

Seed latex.

a) Inlay; The tank was filled with *300 ml* water with some dissolved *SDBS*. The particle size of the synthesized latex is controlled by the amount of *SDBS* in the inlay when all other parameters are held constant during the emulsion polymerization process. Then the inlay is heated up to *80 ^{o}C*.

b) Pre-emulsion; The pre-emulsion consisted of *400 g Styrene* (Core monomer to which sometimes some *DVB* (crosslinker) is added), *100 g H_2O* and *8.5 g SDBS*. The pre-emulsion was stirred until a stable viscous emulsion was obtained.

c) Initiator; The initiator consisted of *1.3 g $(NH_4)_2S_2O_8$* dissolved in *10 g* of water.

When the inlay reached a temperature of *80 ^{o}C*, the initiator was added to the reactor. After one minute the pre-emulsion was dosed to the reactor over a period of

2.5 hours. After that, the temperature was increased to 87 ^{o}C for a period of 1 hour (*to get 100 % conversion*). Then the reaction mixture (*seed-latex*) was cooled slowly to room temperature. The physical parameters and chemical compositions of the seed latices are given in *Table 6.I.*

Core-shell latex

The core-shell latex is made from the prepared seed latex with the same seeded emulsion polymerization procedure.

a) Inlay; The tank was filled with *300 g* Seed-latex and *70 g* water.

b) Pre-emulsion; The pre-emulsion consisted of X *g Shell-monomer* (X depends on the wanted shell thickness), *40 g* H_2O and *1.5 wt %* of *shell-monomer* content *SDBS*.

c) Initiator; The initiator consisted of *0.25 g* $(NH_4)_2S_2O_8$ dissolved in *5 g* of water.

The pre-emulsion was dosed to the reactor over a period of *1.5* to *2* hours, which depended on the amount of pre-emulsion. The physical parameters and chemical compositions of the core-shell latices are given in *Table 6.I.*

Table 6.I Composition and Physical Properties Seeded Emulsion Polymerization

Seed latex	*P8*	*P12*	*P13*	*P16*	*P17*	*P21*	*P22*
Monomer	*S*	*BMA*	*S*	*S*	*S*	*S*	*S*
DVB (wt %)	-	-	*2*	*5*	*10*	*2*	*2*
SDBS (wt %)	*2*	*2*	*2*	*2*	*2*	*2*	*2*
d_p *(nm)*	*199*	*195*	*173*	*186*	*208*	*191*	*155*
W_f *(nm)*	*44.2*	*48.9*	*45.9*	*47.5*	*45.5*	*47.9*	*48.2*

Core-shell latex	*P9*	*P10*	*P14*	*P15*	*P18*	*P19*	*P24*	*P25*	*P26*
Seed latex	*P8*	*P8*	*P13*	*P13*	*P16*	*P17*	*P21*	*P21*	*P22*
Shell monomer	*BMA*	*BMA*	*BMA*	*BMA*	*BMA*	*BMA*	*BMA*	*BMA*	*BMA*
SDBS	*1.7*	*1.7*	*1.7*	*1.3*	*1.6*	*1.6*	*1.2*	*1.1*	*1*
d_p *(nm)*	*223*	*237*	*210*	*222*	*232*	*265*	*273*	*295*	*265*
W_f *(wt %)*	*46.0*	*45.3*	*49.0*	*50.2*	*48.5*	*47.8*	*44.7*	*45.5*	*48.7*

6.2.2. Procedure Shot-growth Emulsion Polymerization

The shot-growth procedure is almost the same as the seeded procedure. First the inlay is heated up, when it reached a temperature of *80* ^{o}C the initiator was added to the reactor. After one minute a pre-emulsion with the core monomer is dosed to the reactor. After all the core monomer is added to the reactor a second pre-emulsion with the shell monomer was directly dosed to the reactor. The physical parameters and chemical compositions of the shot-growth latices are given in *Table 6.II.*

Table 6.II Composition and Physical Properties Shot-growth Emulsion Polymerization

Latex	*P30*	*P31*
Pre-emulsion 1		
Monomer	*S*	*S*
DVB (wt %)	*2*	*2*
SDBS (wt %)	*2.9*	*2.9*
Pre-emulsion 2		
Monomer	*BMA*	*BMA*
SDBS	*1.4*	*1.8*
W_f *(core/shell) (wt %)*	*1.126*	*0.561*
d_p *(nm)*	*160*	*155*
r_{cs}/r_c *(-)*	*1.29*	*1.41*
W_f *(%)*	*47.3*	*----*

6.3. CHARACTERIZATION CORE-SHELL MORPHOLOGY

6.3.1. Particle Size

By measuring the particle size of the seed (*core*) latex and its corresponding core-shell, the ratio of the core and shell size can be determined. Three different techniques were used to verify the particle sizes, viz. *QELS, SEM/TEM* and interparticle interference. The results are shown in *Table 6.III.*

Table 6.III Core-Shell Particle Sizes Determined with Different Techniques.

Seed emulsion polymerization			*Theoretical*	*QELS*		*TEM/SEM*		*Interparticle Interference*	
Seed Latex		*Core/Shell Latex*	r_{cs}/r_c	r_c *(nm)*	r_{cs}/r_c	r_c *(nm)*	r_{cs}/r_c	r_c *(nm)*	r_{cs}/rc
P8	→	*P9*	*1.11*	*117*	*1.11*	*100*	*1.05*	*99*	*1.12*
		P10	*1.19*		*1.13*		*1.10*		*1.19*
P13	→	*P14*	*1.23*	*104*	*1.03*	-	-	*86*	*1.21*
		P15	*1.28*		*1.07*		-		*1.28*
P16	→	*P18*	*1.23*	*102*	*1.13*	-	-	*93*	*1.25*
P17	→	*P19*	*1.23*	*111*	*1.26*	-	-	*104*	*1.27*
P21	→	*P24*	*1.42*	*108*	*1.35*	-	-	*95*	*1.43*
		P25	*1.57*		*1.50*		-		*1.55*
P22	→	*P26*	*1.72*	*90*	*1.61*	-	-	*77*	*1.71*

The results of the *QELS* and *SEM/TEM* measurements deviate much from the theoretical expected ratios of r_{CS}/r_C, whereas the interparticle interference measurements correspond very well to the theoretical expected ratios of r_{CS}/r_C.

Figures 6.2/3/4 show three TEM-photographs, one of the seed latex P8 *(Fig. 6.2)* and two of the corresponding core-shell latices P9 *(Fig. 6.3)* and P10 *(Fig. 6.4)*.

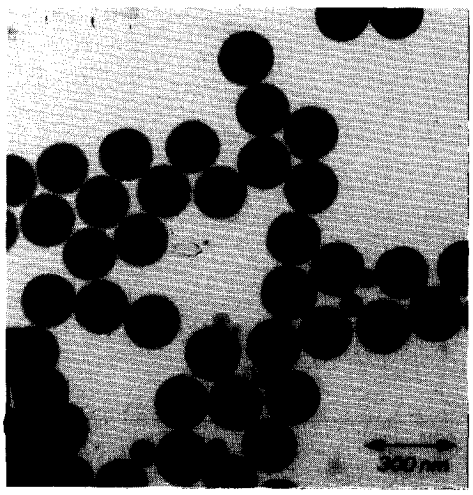

Fig. 6.2 TEM-photograph of seed latex particles P8.

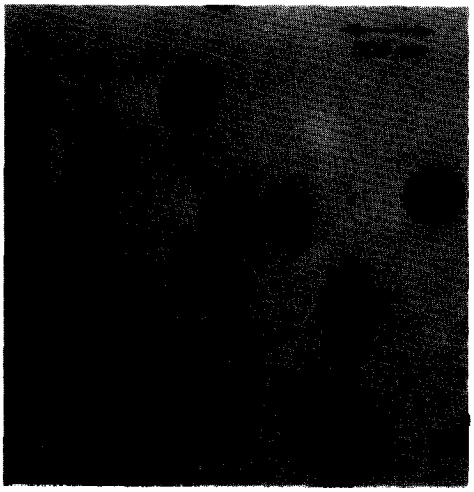

Fig. 6.3 TEM-photograph of core-shell latex particles P9

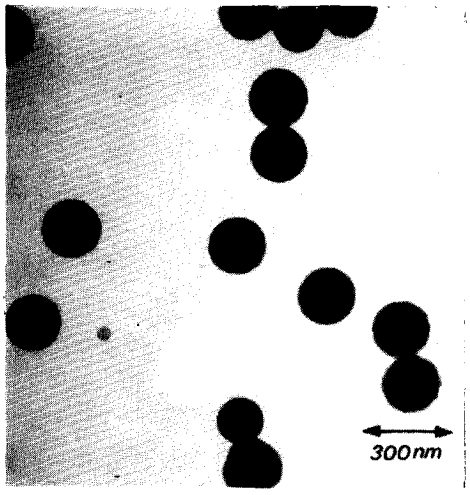

Fig. 6.4 TEM-photograph of core-shell latex particles P10.

The photographs clearly show that all the seed latex particles are covered, somewhat irregularly, with the new shell material. The irregular covering is more distinctively present in latex (P10) which has a higher *PBMA* content. This could mean that the core-shell particles are not ideal, but that they have a kind of *"domain" or "raspberry"* morphology [17].

6.3.2. Soap Titrations.

By measuring the specific absorption area of soap-molecules at the surface of the seed (A_C) and core-shell (A_{CS}) latex particles gives information over the polymer contents at the surface (by means of determination of the critical micelle concentration). Because the difference in absorption area between *PBMA* and *PS* is very small [23], this kind of data can only be used qualitatively. *Figure 6.5* shows the specific absorption area ratio found as function of the ratio r_{CS}/r_C. The specific absorption ratio is given by :

$$R_A = A_{CS}/A_C \qquad (1)$$

Figure 6.5 suggest that for all core shell latices some *PS* is present at the surface. This confirms that the core-shell morphology of our synthesized latices is not ideal and that the morphologies mentioned earlier are probably present.

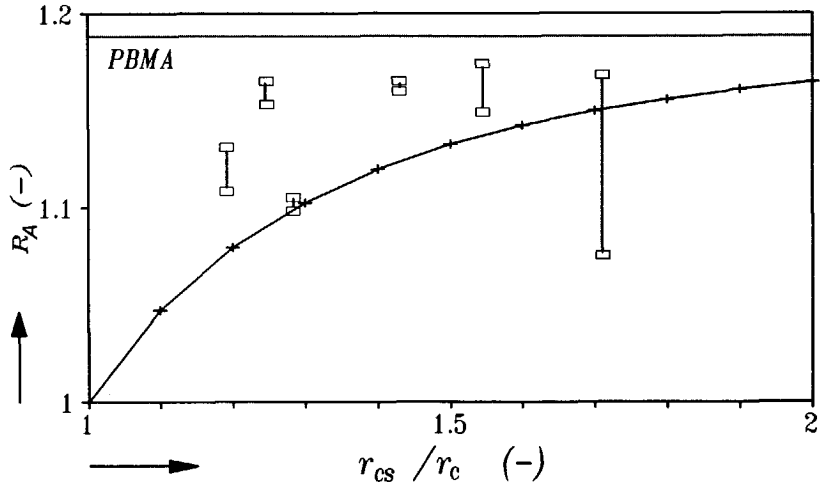

Fig. 6.5 Specific absorption area ratio of SDBS-molecules on the surface of core-shell latex particles as function of r_{CS}/r_C.
□ Experimental + Copolymer (theory)

6.3.3. DSC-T_g

The synthesized core-shell latices consist of a *PBMA*-rich shell and a *PS* core. This must result into two transitions in a *DSC* plot, where the two transitions correspond to the T_g's of the core (*PS*) and of shell (*PBMA*) material. The *DSC* results are shown in *Table 6.IV.* All investigated core-shell latices clearly have two T_g's, these measured T_g's correspond accurately to the T_g of *PBMA* (P12) and to the T_g of *PS* (*104 °C*). The seed latices that have been crosslinked with *DVB* have a higher T_{g2}, where the T_g depend on the amount of *DVB*. Also the T_{g1} of the core-shell latices are slightly higher than the T_g of *PBMA* (P12), due to the presence of *PS* in the shell.

Table 6.IV DSC and MFFT Measurements.

Latex	*DSC*		*Film Formation*		*Fox*
(°C)	T_{g1}	T_{g2}	*MCT*	*MFFT*	T_g
P9	*47*	*104*	*88*	--	*71*
P10	*30*	*104*	*50*	*88*	*70*
P12	*30*	---	--	*31*	--
P14	*32*	*107*	*49*	*62*	*69*
P15	*31*	*108*	*46*	*58*	*62*
P18	*33*	*112*	*40*	*62*	*68*
P19	*34*	*124*	*39*	*54*	*69*
P24	*35*	*108*	*40*	*42*	*53*
P25	*35*	*109*	--	*37*	*48*
P26	*35*	*105*	--	*36*	*43*
P30	*35*	*96*	--	--	*67*
P31	*33*	*104*	---	*41*	*54*

6.3.4. Latex Coalescence

6.3.4a. Interparticle Interference

The deformation of the core-shell particles can be followed by measuring the change of the interparticle interference (λ_{min}) of a drying latex film. This reveals the maximum extend of the indentation of the coalescing core-shell latex particles at a given drying temperature. By doing this at different drying temperatures the maximum indentation as function of temperature can be found. Six core-shell latices were investigated, having ratios of r_{cs}/r_c varying from *1.2* to *1.7*, and crosslinker content varying from *0* to *10 wt % DVB*. The pattern of the indentation/temperature plot as function of the ratio r_{cs}/r_c gives very accurate information about the morphology of the core-shell latex over the indentation region.

In *Fig. 6.6* is given $\lambda_{min}/(r_p.n_d)$, which is proportional to e_p^*/r_p (*bi-axial indentation - section 4.4.2.)*, as a function of the drying temperature. The core-shell latex particles begin to deform at temperatures between *40* and *50 °C*.

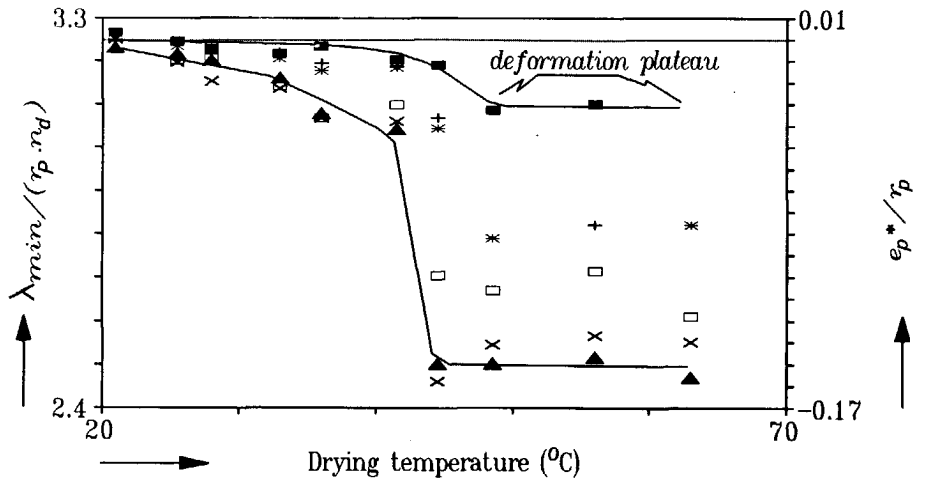

Fig. 6.6 Influence of the drying temperature on the interparticle interference c.q. bi-axial indentation of core-shell particles.
■ = P10, + = P18, ✱ = P19, □ = P24, X= P25, ▲ = P26.

For some core-shell particles the deformation does not continue, but stops at a certain indentation (*deformation plateau*). This deformation plateau lowers for an increasing ratio of r_{cs}/r_c. Eventually the deformation plateau changes into complete latex coalescence at a temperature corresponding to the *MFFT*, which still has a lower temperature than the T_g of *PS*-core. For complete latex coalescence the core-shell latex particles need a deformation of $0.164*r_{cs}$ (*bi-axial indentation - section 4.2.2c*). *Figure 6.7* shows the deformation ratio of latices P10/P18/P19/P24/ P25/P26 resulted from *Fig. 6.6* as function of r_{cs}/r_c, where the the deformation ratio is given by :

$$R_{def.} = e_p^*/(0.164.r_{cs}) \qquad (2)$$

where e_p^* is the indentation corresponding to the deformation plateau. When the particles deform completely $R_{def.}$ is *1* and when there has been no deformation $R_{def.}$ is 0. *Figure 6.7* shows that the core-shell latex coalescence is complete when the ratio r_{cs}/r_c reaches 1.7 and that $R_{def.}$ increases quickly for ratios of r_{cs}/r_c from *1.1* to *1.3* and slowly from 1.3 to 1.7.

It was expected that when the shell was thicker than the maximum indentation needed for complete coalescence, the deformation behaviour could be explained by the elastic properties of the shell material.

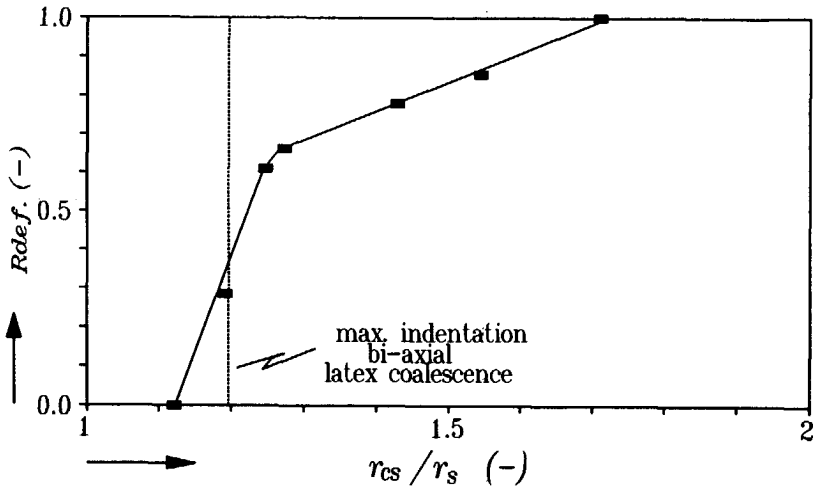

Fig. 6.7 Influence of shell thickness on the deformation ratio of core-shell particles.

However, in our case all the investigated latices had thicker shells than this maximum indentation, so that no deformation plateaus were expected. Therefore the typical indentation plots shown can't be explained by our initially assumed deformation mechanism, other possible explanations are :

a) The core is strongly influencing the deformation of the core-shell latices. Obviously *Fig. 6.7* shows that the core has no influence on the coalescence process (anymore) for ratios r_{cs}/r_c bigger than 1.7 (P26 with *PS* content of only *20 vol %*). The same kind of results was found by Devon [22];

b) The shell material has a *"domain"* morphology of *PS* and *PBMA*, where the *PS* content is increasing from the surface towards the core. The evaluation of *Fig. 6.7* obviously shows that the *PS* content increases faster in core-shell particles with thin shells (e.g. faster decrease of elasticity over the deformation zone) and slower for thick shells.

6.3.4b. Rayleigh Scattering

The transmission spectrum of completely coalesced latices can be fitted with Rayleigh scattering. For that purpose it was assumed that the system of fully coalesced core-shell latex particles consists as a film of spherical *PS* particles in a continuous matrix of *PBMA*. We see in *Fig. 6.8* that the theoretical spectra (*Rayleigh Scattering Models - section 2.3.3.*) corresponds accurately to the measured spectrum of two dried

latex films (P24 and P31); the magnitude of dimensions used corresponds to the dimensions of the core-shell latex particle. This undoubtedly proves that the latex particles prepared with seeded and shot-growth emulsion polymerization have a core-shell morphology.

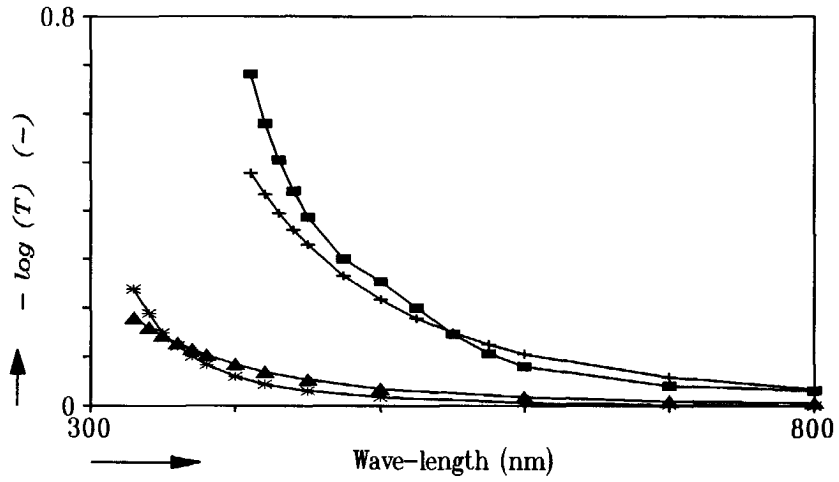

Fig. 6.8 Transmission spectra of completely coalesced dried latex films.
Latex P24 ■ = experimental, + = model 2 with r_c= 94 nm and r_{cs}=136 nm.
*Latex P31 * = experimental, ▲ = model 2 with r_c= 55 nm and r_{cs}= 77 nm.*

6.3.4c. Minimal Film Formation Temperatures Core-shell Latices

In *section 6.6.3a* it was found that some core-shell latices will deform partly at a given temperature and the extent of the deformation remains constant over a certain temperature range ("*deformation plateau*"). The temperature where the deformation plateau starts, is called Minimal Coalescence Temperature (*MCT*). Because the interparticle interference technique has a limited temperature range, *MFFT* measurements were used to measure the temperature when the "*deformation plateau*" eventually goes over in completely coalesced latex particles (*MFFT*).

The minimum film formation temperature is determined by using a messing bar over which a temperature gradient is established from *24* to *88* ^oC. The bar is then coated with a *50* μm thick latex film. The temperature at which the coating becomes "transparent" and crack free is called the *MFFT*. The results are given in *Table 6.IV*. The latices P10/P14/P15/P18/P19/P24 have a *MCT* and *MFFT*, whereas latices P25/P26 only have a *MFFT*. The *MCT*, *MFFT* and the *Fox-*T_g of the latices are given in *Fig. 6.9* as

function of volume fraction *PS*. *Figure 6.9* shows that the *MFFT* of the core-shell latices increases when the shell thickness decreases and that the *MFFT*'s coincidently correspond to the theoretical *Fox-*T_g of the gross chemical composition of core and shell polymer until a fraction of *55 vol %*. Above this fraction the *MCT* and *MFFT* increase quickly, which means that for thin shells the coalescence process depends mainly on the core material. The same kind of results were found by Eliseeva [21] for a *PMMA/PEA* core-shell latex.

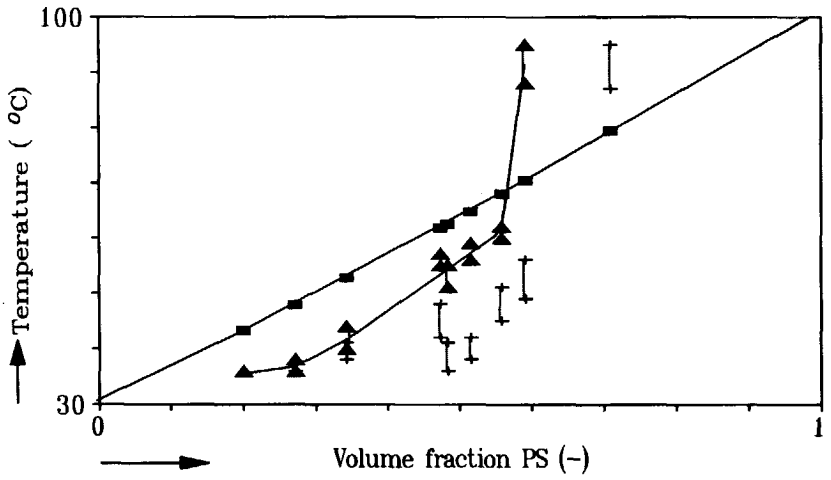

Fig. 6.9 Influence of PS content in core-shell particles on the MFFT (▲), MCT (+) and Fox-T_g *(■).*

6.3.4d. DMTA

In *chapter 3*, we stated that the coalescence process of copolymer latices as function of temperature can be related to the *DMTA* properties of the dried latex film with the Vanderhoff/JKR deformation model. With this model it is possible to calculate the Young's modulus as a function of temperature of the core-shell particles from the indentation-temperature plot (*Fig. 6.6*) during latex coalescence. Theoretically the latex particles can coalesce completely, when the Young's elastic modulus of the particles becomes lower than 10^7-$10^{7.5}$ N/m^2. Therefore, assuming that the Young's modulus of the latex particles have a value of 10^7 to $10^{7.5}$ N/m^2 for temperatures around their *MFFT*. In *Fig. 6.10* is the Young's modulus reconstructed as a function of temperature from the interparticle interference data and *MFFT* of latex P10. The theory assumes two transitions, a first transition at *30-50 °C*, which is caused by the elastic

properties of the *PBMA* shell material and a second transition which depend on the gross elastic properties of *PS* and *PBMA*. The Young's modulus remains constant between the two transition temperatures. Therefore the experimental *DMTA* measurements of completely coalesced dried core-shell latex film should result in two well defined transitions with a kind of rubber plateau. This expected *DMTA* behaviour already has been found by many investigators [23,24,26] and is common for polymers with a core-shell morphology. However, only the *DMTA* measurement of latex P10 did reveal two well defined transitions *(see Fig. 6.10)*.

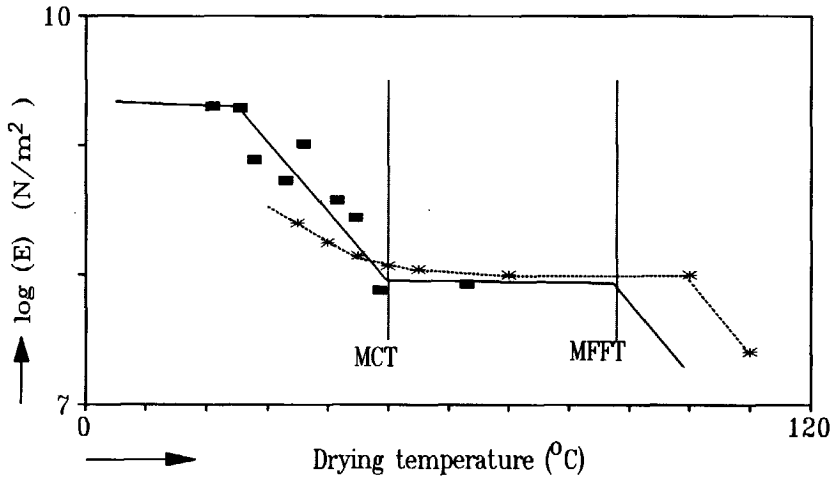

Fig. 6.10 Influence of drying temperature on the Young's modulus of coalescing core-shell particles (■) and the influence of temperature on the Young's modulus (0.1 Hz) of completely coalesced dried latex film (*). [Latex P10]

6.4. CONCLUSIONS

The measurements discussed in this chapter are a first attempt to investigate the mechanism of coalescence of latices with a core-shell morphology. These preliminary results demonstrate that the morphology of particles with a *PS*-core and a *PBMA*-shell can be characterized.

The transmission spectrum of the completely coalesced core-shell latex particles can be fitted accurately with the Rayleigh Scattering model 1, assuming *PS*-cores imbedded in a *PBMA* polymer matrix. This proves that the synthesized two stage latex particles

have a core-shell morphology. *TEM*-photographs, soap-titrations and DSC revealed that the core-shell morphology is not ideal, but that it has a kind of *"domain" or "raspberry"* morphology.

With the interparticle interference technique it was established that the shell and the core materials are important for the coalescence process, even for shells much thicker than the maximum indentation needed for complete coalescence of the core-shell particles. This means that the core material is strongly affecting the coalescence.

The results found between the latex coalescence behaviour and the elasticity behaviour of the completely coalesced latex film (latex P10) as function of temperature evidently proves that the *DMTA* measurements can predict the coalescence behaviour of particles with a core-shell morphology.

References

1 Erickson, J.R., 'Emulsio polymers and emulsion polymerization ACS Symposium series **165**,' Washington D.C., 1981 ,p. 483.
2 Okubo, M, Ando, M., Yamada, A., Katsuta, Y., Matsumoto, T., *J. Polym. Sci., Polym. Lett. Ed.* **19**, 143 (1981).
3 Okubo, M, Katsuta, Y., Matsumoto, T., *J. Polym. Sci., Polym. Lett. Ed.* **20**, 45 (1982).
4 Shaffer, O.L., Dimonie, V.L., El-Aasser, M.S., Vanderhoff, J.W., *J. Polym. Sci., Polym. Chem. Ed.* **25**, 2595 (1987).
5 Min, T.I., Klein, A., El-Aasser, M.S., Vanderhoff, J.W., *J. Polym. Sci., Polym. Chem. Ed.* **21**, 2845 (1983).
6 Brown, R.A., Price, C., Randall, P.D., Satgurunathan, R., *Polym. Common.* **30**, 349 (1989).
7 Hergeth, W.D., *Acta polym.* **36**, 472 (1985).
8 Verdurmen, E.M.F.J., 'The influence of crosslinks on particle morphology of styreen acrylic latices.' Graduate Thesis, Eindhoven University of Technology, Department Emulsion Polymerization, The Netherlands, 1989.
9 Chainey, M, Wilkinson, M.C., Hearn, J., *J. Ind. Eng. Chem., Prod. Res. Dev.* **21**, 171, (1982).
10 Chainey, M, Hearn, J, Wilkinson, M.C., *Brit. Polym. J.* **13**, 132 (1981).
11 Stutman, D.R., Klein, A., El-Aasser, M.S., Vanderhoff, J.W., *Ind. Eng. Chem., Prod Res. Dev.* **24**, 404, (1985).
12 Eliseeva,V.I., Bogdanova, S.V., *Progr. Org. Coat.*, **19**, 141 (1991).
13 Williams, D.J., *J. Elastoplastics*, **3**, 187 (1971).
14 Muroi, S., Hashimoto, H., Hasoi, K., *J. Polym. Sci., Polym. Chem. Ed.*, **22**, 1365 (1984).
15 Lee, D.I., Ishikawa, T., *J. Polym. Sci., Polym. Chem. Ed.*, **21**, 147 (1983).
16 Cho, I., Lee, K.W., *J. Applied Polym. Sci.*, **30**, 1903 (1985).
17 Okubo, M, Yamada, A., Tsunetaka, Matsumoto, *J. Polym. Sci., Polym. Chem. Ed.*, **16**, 3219 (1980).
18 Paxton, T.R., *J. Coll. Int. Sci.* , **31**, 19 (1969).
19 Kong, X.Z., Pichot, C., Guillot, J., *J. Coll. Polym. Sci.* , **265**, 791 (1987).
20 Morgan, L.W., *J. Appl. Polym. Sci.*, **27**, 2033 (1982).
21 Eliseeva,V.I., *Progr. Org. Coat.*, **13**, 195 (1985).
22 Devon, M.J., Gardon, J.L., Roberts, G., Rudin, A., *J. Applied Polym. Sci.*, **39**, 211 (1990).

23 Basset, D.R., ' Science and Technology of polymer colloids vol. 1, Nato ASI Series no. 67.' Martinus Nijhoff Publisher, Dordrecht, 1983, p. 64.
24 Merkel, M.P., Dimonie, V.I., El-Aasser, M.S., Vanderhoff, J.W., *J. Polym. Sci., Polym. Chem. Ed.* **25**, 1219 (1987).
25 Cavaile, J.Y., Jourdan, C., Kong, X.Z, Perez, J., Pichot, C., Guillot, J., *Polymer* **27**, 693 (1986).
26 Lambla, M., Schlund, B., Lazarus, E., Pith, T., *Macromol. Chem. Suppl.* **10/11**, 463 (1985).
27 O'Connor, K.M., Tsaur, S.L., *J. Appl. Polym. Sci.* **33**, 2007 (1987).
28 Fischer, L.W., Melpolder, S.M., O'Reilly, J.M., Ramakrishnan, V., Wignall, G.D., *J Colloid Interface. Sci.* **123**, 24 (1988).
29 Wai, M.P., Gelman, R.A., Fatica, M.G., Hoerl, G.H., Wignall, G.D., *Polymer*, **28**, 91 (1987).
30 Woerkens, P.H. van, 'De Synthese en Karakterisering van Core-shell Waterafdunbare Dispersies.' Graduate Thesis, Delft University of Technology, The Netherlands, 1990.
31 Tent, A. van, Nijenhuis, K. te, *in* "Proceedings 17, XVIIth International Conferenc in Organic Coatings Science and Technology, Luzern, Switzerland," 1991, p.317.
32 Tent, A. van, Nijenhuis, K. te, *J. Colloid Interface Sci.* **150**, 97 (1992).

APPENDIX I

RAYLEIGH SCATTERING MODEL 2

Calculation of the projected area of the inclusion.

The area (A_i) of the projected inclusion is equal to :

$$A_i = A_{m_1m_2m_3} - 6.\left(A_{ab'o} + A_{b'm_1o}\right) \tag{I1}$$

The area $a_{ab'o}$ will be given by :

$$A_{ab'o} = \frac{1}{3}.\int_{\frac{1}{2}.r_p}^{r_p} \sqrt{r_p^2 - x^2}\, dx \tag{I2}$$

By substituting $x = r_p.sin\ t$ into Eq. (I2), we obtain :

$$A_{ab'o} = \frac{1}{6}.r_p^2.\int_{\frac{\pi}{6}}^{\frac{\pi}{2}}\left(1+cos\ 2t\right).dt = r_p^2\left(\frac{1}{18}.\pi - \frac{1}{24}.\sqrt{3}\right) \tag{I3}$$

The area $A_{b'm_1o}$ is equal to :

$$A_{b'm_1o} = \frac{1}{2}.\frac{1}{2}\ r_p.\frac{1}{2}\ r_p\ tan\ 30^o = \frac{1}{24}.\sqrt{3}.r_p^2 \tag{I4}$$

In general, the area $A_{m_1m_2m_3}$ (*in Fig. 2.10* $e_p = 0$) is equal to :

$$A_{m_1m_2m_3} = \sqrt{3}.\left(r_p+e_p\right)^2 \tag{I5}$$

Substitution of Eqs. (I3), (I4) and (I5) into Eq. (I1), yields :

$$A_i = \sqrt{3}.\left(r_p+e_p\right)^2 - \frac{1}{3}.\pi.r_p^2 \tag{I6}$$

Calculation of the perimeter of the inclusion.

In general, the perimeter κ_i of the water inclusion is equal to :

$$\kappa_i = 6.\left(|ab'| + e_p\right) \tag{I7}$$

The perimeter $|ab'|$ is given by :

$$|ab'| = \int_{\frac{1}{2}.r_p}^{r_p} \left[\frac{r_p^2 - \frac{8}{9}.x^2}{r_p^2 - x^2}\right]^{\frac{1}{2}} .dx \tag{I8}$$

By substituting $x = r_p.sin\ t$ into Eq. (I8) we obtain :

$$|ab'| = r_p.\int_{\frac{\pi}{6}}^{\frac{\pi}{2}} \sqrt{1 - \frac{8}{9}.sin^2 t}\ .dt \tag{I9}$$

Numerical solution of Eq. I9 with the Simpson rule gives as an answer $0.6105.r_p$. Substitution of this result into Eq. (I7) gives :

$$\kappa_i = 3.66.r_p + 6.e_p \tag{I10}$$

By rewriting Eq. (17, chp. 2) with $m = m^*$, $\pi.r_p^2 = A_i$ and $x = \kappa_i/\lambda$, and substituting this into Lambert-Beer's Eq. (15, chp. 2), we obtain Eq. (30, chp. 2):

$$ln\ T_{model2} = \left(\frac{-2.A_i.\kappa_i^4.V_f.d_l}{\pi.r_p^2.\lambda^4}.\left(\frac{m^{*2}-1}{m^{*2}+2}\right)^2\right) \tag{I11}$$

APPENDIX II

CALCULATION OF THE SIZE OF THE STABILIZING LAYER.

The wave-length (λ_{min}) at which a sharp minimum in the transmission spectrum arises, depends on the particle radius, the interparticle distance and the number of structured particle layers. This leads to the following equation (for more details see chapter 2):

$$\lambda_{min} = 4.A.n_d \tag{II1}$$

where n_d is the refractive index of the latex and $A=(r_p+\kappa)\ sin\ 54.75^o$, which is one fourth of the height of a *h.c.p.*-unit. From the change of λ_{min} of interstices filled with water to λ_{min} of interstices filled with air, the change in interparticle distance (ΔA) can be calculated. This change is almost equal to the size of the stabilizing layer (κ). The results for latices B4 and B6 are given in *Table 3.II.*

APPENDIX III

INDENTATION AS A FUNCTION OF THE VOLUME FRACTION OF SPHERES IN A H.C.P.-UNIT.

Figure III.1 shows a *h.c.p.*-unit, where :

$$b = 2.\left(r_p+e_p\right)\ ,\ l = 2.\left(r_p+e_p\right).sin\ 60^o \text{ and } h = 4.\left(r_p+e_p\right).sin\ 54.75^o$$

$$V_f = \frac{Volume\ particles\ per\ unit}{Volume\ unit\ (blh)} = \frac{\pi}{3\sqrt{2}}.\left(\frac{r_p}{r_p+e_p}\right)^3 \qquad \text{(III1)}$$

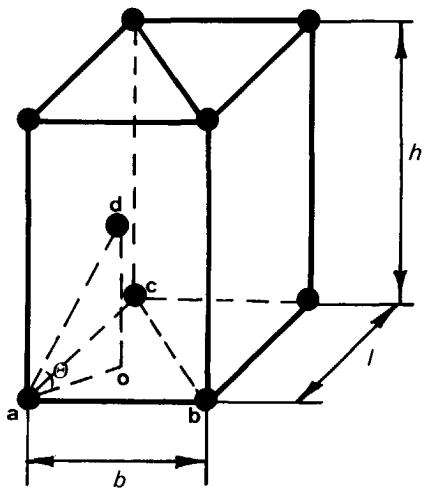

Fig. III-1 Schematic representation of a h.c.p.-matrix.

For *isotropic deformation* the interparticle distance decreases isotropically between all the particles of the unit. The indentation as a function of the volume fraction is then given by :

$$e_p = \left[\left(\frac{\pi}{3\sqrt{2}.V_f} \right)^{\frac{1}{3}} - 1 \right] .r_p \qquad \text{(III2)}$$

For *bi-axidl deformation* only the height (h) of the h.c.p-unit decreases, the sizes of b and l remain constant. Deformation starts when e_p is zero, so that the size of b and l are : $b = 2.r_p$ and $l = 2.r_p.sin\ 60^o$. Substitution of these values into Eq. III2 yields :

$$V_f = \frac{4}{9}.\sqrt{3}.\pi.r_p.h^{-1} \qquad \text{(III3)}$$

The deformations only take place between spheres AD,BD and CD. The indentation is now given by :

$$e_p^* = \frac{1}{2}.\left(|AD| - 2.r_p \right) \qquad \text{(III4)}$$

where $|AD| = \sqrt{\frac{1}{4}.h^2 + \frac{4}{3}.r_p^2}$

APPENDIX IV

THEORETICAL INTERPARTICLE INTERFERENCE CHANGE FOR ISOTROPIC AND BI-AXIAL DEFORMATION MECHANISMS [1-7]

The wave-length (λ_{min}) at which a sharp minimum in the transmission spectrum arises, depends on the particle radius, the interparticle distance and the number of structured particle layers. This leads to the following equation (for more details *chapter 2*) :

$$\lambda_{min} = 4.A.n_d = h.n_d \qquad \text{(IV1)}$$

where n_d is the refractive index of the latex and A is one fourth of the height of *h.c.p.*-unit in *figure III.1* This means that h equals λ_{min}/n_d. Substituting this into the Eq. III1 yields for the isotropic deformation mechanism :

$$V_f = \frac{128}{27}.\pi.\sqrt{3}.\left(\frac{r_p.n_d}{\lambda_{min}} \right)^3 \qquad \text{(IV2)}$$

and for the bi-axial deformation mechanism :

$$V_f = \frac{4}{9}.\pi.\sqrt{3}.\left(\frac{r_p.n_d}{\lambda_{min}}\right) \qquad \text{(IV3)}$$

Following the experimental change of λ_{min} as a function of volume fraction the coalescence mechanism of the latex particles can be determined.

References

1 Luck, W, Klier, M., Wesslau, H., *Ber. Bunsen-Ges. Phys. Chem* **67**, 75 (1963).
2 Luck, W, Klier, M., Wesslau, H., *Ber. Bunsen-Ges. Phys. Chem* **67**, 84 (1963).
3 Hiltner, P.A., Krieger, I.M., *J. Phys. Chem.* **73**, 2386 (1969).
4 Hiltner, P.A., Papir, Y.S., Krieger, I.M., *J. Phys. Chem.* **75**, 1881 (1971).
5 Furusawa, K, Tobori, N., Hachisu, S., *J. Chem. Soc., Faraday Trans.* **84**, 4397(1988)
6 Tent, A. van, Nijenhuis, K. te, *J. Colloid Interface Sci.* **150**, 97 (1992).
7 Tent, A. van, Nijenhuis, K. te, "Proceedings XVIIth International Conference in Organic Coatings Science and Technology", Luzern, Switzerland, 1991, p. 317.

APPENDIX V

RAYLEIGH LIGHT SCATTERING OF ELLIPSOIDS [1]

The attenuation of a light beam which passes a scattering medium, is defined by Lambert-Beer's relation :

$$S = - d_l^{-1}.ln\ T \qquad \text{(V1)}$$

where S is the scattering coefficient, d_l the thickness of the swollen latex film and T the transmittance. For Rayleigh scattering, the scattering coefficient for non-absorbing particles is given by :

$$S = N.Q_{sca}.A_e = N.C_{sca} \qquad \text{(V2)}$$

where N is the particle number concentration (m^{-3}), Q_{sca} the scattering efficiency factor, A_e the area of the cross section of the particle (m^2) and C_{sca} the scattering cross section (m^2).
The scattering cross section for Rayleigh scattering is given by :

$$C_{sca} = \frac{8}{3}.\pi.k^4.|\alpha|^2 \qquad \text{(V3)}$$

where k is the wave-number $2.\pi/\lambda$ and α the isotropic polarizability, defined as :

$$\alpha^2 = \frac{1}{3}.\alpha_a^2 + \frac{1}{3}.\alpha_b^2 + \frac{1}{3}.\alpha_c^2 \qquad \text{(V4)}$$

where α_a, α_b and α_c are the polarizability tensors in the direction of the applied field along any of the x,y,z-axes of the ellipsoids.
For ellipsoids Lorentz derived the following relationship [1] :

$$\frac{V}{4.\pi.\alpha_j} = L_j + \frac{1}{m^2-1} \qquad \text{(V5)}$$

where V is the volume of an ellipsoid (m^3), m the relative refractive index (-), L_j the ratio of the axes of the ellipsoid. When all interfaces are intact (N_f=1) the amount of interfaces equals the number of polymer particles in the dried latex film. The volume of every ellipsoid is equal to the volume absorbed water divided by the number of latex particles :

$$V = \frac{1-V_f}{V_f}.\frac{4}{3}.\pi.r_p^3.\ N_f^{-1} \qquad \text{(V6)}$$

where N_f is the fraction remaining interfaces. If the semi-axes of the ellipsoid are given by a,b and c, then the ratios L_j are given quite accurately by :

$$L_a = \frac{1}{1 + \frac{a}{b} + \frac{a}{c}}, \quad L_b = \frac{1}{1 + \frac{b}{a} + \frac{b}{c}}, \quad L_c = \frac{1}{1 + \frac{c}{a} + \frac{c}{b}} \qquad \text{(V7)}$$

The semi-axes of the swollen interfaces are symmetric in two direction, so that b/c=1. The sizes of b and c are equal to the characteristic size of the projection of the swollen interface in the hexagonal packing structure. The length (a) of the swollen ellipsoid is equal to one fourth of the height (h Eq. III3) of the h.c.p-structure (*Fig. III.1*) minus the particle radius (r_p).

$$b = c = \frac{1}{3}\sqrt{3}.r_p \quad \text{and} \quad a = \frac{1}{9}.\sqrt{3}.\pi.r_p.V_f^{-1} - r_p \qquad \text{(V8)}$$

The scattering cross section is found by calculation of α_a, α_b and α_c from Eqs. V5-V8.

Reference

1 van de Hulst, H.C., "Light scattering by small particles." Wiley, New York, 1957, p. 63-74.

LIST OF SYMBOLS

ABBREVIATIONS

OSV	Onderzoeks Stimulerings-programma Verf
IOP	Innovatie gericht Onderzoeks Programma
Coulter	Particle size measurement apparatus by QELS
DET	Direct non-radiative Energy Transfer
DMTA	Differential Mechanical Temperature Analyzer
DSC	Differential Scanning Calorimeter
GPC	Gel Permeation Chromatography
Malvern	Particle size measurement apparatus by QELS
QELS	Quasi Elastic Light Scattering
SANS	Small Angle Neutron Scattering
SEM	Scanning Electron Microscopy
SF_3	Sedimentation Field Flow Fractionation
SLAM	Scanning Laser Acoustic Microscopy
TEM	Transmission Electron Microscopy
UV-Vis	Ultra Violet and Visible light
h.c.p.	hexagonal close packing
f.c.c.	face centered cubic
s.c.p.	simple close packing
s.h.p.	simple hexagonal packing

CHEMICAL COMPOUNDS

BA	Butyl Acrylate
BMA	Butyl Methacrylate
MAA	Methacrylic Acid
MMA	Methyl Methacrylate
NF26eo	Nonylphenol 26 ethylene oxide
PBMA	Poly Butyl Methacrylate
PMMA	Poly Methyl Methacrylate
PS	Poly Styrene
S	Styrene
SDBS	Sodium Dodecyl Benzene Sulfonate

SYMBOLS

a_0	radius contact area	nm
A	characteristic length for interparticle interference	nm
A_h	Hamaker's constant	J
A_i	area of the projection of a inclusion	nm^2
A_c	specific absorption area core particle	m^2/mol
A_{cs}	specific absorption area core-shell particle	m^2/mol
C_1, C_2, C_3	geometric constants	-
C_{sca}	scattering cross section	m^2

d_j	thickness of the *jth* layer	*nm*
d_l	film thickness or optical path-length sample	*μm*
d_h	thickness polymer layer	*nm*
d_ℓ	thickness water layer	*nm*
e_p	interparticle distance and indentation particles	*nm*
e_p^*	indentation biaxial mechanism	*nm*
E	Young's elastic modulus	*Pa*
$E_{B/H}$	Young's elastic modulus by Brown/Hertz model	*Pa*
$E_{S/H}$	Young's elastic modulus by Sheetz/Hertz model	*Pa*
$E_{V/JKR}$	Young's elastic modulus by Vanderhoff/JKR model	*Pa*
E_e^+	electric field vector of incident light	
E_r^-	electric field vector of reflected light	
E_t^+	electric field vector of transmitted light	
$F_{B/V}$	deformation force of Brown /Vanderhoff	*N*
F_s	shearing force	*N*
F_n	normal force	*N*
F_o	contact force, load	*N*
F_z	interaction pressure	N/m^2
ΔG	cohesive energy	*N/m*
i	$\sqrt{-1}$	-
i_j	angle of incidence of the *jth* layer	*rad*
i_1	angle of incidence	*rad*
i_2	angle of refraction	*lux*
I_t	intensity transmitted light	*lux*
I_o	intensity incident light	*lux*
K_{lp}	number of regularly packed layers two step model	-
K_{cp}	number of regularly packed layers multi step model	-
K_{max}	number of regularly packed layers maximum	-
L_j	ratio semi-axes ellipsoid	-
m,m^*	relative refractive index	-
M	molecular weight polymer	*g/mol*
M_c	mass coalesced latex	*g*
M_f	weight latex at t=0	-
M_t	total weight polymer	*g*
M_o	molecular weight monomer	*kg/mol*
M_n	number average molecular weight polymer	*kg/mol*

M_w	weight average molecular weight polymer	*kg/mol*
MCT	minimal coalescence temperature	^oC
MFFT	minimal film formation temperature	^oC
n	refractive index	-
n_{eff}	effective index of refraction	-
n_d	refractive index latex	-
n_g	refractive index glass	-
n_j	absolute refractive index of the *jth* layer	-
n_s	refractive index solvent	-
n_p	refractive index latex particle (polymer)	-
n_x	average refractive index	-
N	concentration	*mol/l*
N	degree of polymerization	-
N_f	fraction remaining interfaces	-
N_p	particle concentration	m^{-3}
Q_{sca}	scattering efficiency factor	-
p	number of secondary interference minima	-
P_c	capillary pressure	*Pa*
P_v	capillary pressure of Vanderhoff	*Pa*
$<r>$	average square end-to-end polymer chain length	nm^2
r_c	radius capillary	*nm*
r_c	radius core	*nm*
r_{cs}	radius core-shell	*nm*
r_p	particle radius	*nm*
R	gas constant	*J*
R	reflection coefficient	*% or -*
R_a	specific absorption ratio	-
R_r	reflection coefficient of Fresnel	*% or -*
$R_{def.}$	deformation ratio	-
R.H.	relative humidity	*%*
S	scattering coefficient	m^{-1}
Steps	number of transitions to simulate n_x-pattern	-
T	temperature	*K*
T	transmission coefficient	*% or -*
T_g	glass transition temperature polymer	^oC
T_{min}	transmission minimum caused by interparticle interference	*% or -*

V_a	average volume fraction polymer	*% or -*
V_i	volume fraction polymer from interparticle interference data	*% or -*
V_f	volume fraction polymer	*% or -*
W_f	weight fraction polymer	*% or -*
W_a	average weight fraction	-
W_{nc}	weight fraction non-coalesced latex	-
x	position in the particle packing structure	*nm*
z	characteristic length water inclusion scatterer	*nm*
z_o	minimal separation distance between two surfaces	*nm*
z	separation distance between two surfaces	*nm*
α	polarizability	m^3
α_m	polarizability dilute polymer solution	m^3
γ	interfacial or surface tension	*N/m*
$\gamma_{\ell/a}$	surface tension water	*N/m*
$\gamma_{p/a}, \gamma 1$	surface tension polymer	*N/M*
$\gamma_{p/\ell}, \gamma 12$	interfacial tension polymer-water	*N/m*
λ	wave-length	*nm*
λ_{min}	wave-length at the transmission minimum	*nm*
η	viscosity latex	*mPa.s*
ρ	density latex	kg/m^3
ϕ	phase difference	*rad*
ϕ_j	phase shift *jth* layer	*rad*
ϕ_{min}	phase difference is π, 3π, 5π..	*rad*
μ_i	optical admittance of medium i	-
ε	relative dielectric constant	-
ε_{ps}	relative dielectric constant pure solvent	-
θ	coalescing angle	*rad*
Φ	contact angle water/polymer	*rad*
ν	Poisson's ratio	-
$\mathbb{D}$	interdiffusion constant polymer	m^2/s
κ^1	interparticle distance before flocculation	*nm*
κ^2	,, after flocculation	*nm*
κ_i	perimeter of the projection of a water inclusion	*nm*
κ_m	marker displacement	*nm*
κ_p	polymer displacement	*nm*
κ_{SDBS}	size stabilizing layer	*nm*

SUMMARY

The study described in this thesis was performed as part of an innovation oriented research program, funded by the Dutch Ministry of Economic Affairs and called Onderzoeks Stimuleringsprogramma Verf (*OSV*), to arouse interest and to stimulate the paint industry to a more scientific approach of the problems concerning aqueous dispersion paints.

The aim of this study is to characterize the process of film formation and to investigate the influence of different factors such as drying temperature, humidity, drying time, particle size and latex morphology. The process of film formation of industrial aqueous dispersion coatings is very difficult to describe, because of the many chemical components in the paint and the multi-disciplinary character of the process. This leads to a complicated macroscopic behaviour, which is difficult to separate into contributions of the various microscopical properties. Therefore, the number of chemical components was reduced to three to get a better insight in the problems involved in the film formation process. The three basis components were binder (acrylic (co)polymer), solvent (water) and emulsifier (*SDBS*).

The film formation process of these acrylic latices was studied by transmission spectrophotometry. With this technique the light attenuation (transmission) of a thin latex film is measured. The pattern of the transmittance as a function of the wave-length (transmission spectrum) reveals the internal structure of the latex film. The transmission spectrum in the *UV/Vis* wave-length area is determined mainly by Rayleigh scattering and interparticle interference. In particular, the interparticle interference, which causes beautiful iridescent colour patterns, is related accurately to the particle size, interparticle distance and packing structure.

Chapter 2 describes how the transmission spectra of thin latex films are related to the physical properties of the latex, like particle size, weight fraction, particle size distribution and film thickness. This results in an empirical Rayleigh scattering equation, based on the size of the water interstices between the densely packed latex particles, which describes the scattering behaviour of thin latex films very well. The interparticle interference can be described with the multilayer interference theory, if the latex film is considered as a homogeneous medium with small variations in optical density. These optical density variations in a medium with a very regular structure can be considered as a gradual variation of the refractive index between a relatively high

and low value. This represents the so called lamellar phase of the latex, where layers with a high polymer content are separated by layers with a relatively high water content.

In chapter 2 aspects of scattering and interparticle interference have been discussed for thin latex films fixed between glass plates, so that no evaporation of water takes place. In chapter 3 the changing scattering and interparticle interference patterns are studied corresponding to drying thin latex films coated on glass plates. The change of the interparticle interference during the drying process of a latex film is primarily related to the internal displacements, but these patterns are also related to the regularity of the interparticle structure, the critical interparticle distance (where flocculation of the particles is initiated) and the size of the stabilizing layer around the latex particles. The latex particles lie in a hexagonal close packing when they are flocculated in the latex film. When this film is dried above the MFFT, then, during the evaporation of water, the particles will deform into a polyhedric structure under the influence of the capillary forces. The observed changes in the interparticle interference are then related to the deformation of the latex particles. In chapter 4 is described how, from the changes in interparticle interference, the mechanism by which the particles deform, can be determined.

In the literature the wet sintering theory is proposed, which can describe latex coalescence. The concept of this theory is the application of the principle of capillary pressure, where the polymer/air, polymer/water and air/water interfacial tensions are responsible for the deformation of the latex particles. The principle of capillary pressure is applied to the small interstices in the packing structure and to the radii of curvature formed between the latex particles.

From the change of the interparticle interference during the coalescence process it follows that the deformation of the latex particles is one-directional and can be described by a bi-axial mechanism. This result, in combination with the wet sintering theory, has lead to a Vanderhoff/JKR coalescence model, which calculates Young's elastic modulus as a function of temperature of the latex particles from the particle deformations as a function of drying temperature. The calculated elastic properties of the latex particles are in reasonable agreement with the elastic properties (*DMTA at 0.01 Hz*) found for the dried latex film.

The latex film becomes transparent only if the interfacial boundaries or interstices between the deformed latex particles disappear or if they become so small that they

scatter hardly any light in the visual wave-length region. The size of these interfacial boundaries depends on the particle size and the extent of the deformation. This means that latices with relatively big particles have to deform more than those with relatively small particles, in order to get the same transparent latex film. Investigated is how the particle size and relative humidity influence latex coalescence. At relatively high humidities it is found, that there are no major differences in latex coalescence of latices with particle sizes of *94* and *119 nm*, however, at relatively low humidities there is a difference found in latex coalescence. At these low humidities the bigger latex particles coalesced completely at much higher drying temperature than the smaller latex particles. This means that the capillary forces in a system with small particles is higher than in a system with larger particles.

A transparent latex film will be formed when the latex particles are coalesced completely. If this latex film is immersed in an acid solution the remaining internal interfacial boundaries between the contacting latex particles will swell, resulting in a regeneration of scattering and interference patterns. These patterns are related to the size and the number of swollen interfacial boundaries. It is expected, that the number of remaining interfacial boundaries of an dried latex film decreases with time. The process in which the individually particles lose their identity, is called autohesion. Measuring the decrease of the number of interfacial boundaries as a function of ageing time gives information on the time scale of the mechanisms that play a role during the autohesion process. However, the experiments discussed in chapter 5 showed no decrease of the number of interfacial boundaries during an ageing time of *1* and *24* hours. This means that the autohesion of the dried latex films did not improve in a period of *24* hours.

The remaining interfacial boundaries could also be shown by *TEM*. On the *TEM* photographs of partly deformed latex particles dark elliptical ring shapes were visible between the particles. These dark elliptical ring shapes were interpreted as emulsifier molecules concentrated around the area of contact, so that the contact area consists only of polymer-polymer interface. This means that the autohesion will improve only when emulsifier molecules disappear from the dried latex film. It also means that the mechanisms proposed in the literature, i.e. polymer interdiffusion across the interfacial boundaries or the formation of a polymer intermolecular interface by means of viscous flow, can not be responsible for the autohesion process.

The last chapter describes the application of the methods developed so far to characterize latex particles with a core-shell morphology. Core-shell morphology in latices has been used to improve latex coalescence process and the elastic properties of the finally dried latex film.

In the first instance it is checked whether the synthesized latex particles have the expected core-shell structure. *QELS*, interference and scattering measurements showed that the synthesized particles have a core-shell morphology. However, soap titrations, *TEM* and *DSC* measurements revealed that the core-shell morphology was not ideal, but that it has a kind of "domain" or "raspberry" morphology.

In the second part it was investigated whether the Vanderhoff/JKR coalescence mechanism described in chapter 4, can be used for the deformation behaviour of core-shell latex particles. In some cases latex coalescence of core-shell latex particles is very different from that of homogeneous latex particles. It was expected that the deformation mainly will be determined by the elasticity of the shell polymer, if the shell thickness is larger than the maximum possible indentation during latex coalescence. However, experiments showed that shell thicknesses of three times the maximum indentation distances were needed to exclude the influence of the core on the deformation behaviour. In spite of these results, this specific deformation behaviour of the core-shell latex particles could be predicted well from the elastic properties of the dried latex film (measured in a *DMTA at 0.1 Hz*) in combination with the Vanderhoff/JKR coalescence model of chapter 4.

The turbidity measurements discussed in this thesis are a first attempt to investigate the mechanisms of film formation. The information ensuing from this investigation is necessary to understand the influences of additives and morphology on the film formation process of industrially synthesized latices. These preliminary results demonstrate that turbidity spectrophotometry could be a valuable tool for further latex film research.

SAMENVATTING

Het onderzoek beschreven in dit proefschrift werd gedaan in het kader van een innovatie gericht onderzoeksprogramma om de verfindustrie te ondersteunen, te interesseren en te stimuleren voor een wetenschappelijke aanpak van de problemen die betrekking hebben op waterafdunbare dispersieverven. Het programma wordt Onderzoeks Stimulerings-programma Verf (*OSV*) genoemd en wordt gesubsidieerd door het Nederlandse Ministerie van Economische Zaken.

Mijn onderzoek was gericht op de karakterisering van het filmvormingsproces en op de mate waarin verschillende factoren het proces beïnvloeden, zoals droogtemperatuur, relatieve vochtigheid, droogtijd, deeltjesgrootte en de morfologie van de latex-deeltjes. Het filmvormingsproces van industriële waterafdunbare dispersieverven is moeilijk te beschrijven, vanwege het grote aantal chemische componenten in de verf en het multi-disciplinaire karakter van het proces. Dit leidt tot een zeer gecompliceerd macroscopisch gedrag, waarbij de invloeden van de afzonderlijke microscopische eigenschappen niet eenvoudig te herleiden zijn. Om toch enig inzicht te verkrijgen in de algehele filmvormingsproblematiek, is het aantal chemische componenten teruggebracht tot 3. De drie basis componenten zijn binder (acrylaat(co)polymeer), oplosmiddel (water) en emulgator (*SDBS*).

Het filmvormingsproces van deze acrylaatlatices werd bestudeerd met behulp van transmissiespectrofotometrie. Deze techniek meet de lichtdoorlaatbaarheid (transmissie) van een dunne latexfilm. Het patroon van de lichttransmissie als funktie van de golflengte (transmissiespectrum) van het licht onthult de interne structuur van de latexfilm. Het transmissiespectrum in het UV/Vis-golflengtegebied wordt voornamelijk bepaald door Rayleigh lichtverstrooiing en door de onderlinge deeltjesinterferentie. Met name de onderlinge deeltjesinterferentie, die zich visueel in zeer mooie irizerende kleuren uit, is nauwkeurig gerelateerd aan de onderlinge afstand en pakkings-structuur der deeltjes.

In hoofdstuk 2 wordt beschreven hoe de transmissiespectra van dunne latexfilms gerelateerd kunnen worden aan de fysische eigenschappen van de latex, zoals deeltjesgrootte, gewichtsfractie, deeltjesgrootteverdeling en filmdikte. Dit resulteert in een empirische Rayleigh verstrooiingsvergelijking, gebaseerd op de grootte van de water-inclusies tussen de dicht gepakte latexdeeltjes, die het verstrooiingsgedrag van een dunne latexfilm goed benadert. De onderlinge deeltjesinterferentie kan beschreven

worden door de multilagen interferentietheorie, die de latexfilm beschouwt als een homogeen medium met kleine variaties in optische dichtheid. Deze optische dichtheidsvariaties kunnen in een medium met een zeer regelmatige structuur beschreven worden als een variatie in refractie-index, die geleidelijk oscilleert tussen een relatieve hoge en lage waarde. Dit representeert de zogenaamde lamellaire fase van de latex film, waarbij lagen met relatief hoge concentraties polymeerdeeltjes gescheiden worden door lagen met relatief hoge concentraties water.

De in hoofdstuk 2 behandelde lichtverstrooiings- en interferentieaspecten hebben betrekking op dunne latexfilms gefixeerd tussen twee glasplaatjes, zodat geen droging kan plaatsvinden. In hoofdstuk 3 wordt vervolgens onderzocht hoe de lichtverstrooiings- en interferentiepatronen veranderen van drogende dunne latexfilms gecoat op glasplaatjes. De verandering van de onderlinge deeltjesinterferentie in een drogende latexfilm is in eerste instantie gerelateerd aan de onderlinge afstand en verplaatsing der deeltjes. Maar deze veranderende patronen geven ook gedetailleerde informatie over de regelmatigheid van de intrastructuur, kritische onderlinge deeltjesafstand (waarbij de deeltjes juist beginnen te flocculeren) en de grootte van een stabilisatielaag rond de latexdeeltjes. Als alle deeltjes in de latexfilm geflocculeerd zijn, liggen deze in een dichte hexagonale pakking. Als deze latexfilm gedroogd wordt bij een temperatuur boven de minimale filmvormings temperatuur, zullen gedurende de verdere verdamping van water, onder invloed van capillaire krachten, de deeltjes deformeren tot een honingraat structuur. De daarbij waargenomen veranderingen in onderlinge deeltjesinterferentie zijn dan gerelateerd aan de vervormingen van de latexdeeltjes. In hoofdstuk 4 wordt beschreven hoe hieruit het mechanisme waardoor de latexdeeltjes vervormen bepaald kan worden.

In de literatuur wordt de natte-sinterings theorie voorgesteld welke het coalescentieproces kan beschrijven. Het concept van deze theorie is de toepassing van het principe van de capillairdruk in een latexsysteem, waarbij de grensvlakspanningen tussen polymeer/water, polymeer/lucht en water/lucht verantwoordelijk zijn voor de vervorming van de latexdeeltjes. Het principe van de capillairdruk wordt toegepast op de kleine openingen in de bolstapelingsstructuur en op de kromtestralen die ontstaan tussen de deeltjes.

Uit de veranderingen van de onderlinge deeltjesinterferentie gedurende het coalescentieproces is gebleken dat de latexdeeltjes volgens een bi-axiaal mechanisme vervormen (afplatten). Dit resultaat in combinatie met de natte-sinteringstheorie heeft geleid

tot het Vanderhoff/JKR coalescentiemodel, dat aan de hand van de deeltjesvervorming als functie van de droogtemperatuur de elastische eigenschappen (Youngmodulus) van de latexdeeltjes kan berekenen als functie van de droogtemperatuur. Deze elastische eigenschappen komen redelijk overeen met de elastische eigenschappen (gemeten in een DMTA bij 0.01 Hz) van de gedroogde latexfilm.

Een latexfilm wordt pas transparant als de grenslagen, cq. inclusies tussen de vervormde latexdeeltjes verdwenen zijn of dat deze zo klein geworden zijn dat ze in het zichtbare golflengtegebied geen of nauwelijks licht verstrooien. De grootte van de grenslagen, cq. inclusies hangt sterk af van de grootte en mate van vervorming der deeltjes. Dit betekent dat latices met relatief grotere deeltjes meer moeten vervormen om dezelfde transparante films te vormen dan die van latices met relatief kleine deeltjes. Onderzocht is in welke mate de deeltjesgrootte en de relatieve-vochtigheid het vervormingsgedrag van de latexdeeltjes beinvloeden, dit als funktie van de droogtemperatuur. Bij relatief hoge vochtigheden is gebleken dat er nauwelijks verschillen zijn in het vervormingsgedrag voor latices met deeltjes van respectivelijk *94* en *119 nm*, echter bij een relatief lage vochtigheid zijn er duidelijke verschillen in het vervormingsgedrag waargenomen. Bij lage vochtigheden vervormden de grotere latex deeltjes t.o.v. de kleinere latexdeeltjes pas bij veel hogere droogtemperaturen compleet. Dit betekent dat de capillairkrachten in een latexsysteem met kleine deeltjes hoger zijn dan in een latexsysteem met relatief grote deeltjes.

Als de latexdeeltjes totaal vervormd zijn, ontstaat er een transparante film. Wanneer deze latexfilm ondergedompeld wordt in een zure-oplossing, zwellen de nog aanwezige grenslagen tussen de aaneengeplakte latexdeeltjes op, wat als gevolg heeft dat de lichtverstrooiings- en interferentiepatronen geregenereerd worden. Deze patronen zijn dan gerelateerd aan de grootte en het aantal van de gezwollen grenslagen. Verwacht wordt dat wanneer de latexfilm veroudert, deze grenslagen zullen verdwijnen. Het proces waarbij de vervormde latexdeeltjes hun indentiteit verliezen, wordt autohesie genoemd. Door de afname van het aantal grenslagen tegen de verouderingstijd te meten kan het autohesieproces gekarakteriseerd worden. Echter de in hoofdstuk 5 beschreven experimenten tonen aan dat er geen afname is in het aantal grenslagen gedurende droogtijden van *1* en *24* uur. Dit betekent dat de autohesie van deze gedroogde latexfilm niet verbetert gedurende een periode van 24 uur.

De achtergebleven grenslagen zijn ook m.b.v. een Transmissie Electronen Microscoop onderzocht. Op de *TEM*-foto's van gedeeltelijk vervormde latexdeeltjes waren donkere elliptische ringvormen waarneembaar tussen de deeltjes. Deze donkere elliptische ring-

vormen zijn geinterpreteerd als emulgatormolekulen die zich geconcentreerd hebben rond het contactoppervlak van de vervormde latexdeeltjes. Het contactoppervlak zelf bestaat dus alleen uit een polymeer-polymeer grensvlak. Dit betekent dat de autohesie alleen verbetert wanneer de emulgatormoleculen verdwijnen uit de gedroogde latexfilm. Dit betekent ook dat de in de literatuur voorgestelde mechanismen, interdiffusie van polymeerketensegmenten over de grenslagen of de vorming van intermoleculaire grenslagen doormiddel van visceuse vloei, niet verantwoordelijk zijn voor het autohesieproces.

In het laatste hoofdstuk is beschreven hoe de latexcoalescentiemethode uit hoofdstuk 4 toegepast kan worden om latexdeeltjes met kern-schil "core-shell" morfologieën te karakteriseren. Latexdeeltjes met een kern-schilmorfologie worden toegepast om het vervormingsproces en de elastische eigenschappen van de uiteindelijke gedroogde latexfilm te verbeteren. In eerste instantie is onderzocht of de gesynthetiseerde latexdeeltjes de verwachte kern-schilstructuur hebben. M.b.v. van *QELS*, interferentie en lichtverstrooiing metingen is de kern-schilmorfologie aangetoond; echter zeeptitratries en TEM en DSC metingen tonen aan dat de kern-schilmorfologie niet ideaal is, en dat deze bestaat uit een soort van "domein-" of "framboos"-morfologie.

In het tweede deel is onderzocht of het Vanderhoff/JKR vervormingsmechanisme beschreven in hoofdstuk 4 toepasbaar is op het vervormingsgedrag van de kern-schildeeltjes. Gebleken is dat het vervorminggedrag van kern-schil-latexdeeltjes sterk kan afwijken van die van homogene latexdeeltjes. Verwacht werd dat wanneer de schildikte groter is dan de maximaal mogelijke vervorming van de latexdeeltjes, de vervorming voornamelijk bepaald wordt door de elasticiteit van het schilpolymeer. Experimenten toonden echter aan dat schildikten van meer dan drie maal de maximale vervormingsafstand noodzakelijk waren om de invloed van de kern op het vervormingsgedrag uit te sluiten. Maar ook hier blijkt dat uit de elastische eigenschappen van de gedroogde latexfilm (gemeten in een *DMTA* bij *0.1 Hz*) en het Vanderhoff/JKR vervormings model van hoofdstuk 4 het specifieke vervormingsgedrag van de kern-schil latexdeeltjes goed te voorspellen is.

De lichtverstrooiings- en interferentiemetingen besproken in dit proefschrift zijn eerste pogingen om de mechanismen die het filmvormingsproces bepalen te onderzoeken. De informatie verkregen uit dit onderzoek is noodzakelijk om de invloeden van additieven en morfologieën op het filmvormingsproces van industrieel gesynthetiseerde latices te begrijpen. Deze eerste onderzoeksresultaten demonstreren dat transmissiespectrofotometrie een belangrijke meetmethode is voor het verdere filmvormingsonderzoek.

DANKWOORD

Voor het goede verloop van mijn promotie onderzoek wil ik graag allen bedanken die op enigerlei wijze hebben bijgedragen aan de totstandkoming van dit proefschrift.

Allereerst wil ik mijn ouders bedanken, die mij altijd gestimuleerd hebben om verder te gaan studeren en steeds grote belangstelling hebben getoond. Ook wil ik mijn vriendin en schoonouders bedanken voor hun steun gedurende de periode dat ik met het onderzoek bezig was.

Klaas te Nijenhuis en Abe Posthuma de Boer, mijn promotoren, wil ik bedanken voor hun grote interesse en steun tijdens het onderzoek.

Verder wil ik bedanken de afstudeerders Mark Henfling, Edith van der Reijden, Peter den Besten en Paul van Woerkens. Hun bijdragen hebben tot een beter inzicht en tot zeer ver(r)assende en interessante resultaten geleid.

Cor van Rossum van DSM Resins en Ron Koel van Brink/Molijn wil ik bedanken voor hun bijdrage in enkele deelprojecten van het onderzoek.

Leon Janssen bedank ik voor de enthousiaste steun en vriendschap, die het verblijf op de universiteit heel plezierig heeft gemaakt. Verder wil ik speciaal noemen : Bert Verwater, Han Neevel, Prim Ramlal, Jan Helmig en Thom van Velzen.

Tenslotte een woord van dank aan alle collega's, medewerkers, afstudeerders en studenten van de vakgroep, vanwege de prettige sfeer tijdens het werk, en vooral ook na het werk.

In memoriam Prof.dr.ir H.C.A. van Beek

Toen ik als toegevoegd onderzoeker werkzaam was in de proeffabriek op de Technische Universiteit Delft, werd ik door promovendus Bert Verwater geattendeerd op het feit dat het in principe mogelijk was om als afgestudeerd HTS-ingenieur te kunnen promoveren. Professor H.C.A. van Beek vond dat ik een goede kans zou hebben om deze promotie met succes te kunnen afronden. Ik merkte tijdens mijn promotie-onderzoek dat ik toch wel een achterstand had ten opzichte van andere promovendi, wat betreft zelfstandigheid en algemene kennis. Door het geduld en de goede begeleiding van Professor H.C.A. van Beek kon ik deze achterstand uiteindelijk toch inhalen. Hiervoor ben ik hem nog steeds zeer dankbaar.

Na het overlijden van Professor H.C.A. van Beek ben ik erg goed opgevangen en begeleid door Dr.Ir. K te Nijenhuis en Professor Dr.Ir. A. Posthuma de Boer. Hun hulp zorgde er uiteindelijk voor dat ik mijn promotie met succes kon afronden.

CURRICULUM VITAE

Abraham van Tent werd geboren op 6 april 1965 te Nunspeet. In 1982 behaalde hij het HAVO-diploma aan de Rijksscholengemeenschap te Harderwijk. In datzelfde jaar begon hij zijn de studie Chemische Technologie aan Christelijke Hogere Technische School te Hilversum. 'Modellering van het menggedrag in fluidbed-reaktoren' was het onderwerp van zijn afstudeerwerk. In 1986 behaalde hij het ingenieursdiploma.

Van augustus tot november 1986 was hij werkzaam als toegevoegd onderzoeker in de groep van Prof. Ir. C.M. van den Bleek en Giel Doesburg aan de Technische Universiteit Delft.

Sinds februari 1987 werkte hij als assistent in opleiding, bij de vakgroep Chemische Technologie, werkgroep Produkt Technologie van Professor H.C.A. van Beek, Technische Universiteit Delft. Na diens overlijden kwam hij terecht bij de vakgroep Technologie van Macromoleculaire Stoffen, onder begeleiding van Dr.Ir. K te Nijenhuis en Professor Dr.Ir. A. Posthuma de Boer.